Doctor Dissertation

Study on Maneuvering of a Large Tanker in Still Water and Adverse Weather Conditions

(平水中および荒天下中における大型タンカーの操縦性能に関する研究)

September 2018

Graduate School of Engineering
Faculty of Engineering
Hiroshima University

Mochammad Zaky

Abstract

Ship maneuverability has a significantly important role in navigation safety point of view. In order to ensure this important role, a ship must certainly have good maneuver during the initial design process before the ship is built. Likewise, a ship should be maneuvered safely without harming the effectiveness of operating costs. Particularly, a Very Large Crude Carrier (VLCC) with a large size sails not only in still waters or inland waterways but also frequently in various sea states with uncertain environmental conditions. These conditions make a VLCC potentially get a serious accident at sea. Therefore, a VLCC must have a good course stability, and it can be well maneuvered and controlled even in stormy weather under any loading conditions. Furthermore, a VLCC also must be efficient that is proven by low fuel consumption to reduce CO_2 emissions as regulated under IMO regulation with respect to the Energy Efficiency Design Index (EEDI). A small main engine output is one of the alternative options to the above constraint. However, an excessive reduction in the engine output will adversely result in a potentially unexpected unsafe situation wherein a helmsman may not be able to maneuver the ship well in adverse weather conditions. As consequences to the engine output reduction, a large-diameter and low-revolution propeller and an energy efficiency device are employed. A high lift rudder has been selected in this research work as an effective way that aims to improve the ship maneuverability since it becomes worse under reduced-engine output.

In this study, the maneuvering performance of a VLCC tanker in both still water and adverse weather conditions is investigated by using a Maneuvering Modeling Group (MMG) model including wind and waves. A free running model test using a VLCC model (KVLCC2) was carried out to evaluate the maneuvering simulation method in waves. Next, maneuvering of a VLCC is investigated in two loading conditions of a full-load condition (DF) and normal ballast load condition (NB) to assess the effect of load conditions. Furthermore, to achieve an energy efficiency of a VLCC in DF, the investigation involved a situation where the engine output of a VLCC was significantly reduced owing to advances in energy-saving technology. A VLCC with 30% reduced EEDI (Step3) is planned for the conventional VLCC (Step0) by the adoption of energy efficiency devices, a large-diameter and low-revolution propeller, etc. Subsequently, to improve the maneuverability of a VLCC in Step3, a high lift rudder (HL rudder) with a fishtail section and end plates was newly designed to increase the rudder force under a restriction that minimizes the increase in rudder resistance. Tank tests were performed by using a scaled ship

model with a HL rudder to capture propulsive performance and rudder force characteristics of the ship with a HL rudder.

Through the research presented in this thesis, it was confirmed that the loading conditions significantly influence the ship maneuverability. The steady-state sailing condition in adverse weather conditions is quite different between DF and NB: the absolute value of the check helm becomes small in NB, but the hull drift angle becomes large. The relative drift direction of the ship in turning to the wave direction is $20^\circ - 30^\circ$ in NB and DF with a rudder angle 35° and almost constant for any wind (wave) directions. The drifting displacement in turning under NB becomes larger than that under DF at the same environmental condition. Advance A_D and tactical diameter D_T become significantly small with an increasing Beaufort scale in head wind and waves when approaching, although A_D and D_T are almost constant in following wind and waves. In beam wind and waves, the tendency depends on the plus and minus of the rudder angle. In zig-zag maneuvers, the first and second overshoot angles (OSAs) in head wind and waves become smaller than those in still water (SW), and those in following wind and waves are almost the same or become larger than those in SW. In the case of 10/10 zig-zag maneuvers of a ship in beam wind and waves, the first OSA increases compared with the value in SW, because the effective rudder angle decreases, and the second OSA decreases, because of the effective rudder angle increases. This tendency becomes opposite for $-10/-10$ zig-zag maneuvers. The effective rudder angle changes owing to the order of magnitude of the check helm in adverse weather conditions. These tendencies with respect to OSAs are the same in between DF and NB, although DF is more significant. However, the situation where the VLCC uncontrollable in DF did not occur. Since the reduction 30% EEDI was applied to a VLCC in Step3, it was observed that Step3 satisfied IMO maneuvering criteria in the still water condition. However, the maneuverability of Step3 was worse than that of Step0 since the rudder force was reduced owing to the low propeller load, which resulted from the small engine output. Additionally, the steady-state sailing performance of Step3 in adverse weather conditions, such as check helm, hull drift angle, and speed drop, generally worsened when compared with those of Step0. Furthermore, course changing ability also deteriorated in the case of Step3. However, the difference between the trajectories of Step0 and Step3 reduced with respect to the large Beaufort scale since the difference in the rudder force became less noticeable owing to the presence of large external lateral forces caused by strong winds and waves. The improvement of step3 was performed by attaching a HL rudder. The results indicated that the

designed HL rudder increased the effective rudder force by approximately 10% when compared to a conventional mariner rudder (MN rudder). And the HL rudder presented in this study is useful in improving maneuverability while maintaining almost the same level as the propulsive performance of a ship with a mariner rudder.

Acknowledgements

Alhamdulillah, praise be to Allah SWT the Almighty and the most merciful that because of His blessings I could finally finish my dissertation. Shalawat and salam may everlastingly be upon our adoration, Great Prophet Muhammad SAW who as the role model for all mankind.

I would like to express my best gratitude to:

- Prof. Hironori Yasukawa as my supervisor who has been helping me in academic and also in settling down for Japan life. Thanks for your time, knowledge, advice and motivation that you have given to the writer since study in this great campus.

- Prof. Yasuaki Doi as my supervisor who gave me many important advice and the valuable input to improve of this thesis.

- Prof. Hidetsugu Iwashita as my supervisor who gave me the valuable input and advice for the improvement of this thesis.

- Asc. Prof. Susumu Tanaka as my supervisor who gave me many important advice in my study.

- Ast. Prof. Masaaki Sano who gave me some information so the writer can accomplish this thesis.

- My beloved wife Damarwulan Pamungkas and my daughter and son Aisyah Nailal Husna and Ali Mirza Fahlevi who always loves me, besides me, supports and shares with me all happiness and difficulties of my whole life. I love them so much.

- My parents and all my family members especially in Surabaya and Cijulang who always pray for me, proud of me, and would have never left me alone.

- All of Management of PT. Biro Klasifikasi Indonesia (Indonesian ship classification society) who gave me support and many important advice in my study, and I am also proud to be a part of this company.

- Dr. Jiangang Shi and Ms. Ayako Yokosu as my internship supervisor in Tsuneishi shipyard who gave me some knowledge about the optimization of ship design based on the CFD method.

- All of students in Marine Transportation Systems Laboratory (Mr.Amirul, Mr.Sasmito, Mr.Timmy, Mr.Matsumoto, Mr.Hamamoto, Mr.Okuda, Mr.Hamasaki, Mr.Mori, Mr.Hori, Mr.Zakiyama, Mr.Shirai, Mr.Fukushima, Mr.Ishikawa, Mr.Sato, Mr.Yamamoto, Ms.Ito, etc), with whom I have had longer or shorter enlightening discussions about the various topics of this work.

- Professors, researchers, students and staffs in Department of Environmental and Transportation Systems who helped me in last three years.

- Mr. Fukumura and Mr. Ohmura as our Japanese parents and teacher while during stay in Japan.

- All of my friends in Indonesian Student Community of Hiroshima (PPIH) and Indonesian Moslem Community of Hiroshima (KMIH) for their support and valuable experiences for last three years.

Glossary

Abbreviations

ACS	Air Circulation System
BHP	Brake Horse Power
CFD	Computational Fluid Dynamic
DF	Design Full
DOF	Degree of Freedom
EEDI	Energy Efficiency Design Index
HL rudder	High Lift rudder
IMO	International Maritime Organization
ITTC	International Towing Tank Conference
LFRP	Low Frictional Resistance Paint
MCR	Maximum Continuous Rating
MMG	Maneuvering Modeling Group
MN rudder	Mariner rudder
NB	Normal Ballast
NOR	Normal output
NRIFE	National Research Institute of Fisheries Engineering
OSA	Overshoot Angle
PSF	Pre-Swirl Fin
RBF	Rudder Bulb Fin
SW	Still Water
VLCC	Very Large Crude oil Carrier

Greek symbols

α_0	relative drift direction in turning to the wave directions ($\equiv \beta_0 - \chi$) (rad)
α_R	effective inflow angle to the rudder (rad)
β	hull drift angle at midship, $\beta = \tan^{-1}(-v_m/u)$ (rad)

β_0	drift turning direction (rad)
β_P	Geometrical inflow angle to propeller in maneuvering motions (rad)
β_R	effective inflow angle to rudder in maneuvering motions (rad)
β_{R0}	Geometrical inflow angle to rudder in maneuvering motions (rad)
χ	wave direction (rad)
χ_0	relative wave direction with respect to ship heading $\chi_0 = \chi - \psi$ (rad)
η	ratio of propeller diameter to rudder span ($= D_P/H_R$) ($-$)
η_H	hull efficiency ($-$)
η_R	relative rotative efficiency ($-$)
δ	rudder angle (rad)
δ_{FN0}	rudder angle where rudder normal force becomes zero (rad)
γ_R	flow straightening coefficient ($-$)
Λ	rudder aspect ratio ($-$)
κ	an experimental constant for expressing u_R ($-$)
∇	displacement volume of ship (m^3)
ψ	ship heading (rad)
ρ	water density ($\mathrm{kg\ m}^{-3}$)
ρ_a	air density ($\mathrm{kg\ m}^{-3}$)
θ_W	wind direction (rad)
θ_A	relative wind direction $\theta_A = \tan^{-1}(v_A/u_A)$ (rad)
ε	ratio of wake fraction at propeller and rudder positions $(= 1 - w_R)/(1 - w_P))$ ($-$)

Roman symbols

A_D	advance (m)
A_e	expanded area of the propeller (m^2)
A_0	disc area of the propeller, $A_0 = \pi {D_p}^2/4$ (m^2)
a_H	rudder force increase factor ($-$)
A_R	rudder area including horn (m^2)
A_X	front wind pressure area (m^2)

A_Y	side wind pressure area (m^2)
B	ship breadth (m)
B_R	averaged rudder chord length (m)
C_b	block coefficient $(-)$
C_{XA}	aerodynamic coefficient in surge $(-)$
C_{YA}, C_{NA}	aerodynamic coefficients in sway and yaw moment, respectively $(-)$
C_{XW}	the wave-induced added resistance coefficient in regular waves $(-)$
C_{YW}, C_{NW}	the wave-induced lateral force and yaw moment coefficients in regular waves, respectively $(-)$
$\overline{C_{XW}}$	the averaged wave-induced added resistance coefficient in irregular waves $(-)$
$\overline{C_{YW}}, \overline{C_{NW}}$	the averaged wave-induced lateral force and yaw moment coefficients in irregular waves, respectively $(-)$
D	ship depth (m)
D_d	displacement of the drift turning (m)
D_P	propeller diameter (m)
D_T	tactical diameter (m)
d	ship draft (m)
d_a	draft at after perpendicular of the ship (m)
d_f	draft at fore perpendicular of the ship (m)
F_N	rudder normal force (N)
F_{nwl}	Froude number based on L_{wl} $(-)$
f_α	rudder lift gradient coefficient $(-)$
GM	metacentric height (m)
g	gravity acceleration (m/s^2)
H_R	rudder span (m)
$H_{1/3}$	significant wave height (m)
I_{zG}	moment of inertia of ship around the center of gravity (kg m^2)
J_z	added moment of inertia (kg m^2)
K_T	propeller thrust open water characteristic $(-)$
k_2, k_1, k_0	coefficients representing K_T $(-)$
K_Q	propeller torque open water characteristic $(-)$
q_2, q_1, q_0	coefficients representing K_Q $(-)$

L	ship length between perpendiculars (m)
L_{wl}	ship length waterline (m)
ℓ'_R	effective longitudinal coordinate of rudder position in formula of β_R $(-)$
m	ship's mass (kg)
m_x, m_y	added masses of x-axis direction and y-axis direction, respectively (kg)
N_A	yaw moment around the midship due to the wind (N m)
N_E	engine revolution at MCR (rpm)
N_H	yaw moment around the midship acting on ship hull with the exception of the added mass component (N m)
N_m	yaw moment around the midship with the exception of the added mass component (N m)
n_P	propeller revolution (rps)
N_R	yaw moment around the midship by steering (N m)
N_W	yaw moment in irregular waves (N m)
$o-xyz$	fixed coordinate system of the ship by considering the origin at the midship
$o_0-x_0y_0z_0$	space fixed coordinate system
p	propeller pitch ratio $(-)$
P_B	main engine output (kW)
P_E	engine power at MCR (kW)
Q	propeller torque (Nm)
r	yaw rate (rad s^{-1})
$\dot{r}$	yaw acceleration (rad s^{-2})
S	wetted surface area of a ship without a rudder and horn (m^2)
$S_{\zeta\zeta}$	wave spectrum (m^2s)
t	time (s)
T	propeller thrust (N)
T_R	transfer (m)
T_v	averaged wave period (s)
t_P	thrust deduction factor $(-)$
t_R	steering resistance deduction factor $(-)$
U	resultant speed, $U=\sqrt{u^2+v_m^2}$ (m s^{-1})
U_0	approach speed (given speed) (m s^{-1})

U_R	resultant inflow velocity to rudder (m s^{-1})
u	surge velocity (m s^{-1})
u_R, v_R	longitudinal and lateral inflow velocity components to rudder, respectively (m s^{-1})
$\dot{u}$	surge acceleration (m s^{-2})
v_m	lateral velocity at midship (m s^{-1})
$\dot{v}_m$	lateral acceleration at the midship (m s^{-2})
V_A	relative wind speed (m s^{-1})
V_s	ship speed (knots)
w	wake fraction in the model (−)
w_P	wake fraction at propeller position in maneuvering motions (−)
w_{P0}	wake fraction at propeller position in straight moving (−)
w_R	wake fraction coefficient at rudder position (−)
w_{R0}	effective wake fraction coefficient at rudder position (−)
w_s	wake fraction in fullscale (−)
X	surge force with the exception of the added mass component (N)
X_A	surge force due to the wind (N)
x_G	longitudinal position of the center of gravity of a ship (m)
X_H	surge force acting on a ship hull with the exception of the added mass component (N)
X_P	propeller force (N)
X_R	surge force by steering (N)
X_W	surge force in irregular waves (N)
x_H	longitudinal coordinate of the acting point of the additional lateral force (m)
x_R	longitudinal coordinate of the rudder position (m)
Y	lateral force with the exception of the added mass component (N)
Y_A	lateral force due to wind (N)
Y_H	lateral force acting on the ship hull with the exception of the added mass component (N)
Y_R	lateral force by steering (N)
Y_W	lateral force in irregular waves (N)
Z	number of propeller blades (−)

Contents

List of Tables

List of Figures

Chapter 1

Introduction

Ship maneuverability has a significantly important role in navigation safety point of view. In order to ensure this important role, a ship must certainly have good maneuver during the initial design process before the ship is built. Likewise, a ship should be maneuvered safely without harming the effectiveness of operating costs. Commonly, the ship with a large size not only sails in still waters or inland waterways but also frequently in various sea states with uncertain environmental conditions. These conditions make a ship potentially get a serious accident at sea. Therefore, the ship must be designed safely, efficiently and Eco-friendly. A reliable ship is a ship that has good course stability, and it can be well maneuvered and controlled even in stormy weather under any loading conditions. Not only that, but the ship also must be efficient that is proven by low fuel consumption, in order to reduce CO_2 emissions as regulated under IMO regulation with respect to the Energy Efficiency Design Index [EEDI] of ships [12, 13]. A small main engine output is one of the alternative options to the above constraint. However, an excessive reduction in the engine output will adversely result in a potentially unexpected unsafe situation wherein a helmsman may not be able to maneuver the ship well in adverse weather conditions. As consequences to the engine output reduction, a large-diameter, low-revolution propeller and an energy efficiency devices are employed. A special rudder namely high lift rudder has been selected in this research work as an effective way that aims to improve the ship maneuverability since it becomes worse under reduced-engine output. The maneuvering criteria

as regulated by IMO [14, 15, 16] is used as the primary guideline to measure quantitatively for ship maneuvering performance in this study.

This chapter presents the purpose, objective and reviews studies as references for this study. Section 1.1 introduces the applied terminologies and the research background. Section 1.2 states the research problems to be resolved. Section 1.3 presents some research questions that appear from the problem statement, and it will be a basis for improvement of maneuverability of a large tanker. Section 1.4 addresses the scope of this research. At the end, Section 1.5 explains the structure of this dissertation and describes the content of each chapter.

1.1 Research Background

1.1.1 Terminologies

The use of the term like ship design and maneuvering commonly appears in some literature, especially in an engineering field. To avoid ambiguity in this thesis, the following terms are briefly defined as below:

- **Tanker** is a ship that is built to carry liquid or gas. in this study a Very Large Crude Carrier (VLCC) as an oil tanker with a deadweight capacity 200,000 - 400,000 tons used as reference ship.
- **Ship maneuverability** is the quality of ship being able to respond to certain navigation orders, which include but not limited to, turning, course keeping, yaw checking and stopping.
- **Energy efficiency** is to use less energy to provide the same energy level. The ship energy efficiency is defined as EEDI which expressed in grams of carbon dioxide CO_2 per ship's capacity-mile (the smaller the EEDI the more energy efficient ship design) and is calculated by a formula based on the technical design parameters for a given ship.
- **Still water** is the sea condition with little or no wind and waves.

- **Adverse weather** is severe weather with strong wind and waves that cause an unsafe condition. In this study, adverse weather is assumed on a Beaufort 6 and above.
- **MMG model** is one of the simulation models for ship maneuvering developed in Japan.
- **Engine output** is the maximum power that an engine can put out. Normally it is defined as a maximum continuous rating (MCR).
- **Loading condition** is a certain load condition, which includes fully loaded departure condition, fully loaded arrival condition, and ballast departure condition, ballast arrival condition. In this study, to evaluate the maneuvering performance of a large tanker based on loading conditions, both of full loaded departure and ballast arrival condition are used.
- **Full load condition** is a fully loaded departure condition with the full cargo, stores, and fuel.
- **Ballast condition** is a ballast arrival condition without cargo and with 10% stores and fuel remaining.
- **Course stability** is the ships ability to return soon to its initial motion characteristics after a momentary disturbance.
- **Mariner rudder** is a rudder with a spade type incorporated with a rudder horn.
- **High lift rudder** is a special rudder with a fishtail section and end plates, and it is designed to increase the rudder force.

1.1.2 Tanker transport

The tanker transports crude oil, refined petroleum products, and chemicals. Tankers have large populations whose operations typically travel beyond the open seas and oceans. The world tanker fleet has greatly expanded in recent years, whose number until 2017 are 12,662 ships totaling 577 million dead-weight tons [17]. It was principally through a major use of large tanker or supertankers. An equivalent number of large tankers are now under construction

throughout the world. It was reported that until 2016, the world tanker trade performing is relatively better than any other sector, although the world tanker production rate was decreased compared with previous years [31]. Those conditions might be triggered by the impact of declining in world oil prices that occur to date. Nevertheless, this situation tends to recover in line with the energy demands which certainly needed in some developed countries. On the other hand, recent estimation shows that one-third of all oil pollution of the world's oceans due to the marine transportation. Tankers understandably are the single most significant contributor to such pollution due to its high fuel consumption and CO_2 emissions generated. Accordingly, this requires international regulation to make a strict policy through the improvement of the energy efficiency index on the ship. As the solutions from those problems, it is necessary to develop and apply new methods and technology in the ship design process. One of the areas of most importance for large tankers is their maneuverability. And the most important point in the design process is to ensure that the tankers have reliable maneuverability in still waters and adverse weather conditions. From the explanation mentioned above, it is necessary to perform a research that concerns the design of tankers to operate safely and efficiently based on the navigation point of view.

1.1.3 Navigation safety

The safety of ships is critical to the world economy. This is due to the international trades which dominantly transported by shipping sector. With increasing sea transportation, the number of ships in operations also increases as well as the risk of marine accidents. During the period of 2007-2016, it was reported that the total losses were 1186 ships throughout the world [1]. Based on statistical data, they have declined 50% over the past decade. It was informed that the cause of total losses with respect to the ship maneuverability such as foundered, stranded and collision over half of all total losses. Additionally, one of the ship's accidents is due to the ship being unable to maneuver appropriately during its operation. Storm weather is often as a factor, even though human error also involved in those accidents. The other statistical data show that most of the ship accidents related to the ocean swell occurred relatively in low sea

states conditions [50]. It is noted that maritime safety has been improving in recent years, driven by continually evolving regulation and the development of a more robust safety culture and many ship-owners are now much more proactive around safety than they were in the past. Based on the explanation described above, studies that concern for marine safety in relation to ship maneuvering are needed.

1.1.4 Loading conditions

International Maritime Organization (IMO) standards for ship maneuverability [15, 16] apply the full load and even keel condition as the fundamental condition for the assessment. However, many trades and voyages require passage without cargo or in a light-cargo condition. When a ship is not fully laden, ballast water is required to compensate for the increased buoyancy and keep the propeller and rudder submerged for navigation safety. The propeller thrust or rudder force may reduce due to not fully-immersed propeller and rudder. Those situations may lead to the unsafe condition of the ship in adverse weather conditions. For instance, the serious accident in stormy weather by grounding occurred for a ship in ballast load condition, in Australia [2].

Several studies were conducted to investigate the effect of loading conditions on maneuvering performances. Eda et al. [6] confirmed that both the water depths and loads significantly influenced the ship maneuverability characteristics. With decreasing water depth, turning performance become worse and dynamic course stability improved, likewise decreased turning capability and increased dynamic course stability are indicated for the ballast condition relative to the full load condition. Kijima et al. [20] proposed a practical method to predict the maneuvering motions of the ships in any loading conditions. The method based on a lot of approximate formulas to estimate the hydrodynamic force coefficients of ships. The prediction accuracy is acceptable, and it is useful for predicting maneuverability of the conventional ships at the initial design stage. Kijima et al. [21] also proposed prediction method that expresses the loading condition effect on the ship maneuverability based on the parameters of flow straightening coefficient γ and effective wake fraction coefficient at rudder position w_{R0}, the prediction

method has relatively good accuracy for turning ability but not for course keeping ability. In addition, a new modification of Kijima's mathematical model was introduced by Yoshimura [42]. It confirmed that a dry cargo with V-shape model becomes worse in ballast condition and conversely improved for U-shape model when compared to that of full load condition, V-shape makes the course stability worse in general, though it produces better resistance and propulsion. Im et al. [19] proposed approximate formulas to estimate the hydrodynamic derivatives of a ship in any loading conditions. Yoshimura et al. [44] investigated the effect of load condition on the rudder force, and it was confirmed that the rudder normal force decreases with decreasing the aft draft in ballast condition. Recently, Yasukawa et al. [40] investigated the impacts of load conditions with series models of a large tanker in full and ballast load conditions. And they confirmed that by increasing the block coefficient (C_b), turning performance increased, zig-zag maneuvers decreased, and the course stability becomes worse. However, in these studies, they did not mention the ship maneuverability in adverse weather conditions.

1.1.5 Maneuverability in adverse weather

Nowadays, ships maneuverability as regulated by the IMO [15, 16], which does not address ship maneuverability in adverse conditions. Meanwhile, well maneuvers of the ship in adverse conditions are required since the introduction of EEDI [12, 13]. Some researchers and experts were involved in these challenging activities. Hirano et al.[10] initiated to investigate the ship maneuverability in regular waves by the simple prediction method where only wave-induced steady forces are considered as the wave effect in a time domain simulation method. A practical maneuvering simulations method in waves was proposed by Yasukawa et al. [35]. In the method, 2nd-order wave-induced steady forces acting on the ship were considered as the wave effect. The simulation method can capture the maneuvering motions of the ship with the sufficient accuracy for practical purposes. Yoshimura et al. [43] and Hasegawa et al. [9] investigated maneuverability of a Pure Car Carrier in the wind by a time domain simulation method. Nagarajan et al. [24] observed maneuverability of a large tanker with the Mariner Schilling Rudder in the strong wind. However, they never mentioned the engine output effect on the

ship maneuverability in adverse weather conditions in relation to EEDI requirements. Hence, in order to increase the index of EEDI effectively, one of the ways is by applying a small main engine output. However, this may lead to worse maneuverability in adverse conditions.

1.1.6 Minimum power requirement

The IMO requires that all ships above 400 GT must reduce EEDI by a maximum of 30% after 2025 [12]. The implementation of the EEDI has raised justified concerns that some ship designers might choose to simply lower the installed power to achieve EEDI requirements. The employment of a small main engine output is an extremely effective way to lower fuel consumption and to reduce CO_2 emissions. However, small engine output leads to a low propeller load, and thereby reduces the rudder force. Therefore, an excessive reduction in minimum power will result in unsafe situations in which the ship is unable to be well maneuvered in adverse weather conditions.

Several studies have been carried out to improve ship maneuverability under a lower engine output in adverse weather, although very few studies deeply discuss with regard to this subject. Takahashi and Asai [29] confirmed that a lower-powered ship has larger speed loss and poorer course keeping ability when compared with a higher-powered ship in stormy conditions. They examined a case in which engine output was reduced with decreases in the design speed and did not consider the impact of specific maneuvering motions such as turning and zig-zag maneuvers.

1.1.7 Improvement of manueverability

There are many ways to improve ship maneuverability, such as reducing ship weight, optimizing hullform, increasing thrust power, modifying rudder design. In practice, it may not be possible to improve ship maneuverability which related to the main particulars and hullform because both constrained by the cargo capacity and the ship lightweight. Likewise, upgraded thrust power by increasing main engine output leads to an increase in fuel consumption. Therefore, the remaining possibilities to improve the maneuvering performance are through optimizing

rudder design. A rudder has a significant contribution to the ship maneuvering performances as well as an underestimated potential for fuel savings [11]. A rudder with special sectional shape achieves the high lift rudder forces, and it will improve the ship maneuverability certainly.

Several studies investigated the impacts of a high lift rudder on maneuvering and propulsive performances of ships. Bingham and Mackey [4] reviewed the maneuvering performance of ships with a high lift rudder, such as the Schilling rudder and a flap rudder, and indicated that the Schilling rudder exhibited better turning ability, was simpler in construction, and cheaper when compared with the flap rudder. Brix [5] indicated that the rudder with various fishtails section produces a larger lift force as compared to the NACA mariner rudder, although the drag increases at all rudder angles. The lift force of this rudder evidently improved about 8-12% when attached on a series of the container ship. Hasegawa et al. [9] investigated the course-keeping ability of a Pure Car Carrier in windy conditions for two rudders (Schilling rudder and mariner rudder), and concluded that the Schilling rudder produces a larger lift force when compared with the mariner rudder. Nagarajan et al. [24] confirmed that maneuverability and fuel efficiency of a VLCC with a Schilling rudder was superior when compared with a ship with a conventional mariner rudder. Nguyen and Ikeda [25] numerically confirmed that a rudder with a fishtail section exhibited a higher lift when compared with a NACA mariner rudder. Liu et al. [22] investigated the impact of the rudder section on maneuvering performance, and the results indicated that the wedge-tail section produces a larger rudder force and smaller turning indexes albeit with least efficiency (i.e., higher rudder resistance). In summary, existing studies have indicated that a rudder with a fishtail or a wedge-tail section similar to a Shilling rudder can potentially be used as a measure to improve maneuverability, although there is a possibility that the propulsive performance worsened due to the rudder resistance increased.

1.1.8 Concluding remarks

In section 1.1 we have discussed the importance of proper maneuverability for a large tanker with various load conditions in still water and adverse weather conditions. A small main engine output due to advances in energy efficiency devices and a propeller with a large-diameter and

low-revolution is proposed for the conventional VLCC to improve the index of EEDI. A high lift rudder is selected as an effective way to improve the maneuverability of a VLCC under reduced-engine output. Furthermore, IMO maneuvering criteria are used to assess the maneuvering performance of ships.

1.2 Problem statement

Presently, studies on ship maneuvering are mainly conducted in still water conditions, whereas in reality, seagoing ships with various load conditions travel in different sea-states, and most likely also sail in stormy conditions. These conditions allow that the ship gets a high risk accident. In order to protect the environment from the pollution at sea and to increase the ship energy efficiency, a strict regulation was issued by IMO [12]. This regulation will impact on the reduction of main engine output to fulfill EEDI requirements. By employing a small main engine output, a ship might have insufficient maneuverability in adverse conditions.

Considering the research challenges as mentioned above, there are the several issues to be explored in this study, as follows:

- **According to the existing research, the effect of loading conditions on ship maneuvering performance in adverse conditions, has not been examined yet.**
  There are several studies which concern related to the ship maneuverability in wind and waves. However, their maneuvering studies only in full load condition but not in ballast load condition. In fact, loading conditions will affect the course stability of the ship. Accordingly, the course stability should be observed to confirm the maneuvering performance based on its loading effects.
- **The importance for the development of maneuvering simulation methods under adverse weather conditions.**
  The ship maneuverability in adverse condition has to be discussed under minimum propulsion power under-regulated by IMO [14]. However, the mentioned assessment procedure

may not be enough to represent the actual condition of the ship maneuvers in adverse conditions. Therefore, some parameters should be added in the simulation, such including, but not limited to wind and waves in any direction together with the engine torque-rich model.

- **Effects of engine output on ship maneuverability are not clear.**
  Some researchers have been investigated the maneuvering performance of a large ship in wind and waves [9, 10, 24, 35, 43]. However, they never mentioned the engine output effect on the ship maneuverability in adverse weather conditions. In fact, Takahashi and Asai [29] performed a maneuvering study in severe weather conditions in conjunction with appropriate reductions in the engine output. However, they did not consider the impact of specific maneuvering motions such as turning and zig-zag maneuvers.
- **Effect of a high lift rudder on maneuvering performance in wind and waves has not been examined yet.**
  One of the effective ways to improve the maneuverability of a ship under a small main engine output is attaching a high lift rudder. Studies related to the effect of a high lift rudder on the maneuverability of a ship in adverse weather conditions are limited. Therefore, it is necessary to extend the advantageous by a high lift rudder to the ship maneuvering performance in adverse conditions.

1.3 Research questions

Some problems were identified in section 1.2. There is a lack of study in the prediction methods of maneuverability of a large tanker in still water and adverse conditions under a small engine output. The effect of load conditions on ship maneuvering in the wind and waves has been not investigated yet. The impacts of high lift rudder on ship maneuverability in adverse conditions are not clear. Following these conditions, this thesis intends to resolve these main problems through the following questions:

(1) ***What is the practical simulation model to evaluate the ship maneuvers in adverse weather conditions?***

If the above question is answered, a maneuvering simulation model including wind and waves will be proposed. The proposed simulation model will be useful for practical purposes, particularly at the initial design stage.

(2) ***How does the effect of loading conditions on ship maneuvering performance?***

Answers to this question will provide some information such as the performance of ship maneuvers in design full and normal ballast conditions in still waters and adverse weather conditions. The course stability will be taken account as the significant parameters for the loading conditions effect on maneuvering performance.

(3) ***How does the engine output effect on ship maneuvering performance?***

Answering this question, a small main engine output with a large diameter and low propeller and applying some energy efficiency devices will be proposed. As a result, a VLCC tanker with energy saving, Eco-friendly and safe maneuvers will be achieved.

(4) ***How to improve the ship maneuverability under a small main engine output?***

Answers to the above question will provide insight into the impacts of a high lift rudder on the maneuvering performance of the ship. This solution aims to improve the maneuvering performance due to low engine output.

1.4 Research boundaries

In this thesis, the study of ship maneuverability based on the assumption that the maneuverability of a ship can be assessed by its maneuvering trajectories and indices in specified test maneuvers. A VLCC tanker was taken as reference ship (length: 320 m, breadth: 58 m, depth: 30 m) with a single propeller and single rudder. Based on the above assumptions, the following research boundaries are determined:

- The maneuvering simulation method based on MMG model [12].
- Human factors are not included.
- Effect of the ship to ship interaction is not included.
- Metacentric height GM for a large tanker is commonly large, and the roll coupling effect on maneuvering is negligible.
- The speed effect on the averaged wave-induced steady lateral force coefficient $\overline{C_{YW}}$ and yaw moment coefficient $\overline{C_{NW}}$ in irregular waves is negligible [34].
- Wind and waves directions as the external forces in the simulations are assumed almost the same.

1.5 Thesis outline

To answer the identified research problems as mentioned in section 1.2 and 1.3, a maneuvering performance of large tanker in any loading conditions under adverse conditions will be investigated, the impacts of small engine output on ship maneuverability will be analyzed, and the improvement of maneuverability will be proposed. Fig. 1.1 shows the thesis structure which describes a relation between chapters. This thesis is organized as follows:

- **Chapter 1** presents research background and reviews state of the art literature on ship maneuverability in still water and adverse weather conditions and a ship with lowered engine output to support the research topic. In this chapter the main purposes and problem identification for this study are explained.
- **Chapter 2** proposes the development of the mathematical maneuvering models which involve wind and waves effect. The engine output is modeled as torque limit line for controlling the propeller revolution. This chapter answers the question 1.

- **Chapter 3** outlines a VLCC tanker as studied ship with the detail of ship particulars that will be as the reference ship for the simulation. This chapter answers the question 1 as subject ship used in Chapter 2.

- **Chapter 4** presents the verification of the simulation method as mentioned in Chapter 2 through free-running model tests in waves with specified maneuvering test. The ship model based on Chapter 3. This chapter answers the question 1 and ensures the reliability of simulation models.

- **Chapter 5** discusses the effect of load conditions on ship maneuverability. By using the simulation maneuvering model in Chapter 2 and the subject ship in Chapter 3, the ship maneuverability in full load and ballast load conditions are investigated. A course stability is observed to confirm the ship maneuvering performance based on its loading conditions. This chapter answers the whole question 2.

- **Chapter 6** presents a maneuvering performance of ship under a small main engine output in full load condition. Using the reference ship in Chapter 3 and hydrodynamic characteristics in Chapter 5, the simulations method corresponds to Chapter 2 is applied to investigate the maneuverability for both a conventional vessel and a ship with 30% reduced EEDI. This chapter answers the question 3.

- **Chapter 7** introduces a new high lift rudder design to improve ship maneuverability of ship with a small engine output based on Chapter 6. The reference ship corresponds to Chapter 3. Tank test is carried out to obtain the self-propulsion performance and rudder force characteristics. This chapter answers the question 4.

- **Chapter 8** summarizes the conclusions of this thesis and outlines the recommendations for further research.

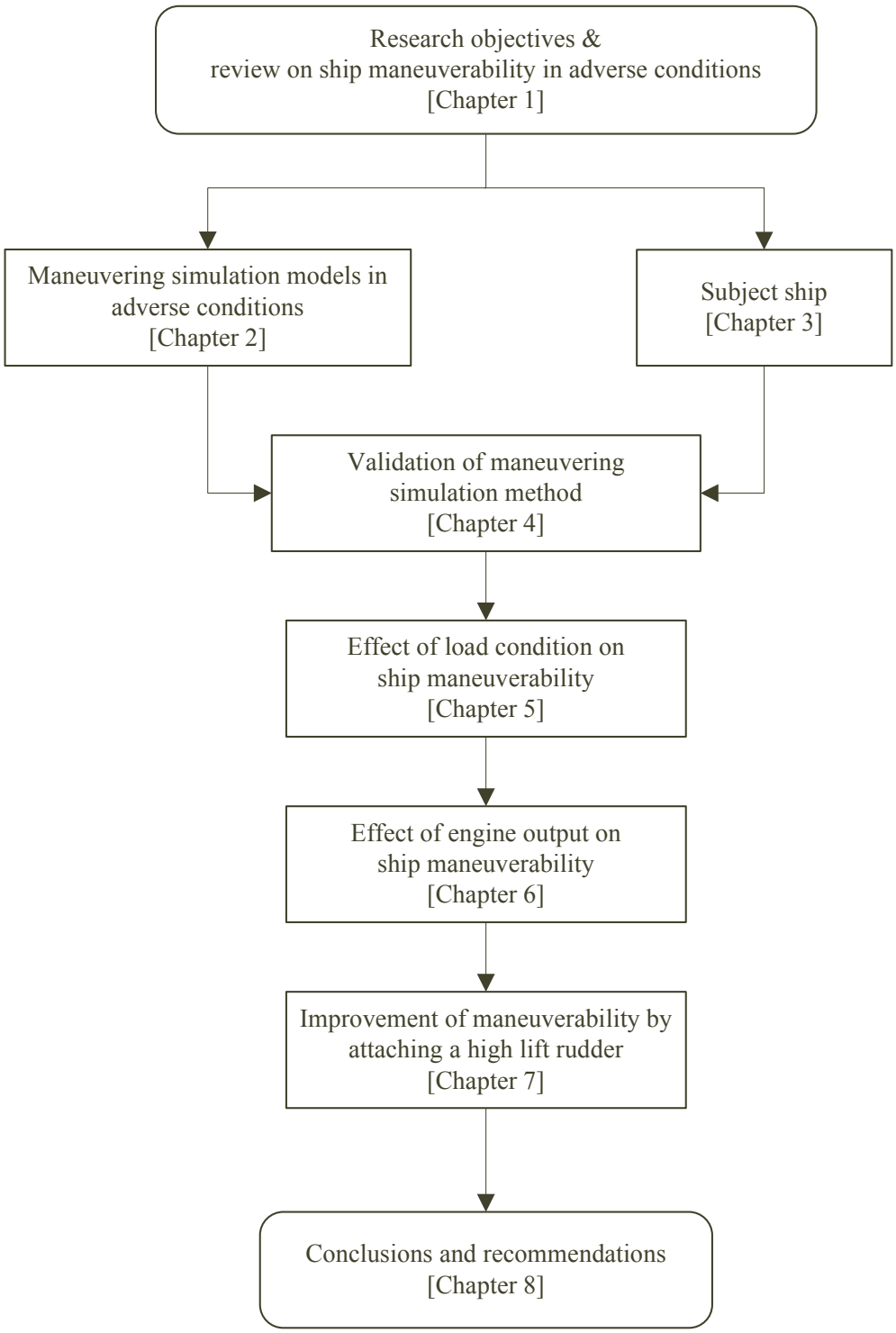

Figure 1.1: Thesis outline

Chapter 2

A Simulation Method for Ship Maneuvering in Wind and Waves

As reviewed in Chapter 1, a mathematical model for maneuvering motion in adverse weather conditions is required, then both wind and waves effects should be incorporated to the motion equations of maneuvers into the MMG simulation model [37], with the following assumptions:

- Ship is a rigid body.
- Ship speed is not fast that wave-making effect can be neglected.
- Hydrodynamic forces acting on the ship are treated quasi-steadily.
- Lateral velocity component is small compared with longitudinal velocity component.
- Roll coupling effect on maneuvering is negligible since metacentric height GM is sufficiently large.

To analyze the ship maneuvering performance in adverse conditions, it is necessary to develop a mathematical model associated with the maneuvering motions involve wind and waves. This chapter describes maneuvering simulations models, and those will be used to simulate the maneuvering of a VLCC with a single propeller and rudder. Section 2.1 introduces the applied

coordinate systems. Section 2.2 describes the motion equations to be solved for maneuvering motions of the ship. In this section, describes the equations of hydrodynamic forces acting on ship hull, the hydrodynamic forces due to the propeller, and hydrodynamic forces by the rudder are described. Section 2.3 expresses the prediction of the wave-induced steady forces in irregular waves. Section 2.4 expresses the wind forces acting on the ship. Section 2.5 presents the torque limit model. In the end, the conclusions of this chapter are summarized in Section 2.6.

2.1 Coordinate system

Fig. 2.1 shows the coordinate systems used in the study. Specifically, the space-fixed coordinate system is denoted as $o_0 - x_0 y_0 z_0$ in which the $x_0 - y_0$ plane coincides with the still water surface, and the z_0-axis points vertically downward. The moving ship-fixed coordinate system is denoted as $o - xyz$ in which o is considered on the midship of the ship, and x, y, and z-axes point toward the ship's bow, i.e., toward the starboard and vertically downward directions, respectively.

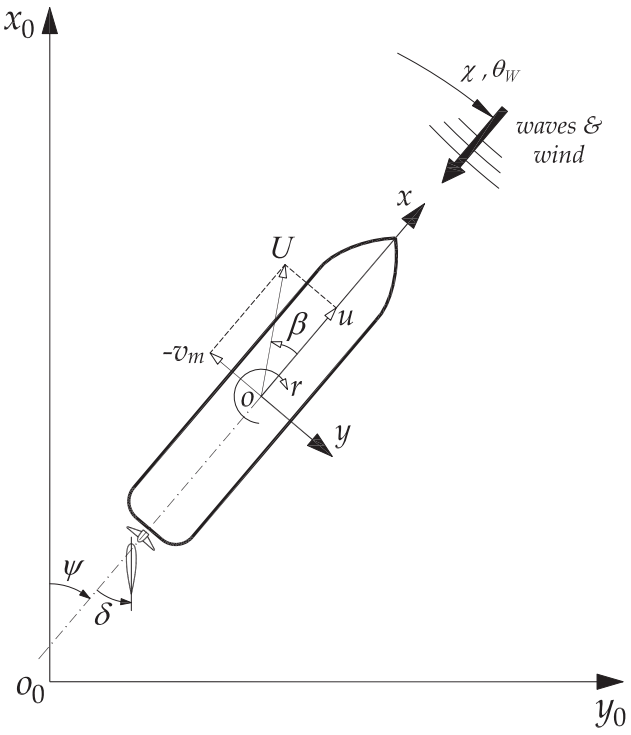

Figure 2.1: Coordinate systems

The heading angle ψ is defined as the angle between the x_0 and x-axes. Furthermore, δ denotes the rudder angle, and r denotes the yaw rate. Additionally, u and v_m denotes the velocity components in x and y directions, respectively. The drift angle at the midship position is defined as $\beta(= \tan^{-1}(-v_m/u))$. The total velocity corresponds to $U(= \sqrt{u^2 + v_m^2})$. The main wave propagation direction is denoted as χ as shown in Fig. 2.1. Subsequently, relative wave direction χ_0 is defined as $\chi_0 \equiv \chi - \psi$. The head wave, the beam wave, and the following wave of the ship are defined as $\chi_0 = 0°$, $\chi_0 = 90°$, and $\chi_0 = 180°$, respectively. The wind direction θ_W is assumed as same as the wave direction χ.

2.2 Motion equations

The motion equations with respect to surge, sway, and yaw are expressed as follows [37]:

$$\left.\begin{aligned} (m + m_x)\dot{u} - (m + m_y)v_m r - x_G m r^2 &= X \\ (m + m_y)\dot{v}_m + (m + m_x)ur + x_G m\dot{r} &= Y \\ (I_{zG} + x_G^2 m + J_z)\dot{r} + x_G m\dot{v}_m + x_G mur &= N \end{aligned}\right\} \tag{2.1}$$

where m denotes ship's mass, I_{zG} denotes the moment of inertia around center of gravity, m_x and m_y denote the added masses of x-axis direction and y-axis direction, respectively, and J_z denotes the added moment of inertia. Eq.(2.1) denotes the equations of motion to be solved. The unknown variables corresponded to u, v_m, and r. Additionally, X, Y, and N in the right hand side of Eq.(2.1) denote the surge force, lateral force, and yaw moment around midship except added mass components, respectively, and are expressed as follows:

$$\left.\begin{aligned} X &= X_H + X_R + X_P + X_W + X_A \\ Y &= Y_H + Y_R + Y_W + Y_A \\ N &= N_H + N_R + N_W + N_A \end{aligned}\right\} \tag{2.2}$$

Here, subscripts H, R, and P denote hull, rudder, and propeller, respectively. The forces with subscripts H, R, and P could be predicted by using the MMG standard method [37]. The

subscript W denotes the wave-induced steady forces in irregular waves, and A denotes the wind forces. By solving the equation of motion, i.e., Eq.(2.1), it was numerically possible to determine the maneuvering motions of the ship.

2.2.1 Hull forces

Surge force (X_H), lateral force (Y_H) and yaw moment (N_H) around midship acting on ship hull can be express as:

$$\left.\begin{aligned} X_H &= (1/2)\rho LdU^2 X'_H(v'_m, r') \\ Y_H &= (1/2)\rho LdU^2 Y'_H(v'_m, r') \\ N_H &= (1/2)\rho L^2 dU^2 N'_H(v'_m, r') \end{aligned}\right\} \tag{2.3}$$

where ρ is water density, L is ship length, d is ship draft, and U is ship speed, v'_m denotes non-dimensionalized lateral velocity ($v'_m \equiv v_m/U$), and r' denotes non-dimensionalized yaw rate ($r' \equiv rL/U$). X'_H, Y'_H and N'_H are expressed as follows:

$$\left.\begin{aligned} X'_H(v'_m, r') &= -R'_0 + X'_{vv}v'^2_m + X'_{vr}v'_m r' + X'_{rr}r'^2 + X'_{vvvv}v'^4_m \\ Y'_H(v'_m, r') &= Y'_v v'_m + Y'_r r' + Y'_{vvv}v'^3_m + Y'_{vvr}v'^2_m r' + Y'_{vrr}v'_m r'^2 + Y'_{rrr}r'^3 \\ N'_H(v'_m, r') &= N'_v v'_m + N'_r r' + N'_{vvv}v'^3_m + N'_{vvr}v'^2_m r' + N'_{vrr}v'_m r'^2 + N'_{rrr}r'^3 \end{aligned}\right\} \tag{2.4}$$

where X'_{vv}, X'_{vr}, X'_{rr}, X'_{vvvv}, Y'_v, Y'_r, Y'_{vvv}, Y'_{vvr}, Y'_{vrr}, Y'_{rrr}, N'_v, N'_r, N'_{vvv}, N'_{vvr}, N'_{vrr} and N'_{rrr} are the hydrodynamic derivatives on maneuvering.

2.2.2 Hydrodynamic forces due to propeller

Surge force due to propeller (X_P) is expressed as follows:

$$X_P = (1 - t_P)T \tag{2.5}$$

t_P is the thrust deduction factor. The thrust T and the torque Q are generated by propeller are written as

$$\left.\begin{aligned} T &= \rho n_P^2 D_P^4 K_T(J_P) \\ Q &= \rho n_P^2 D_P^5 K_Q(J_P) \end{aligned}\right\} \tag{2.6}$$

Here, D_P is the propeller diameter. The propeller thrust open water characteristic K_T and the characteristic of propeller torque in open water K_Q are expressed by the following equation.

$$\left.\begin{aligned} K_T(J_P) &= k_2 J_P^2 + k_1 J_P + k_0 \\ K_Q(J_P) &= q_2 J_P^2 + q_1 J_P + q_0 \end{aligned}\right\} \tag{2.7}$$

Where k_2, k_1, and k_0 are coefficients representing K_T, and q_2, q_1 and q_0 are coefficients representing K_Q. K_T and K_Q are approximately expressed as 2nd polynomial function of propeller advance ratio J_P.

$$J_P = \frac{u(1-w_P)}{n_P D_P} \tag{2.8}$$

w_P in the equation is the effective wake fraction, n_P is the propeller revolution and β_P is the geometrical inflow angle to the propeller in maneuvering motions ($\beta_P \equiv \beta - x'_P r'$), x'_P is longitudinal position coordinate of the propeller and dimensionalized by L. A formula corresponds to w_P is expressed as

$$\frac{1-w_P}{1-w_{P0}} = 1 + [1 - \exp(-C_1|\beta_P|)](C_2 - 1) \tag{2.9}$$

Here, C_1 and C_2 are constants representing the characteristics of $(1-w_P)/(1-w_{P0})$.

2.2.3 Hydrodynamic forces by rudder

The hydrodynamic forces generated by the steering (X_R, Y_R, N_R) are expressed as

$$\left.\begin{aligned} X_R &= -(1-t_R)F_N \sin\delta \\ Y_R &= -(1+a_H)F_N \cos\delta \\ N_R &= -(x_R + a_H x_H)F_N \cos\delta \end{aligned}\right\} \tag{2.10}$$

Here, t_R, a_H, x_H are parameters representing the interaction between the hull and the rudder. F_N is expressed as

$$F_N = (1/2)\rho A_R U_R^2 f_\alpha \sin\alpha_R \tag{2.11}$$

Where A_R denotes rudder area and f_α denotes rudder lift gradient coefficient. The resultant inflow velocity to rudder U_R and effective inflow angle to the rudder α_R are expressed by the following equation:

$$U_R = \sqrt{u_R^2 + v_R^2} \tag{2.12}$$

$$\alpha_R = \delta - \tan^{-1}\left(\frac{v_R}{u_R}\right) \simeq \delta - \frac{v_R}{u_R} \tag{2.13}$$

u_R is longitudinal inflow velocity components to rudder, v_R is lateral inflow velocity components to rudder. v_R can be expressed as follows:

$$v_R = U\gamma_R \beta_R \tag{2.14}$$

where

$$\beta_R = \beta - \ell'_R r' \tag{2.15}$$

Here, γ_R is called the flow straightening coefficient and usually smaller than 1.0. β_R denotes the effective inflow angle to rudder. ℓ'_R is treated as an experimental constant for expressing v_R and can be obtained from the captive model test.

u_R uses the following equation,

$$u_R = \varepsilon u(1-w_P)\sqrt{\eta\left[1+\kappa\left(\sqrt{1+\frac{8K_T}{\pi J_P^2}}-1\right)\right]^2+(1-\eta)} \tag{2.16}$$

where ε means ratio of wake fraction at rudder position to that at propeller position defined by $\varepsilon = (1-w_R)/(1-w_P)$. The κ is an experimental constant. η denotes ratio of propeller diameter to rudder span ($= D_P/H_R$).

2.3 Wave-induced steady forces

The wave-induced steady forces in irregular waves (X_W, Y_W, N_W) are expressed as follows:

$$\left.\begin{aligned} X_W &= \rho g H_{1/3}^2 L\,\overline{C_{XW}}(U, T_v, \chi_0) \\ Y_W &= \rho g H_{1/3}^2 L\,\overline{C_{YW}}(T_v, \chi_0) \\ N_W &= \rho g H_{1/3}^2 L^2\,\overline{C_{NW}}(T_v, \chi_0) \end{aligned}\right\} \tag{2.17}$$

where $H_{1/3}$ denotes the significant wave height, and g denotes the gravity acceleration. The averaged wave-induced added resistance coefficient in irregular waves ($\overline{C_{XW}}$) is expressed as a function of ship speed (denoted as U), averaged wave period (denoted as T_v), and relative wave direction (denoted as χ_0). The speed effect on $\overline{C_{XW}}$ cannot be neglected. In contrast, the speed effect on the averaged wave-induced steady lateral force and yaw moment coefficients in irregular waves ($\overline{C_{YW}}$, $\overline{C_{NW}}$) is assumed as negligible [34]. Then, $\overline{C_{YW}}$ and $\overline{C_{NW}}$ are expressed as a function of T_v and χ_0. The averaged value of wave-induced steady force coefficients in irregular waves are calculated by applying the short-term prediction technique based on the

wave-induced steady force coefficients in regular waves as follows:

$$\left.\begin{aligned}
\overline{C_{XW}}(U, T_v, \chi_0) &= 2\int_{-\pi}^{\pi} G(\theta)d\theta \int_0^{\infty} C_{XW}(U, \omega, \chi_0)\frac{S_{\zeta\zeta}(\omega)}{H_{1/3}^2}d\omega \\
\overline{C_{YW}}(T_v, \chi_0) &= 2\int_{-\pi}^{\pi} G(\theta)d\theta \int_0^{\infty} C_{YW}(\omega, \chi_0)\frac{S_{\zeta\zeta}(\omega)}{H_{1/3}^2}d\omega \\
\overline{C_{NW}}(T_v, \chi_0) &= 2\int_{-\pi}^{\pi} G(\theta)d\theta \int_0^{\infty} C_{NW}(\omega, \chi_0)\frac{S_{\zeta\zeta}(\omega)}{H_{1/3}^2}d\omega
\end{aligned}\right\} \tag{2.18}$$

where $S_{\zeta\zeta}(\omega)$ denotes the wave spectrum, and $G(\theta)$ denotes the wave direction distribution function. C_{XW}, C_{YW}, and C_{NW} denote the wave-induced steady force coefficients in regular waves, and C_{XW} and C_{YW} are non-dimensionalized through the division by $\rho g h_a^2 L$ where h_a denotes amplitude of incident waves, and C_{NW} is non-dimensionalized through the division $\rho g h_a^2 L^2$. The following procedure was employed in the actual simulations: Prior to the simulations, a database of wave-induced steady force coefficients in irregular waves ($\overline{C_{XW}}$, $\overline{C_{YW}}$, $\overline{C_{NW}}$) was provided as the functions of U, T_v, and χ_0. The steady forces at the moment of the maneuvering motion were estimated in the time domain by an interpolation technique based on the database [35].

2.4 Wind forces

Based on the assumption of steady and constant wind, the surge force, lateral force, and yaw moment due to the wind (X_A, Y_A, N_A) are expressed as follows:

$$\left.\begin{aligned}
X_A &= (1/2)\rho_a A_X V_A^2 C_{XA}(\theta_A) \\
Y_A &= (1/2)\rho_a A_Y V_A^2 C_{YA}(\theta_A) \\
N_A &= (1/2)\rho_a A_Y L V_A^2 C_{NA}(\theta_A)
\end{aligned}\right\} \tag{2.19}$$

where

$$\theta_A = \tan^{-1}(v_A/u_A) \tag{2.20}$$

$$V_A = \sqrt{u_A^2 + v_A^2} \tag{2.21}$$

$$u_A = u + U_W \cos(\theta_W - \psi) \tag{2.22}$$

$$v_A = v_m + U_W \sin(\theta_W - \psi) \tag{2.23}$$

Here, ρ_a denotes air density, V_A denotes the relative wind speed, U_W denotes the absolute wind speed, θ_A denotes the relative wind direction, and θ_W denotes the absolute wind direction. C_{XA}, C_{YA}, and C_{NA} denote the aerodynamic force coefficients expressed as a function of the relative wind direction (denoted by θ_A).

2.5 Torque limit line

A large load could act on the main engine in a severe sea. In order to avoid an undesirable situation, the propeller revolution is controlled not to exceed a propeller torque limit. In accordance with a previous study Ref.[30], the limit line is expressed as follows:

$$P_B = \min(P_{BMEP}, P_{BOLP}) \tag{2.24}$$

where P_B denotes the main engine output. Averaged effective pressure limit P_{BMEP} is expressed as follows:

$$P_{BMEP} = MCR\frac{N_E}{N_{MCR}} \tag{2.25}$$

where N_E denotes the engine revolution. Overload protection limit P_{BOLP} is expressed as follows:

$$P_{BOLP} = \alpha^{1-\Gamma} MCR\left(\frac{N_E}{N_{MCR}}\right)^{\Gamma} \tag{2.26}$$

Here, $\alpha = 0.967$ and $\Gamma = 2$ are used.

2.6 Concluding remarks

In this chapter, a model presented was based on the MMG maneuvering simulation method [37]. To observe the maneuvering performance of the ship in adverse condition, both wind and waves effects have been included in the maneuvering motion equations. Further investigations and experiments are required to confirm the accuracy of the simulation method (Chapter 4).

Moreover, research on the ship maneuverability in waves is suggested. Through the further simulation study, it is expected that the present model can roughly capture the maneuvering performance of the reference ship.

Chapter 3

Studied Ship

As explained in Chapter 1, a VLCC tanker will be used as a subject ship to investigate maneuvering performance in still water and adverse conditions. This chapter describes a ship particulars used in this study with a single propeller and a single rudder. Section 3.1 describes ship main dimensions and hullform. Section 3.2 presents the arrangement of superstructure and wind exposed area. Section 3.3 describes rudder and propeller information.

3.1 Ship Particulars

In this study, a VLCC titled KVLCC2 [27] in which hull form data was previously published is used as the target ship. Table 3.1 shows the principal particulars of the ship. The scale ratio between the actual ship and model is 1/110. In the table, L denotes length between perpendiculars, L_{wl} denotes length of the waterline, B denotes breadth, D denotes depth, d denotes draft, ∇ denotes displacement volume, S denotes wetted surface area without a rudder and a horn, x_G denotes longitudinal position of the center of gravity (fore position from the midship is positive), and C_b denotes the block coefficient. The load condition involved a full load even keel. Fig. 3.1 illustrates the body plan of KVLCC2, and a picture of the KVLCC2 model used for the tank test as shown in Fig. 3.2.

Table 3.1: Principal particulars of a target ship (KVLCC2)

symbol	Ship	Model
L (m)	320.0	2.9091
L_{wl} (m)	325.5	2.9591
B (m)	58.0	0.5273
D (m)	30.0	0.2364
d (m)	20.80	0.1891
∇ (m^3)	312,622	0.2349
S (m^2)	27,467	2.2475
x_G (m)	11.2	0.1012
C_b	0.81	0.81

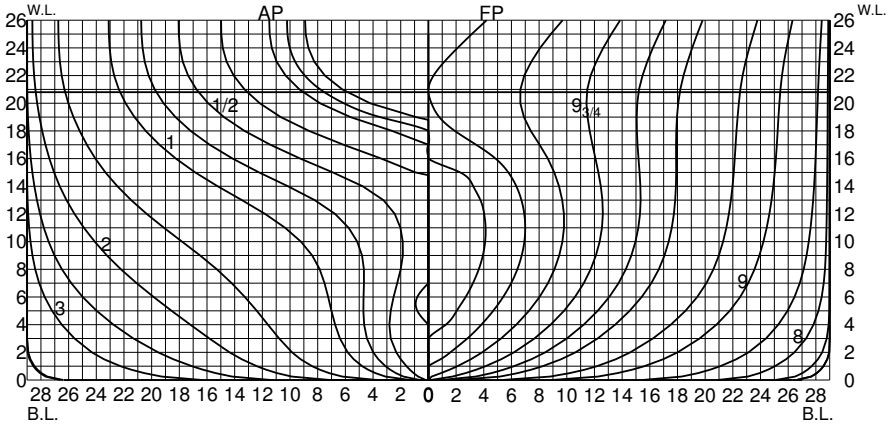

Figure 3.1: Body plan of KVLCC2

Figure 3.2: KVLCC2 model

3.2 Wind exposed area

Fig. 3.3 shows side and front views including the super-structure of the ship used in the study. The configuration and arrangement of the super-structure were estimated based on an existing VLCC tanker with a similar size since an actual fullscale ship corresponding to KVLCC2 was not available. The front wind pressure area A_X corresponds to 1,161 m^2, and the side wind pressure area corresponds to A_Y 4,258 m^2.

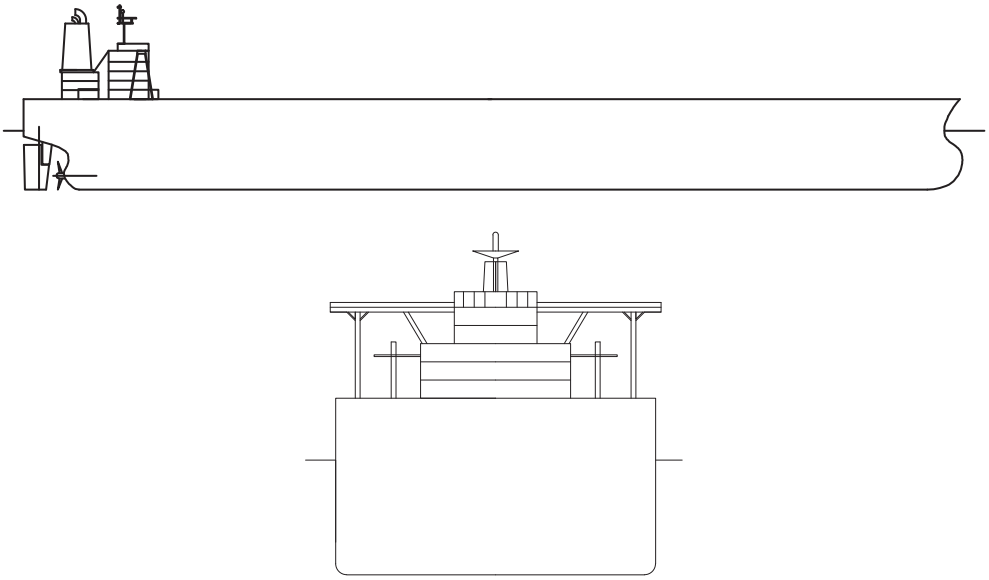

Figure 3.3: Side and front views of a VLCC

3.3 Rudder and propeller

The ship possessed a Mariner rudder (NACA0018) as shown in Fig. 3.4. Table 3.2 shows the principal particulars of the rudder. In the table, H_R denotes span of the rudder, B_R denotes the averaged chord of the rudder including horn, A_R denotes the rudder area of the movable part, and Λ denotes the aspect ratio. η denotes the ratio of propeller diameter and rudder height. $A_R/(Ld)$ denotes the rudder area ratio. f_α denotes the Rudder lift gradient coefficient.

Table 3.2: Principal particulars of the rudder

Symbol	**Fullscale**	**Model**
H_R (m)	15.80	0.14
B_R (m)	8.65	0.08
A_R (m^2)	112.5	0.0093
Λ	1.827	1.827
η	1.827	0.624
$A_R/(Ld)$	1/59.15	1/59.15
f_α	2.747	2.747

Table 3.3 shows the principal particulars of the engine and propeller. In the table, D_P denotes the propeller diameter, p denotes the propeller pitch ratio, A_e/A_d denotes the expanded area ratio, Z denotes the number of blades. k_0, k_1, and k_2 denotes the propeller thrust characteristics. q_0, q_1, and q_2 denotes the propeller torque characteristics. P_E denotes the engine power at

(a) Rudder model

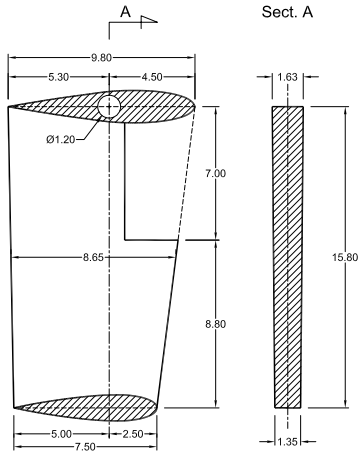

(b) Rudder profiles, units in meter

Figure 3.4: KVLCC2 Rudder

Maximum Continuous Rating (MCR), N_E denotes the engine revolution at MCR. Fig. 3.5 shows the propeller model of KVLCC2.

Table 3.3: Principal particulars of propeller

Symbol	**Fullscale**	**Model**
D_P (m)	9.86	0.0896
p	0.673	0.673
A_e/A_d	0.384	0.384
Z	4	4
k_0	0.2653	0.2653
k_1	-0.1568	-0.1568
k_2	-0.2595	-0.2595
q_0	0.0244	0.0244
q_1	0.00025	0.00025
q_2	-0.03638	-0.03638
P_E (kW)	25,600	
N_E (rpm)	76.0	

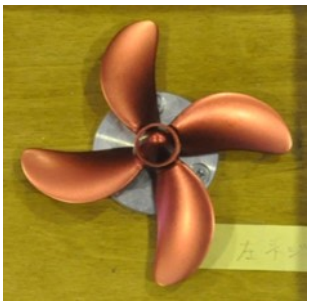

Figure 3.5: Propeller model (KVLCC2)

Chapter 4

Evaluation of the simulation method

In this chapter, maneuvering simulations are performed for ships moving in irregular waves. MMG standard method [37] as explained in Chapter 2 is used as the simulation method. As the wave effect, 2nd order wave induced steady forces (wave drift forces) acting on the ship hull as mentioned in Chapter 2.3 are considered in the simulations. To evaluate ship maneuvering simulation method, a KVLCC2 model as described in Chapter 3 is used for free-running model tests. Turning test and zig-zag maneuver test were carried out in both still water and irregular waves with various speed conditions. Then, the simulation method and the measured results are compared in the same condition. This chapter describes the evaluation of maneuvering simulation method to be used in this study. Section 4.1 outlines the free-running model test. Section 4.2 presents the comparison results of turning and zig-zag maneuvers between experiment and simulation in both still water and irregular waves. Finally, section 4.3 concludes this chapter.

4.1 Outline of free-running model test

The free-running model tests were conducted in a square tank of National Research Institute of Fisheries Engineering (NRIFE), Japan (Tank length: 60m, width: 25m, depth: 3.2m) as shown in Fig. 4.1. In the square tank, short-crested irregular waves can be generated.

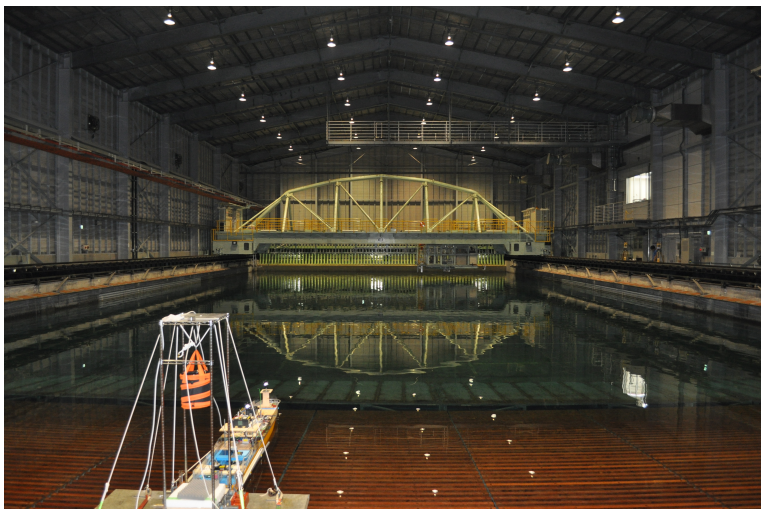

Figure 4.1: National Research Institute of Fisheries Engineering

4.1.1 Test setup and measurements

Turning test with a rudder angle δ $\pm 35°$ and time histories of rudder angle δ and heading angle ψ in $\pm 10°/\pm 10°$ zig-zag maneuver tests are performed in still water and irregular waves. In the tests, the approach speed U_0 and propeller revolution n_P are mentioned in Table 4.1.

Table 4.1: Ship speed and propeller revolution in the test

	still water			irregular waves		
U_0 fullscale (kn)	15.5	10.0	5.0	13.0	10.0	5.0
U_0 model (m/s)	0.760	0.491	0.245	0.636	0.491	0.245
n_P model (rps)	17.2	11.6	6.0	17.2	14.0	8.3

The variation of ship speed in Table 4.1 is intended to observe the speed effect on the maneuvering motions. we made the propeller revolution same in still water and irregular waves. Then, the approach speed U_0 decrease 13.0kn in irregular waves from the previous approach speed 15.5kn in still water. In the medium and low speed cases (U_0=10.0kn and 5.0kn), the approach speed same in both still water and irregular waves. The radius of gyration was set to be 0.25L. GM was 120mm. Steering rate was $19.0°/s$ for fullscale.

The significant wave height $H_{1/3}$ and averaged wave period T_v in the tank tests corresponding to Sea State 6 as mentioned in Table 4.2. ITTC spectrum was used as the wave spectrum $S_{\zeta\zeta}$. The $\cos^2$ function was used as the wave direction distribution function $G(\theta)$. Head wave

Table 4.2: Wave condition in the tank test

	Fullscale	Model
$H_{1/3}$ (m)	6.0	0.0545
T_v (s)	9.46	0.902

direction ($\chi = 0°$) was selected in the ship approach condition as the main wave direction. Total Station system measures the ship positions of surge, sway and heave. The Total Station can truck the ship model automatically from the square tank side and measure the 3D position of a prism equipped to the midship of the model. At the same time, roll, pitch and yaw were measured by a three axes gyro installed to the model. The ship model was launched with the certain approach speed by a catapult set at the beach of the tank. After reaching the target model speed (U_0) and the target heading ($\psi = 0°$) by an autopilot, the model was steered by a radio controller for turning or zig-zag maneuvers.

4.1.2 Test reliability

The repeat tests in irregular waves are carried out to confirm the test reliability during five times under the same conditions. The repeat test result of $\delta = \pm 35°$ turning trajectories in irregular waves is shown in Fig. 4.2.

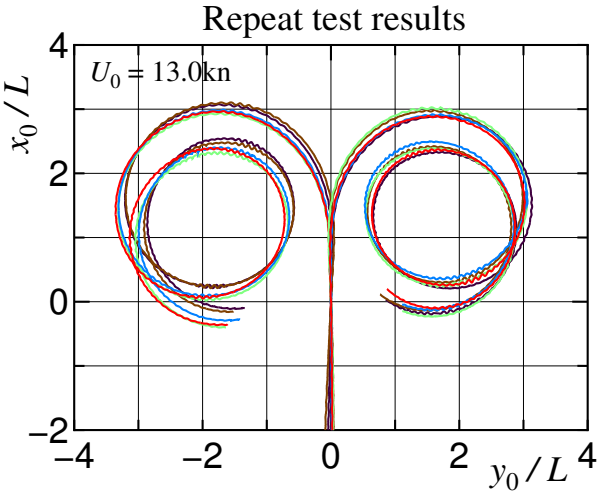

Figure 4.2: Repeat test results: comparison of turning trajectories in irregular waves ($\delta = \pm 35°$)

The comparison of turning indices (A_D, D_T) in irregular waves as mentioned in Table 4.3. The difference is not significant in the measured turning performances and the repeatability.

Table 4.3: Repeat test results: comparison of turning indices in irregular waves (U_0=13.0kn)

	$\delta = -35°$		$\delta = 35°$	
Repeat No.	A_D/L	D_T/L	A_D/L	D_T/L
1	2.82	3.06	2.97	3.13
2	2.92	2.91	2.96	3.19
3	2.92	3.04	2.92	3.19
4	2.85	2.97	2.94	3.19
5	2.80	2.97	2.94	3.23
Averaged	2.86	2.99	2.95	3.19
Standard deviation	0.050	0.054	0.017	0.032

4.2 Comparison results of simulation and experiment

4.2.1 Hydrodynamic force coefficients

Table 5.2 shows the hydrodynamic force coefficients used in the maneuvering simulations. These are the same as the coefficients shown in Ref.[37] except w_{P0}.

Table 4.4: Hydrodynamic force coefficients used in the simulations

Symbol	**values**	**Symbol**	**values**
X'_{vv}	-0.04	m'_x	0.022
X'_{vr}	0.002	m'_y	0.223
X'_{rr}	0.011	J'_z	0.011
X'_{vvvv}	0.771	t_P	0.2
Y'_v	-0.315	t_R	0.387
Y'_r	0.083	a_H	0.312
Y'_{vvv}	-1.607	x'_H	-0.464
Y'_{vvr}	0.379	C_1	2.0
Y'_{vrr}	-0.391	$C_2(\beta_P < 0)$	1.1
Y'_{rrr}	0.008	$C_2(\beta_P > 0)$	1.4
N'_v	-0.137	$\gamma_R(\beta_R < 0)$	0.395
N'_r	-0.049	$\gamma_R(\beta_R > 0)$	0.640
N'_{vvv}	-0.030	ℓ'_R	-0.71
N'_{vvr}	-0.294	ε	1.09
N'_{vrr}	0.055	κ	0.50
N'_{rrr}	-0.013	w_{P0}	0.42

4.2.2 Turning in still water

The comparison of turning trajectories with rudder angle δ $\pm 35°$ in still water are shown in Fig. 4.3. The turning indices (A_D and D_T) both of experiment and calculation are presented in Table 4.5. From those results, it is confirmed that the present method can capture the tendency A_D and D_T become small with decreasing the approach speed, although the simulation results are slightly larger than the experimental values in all cases.

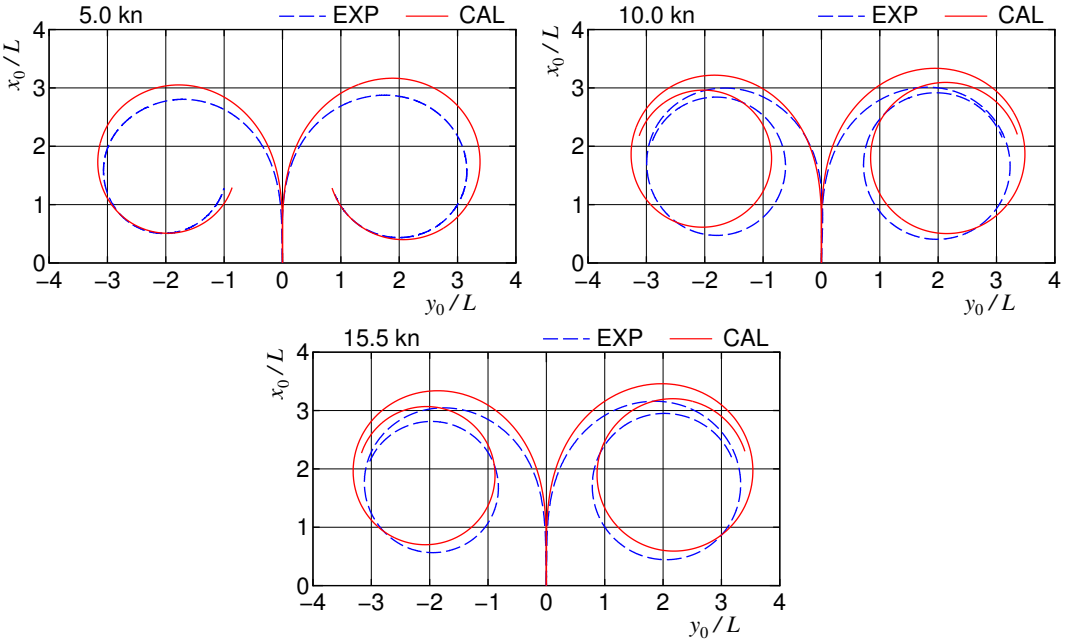

Figure 4.3: Comparison of turning trajectories in still water ($\delta = \pm 35°$)

Table 4.5: A comparison of turning indices in still water

	$\delta = 35°$		$\delta = -35°$	
	A_D/L	D_T/L	A_D/L	D_T/L
EXP (5.0kn)	2.79	3.08	2.73	2.99
CAL (5.0kn)	3.10	3.32	2.98	3.10
EXP (10.0kn)	2.93	3.15	2.92	2.92
CAL (10.0kn)	3.27	3.42	3.15	3.20
EXP (15.5kn)	3.08	3.25	2.97	3.10
CAL (15.5kn)	3.39	3.47	3.27	3.24

4.2.3 Zig-zag maneuvers in still water

The time histories of heading angle ψ and rudder angle δ for 10/10 and $-10/-10$ zig-zag maneuvers in still water are presented in Fig. 4.4, and the comparison of overshoot angle

(OSA) mentioned in Table 4.6. The present simulations agree well with the measured time history changes of ψ and δ. The captured tendencies in the present method are OSA decreases with decreasing the approach speed. This is due to the increase of relative steering rate for low ship speed. The present method has a sufficient accuracy in the practical point of view.

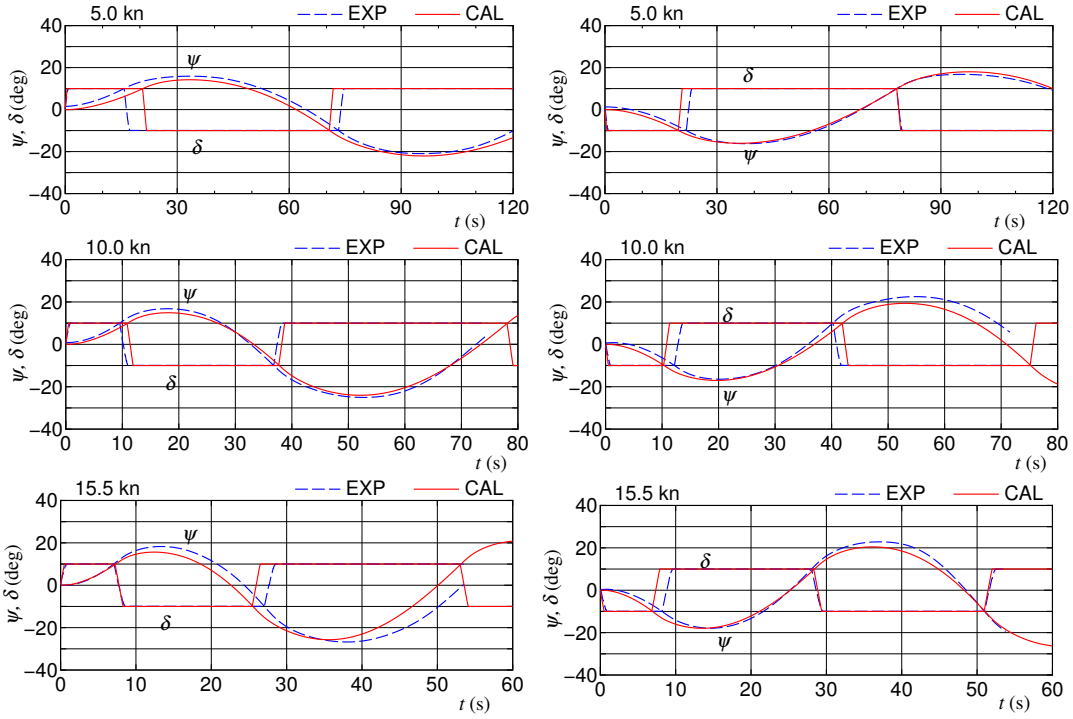

Figure 4.4: Comparison of time histories of the heading angle (ψ) and rudder angle (δ) in still water (left: $10°/10°$ zig-zag, right: $-10°/-10°$ zig-zag)

Table 4.6: A comparison of overshoot angle in still water

	10/10 zig-zag		-10/-10 zig-zag	
	1st OSA (°)	2nd OSA (°)	1st OSA (°)	2nd OSA (°)
EXP (5.0kn)	5.3	10.6	5.8	6.3
CAL (5.0kn)	4.2	12.1	6.1	8.0
EXP (10.0kn)	6.7	14.8	6.4	12.4
CAL (10.0kn)	4.9	14.0	7.0	9.3
EXP (15.5kn)	8.2	16.7	7.9	12.8
CAL (15.5kn)	5.6	15.7	8.0	10.5

4.2.4 Data related to wave-induced steady forces

A theoretical method based on the potential theory is used to predict the wave-induced steady force coefficients in regular waves, i.e., C_{XW}, C_{YW} and C_{NW}. In zero speed case, C_{XW}, C_{YW}

and C_{NW} are predicted by a 3D panel method [18]. A method based on strip theory [32] is used to consider the speed effect on the added resistance (denoted C_{XW}). In the framework of the strip theory, Maruo's far field theory [23] was applied for the added resistance prediction with the empirical correction of the added resistance in short wave length referring proposed by Tsujimoto et al. [30]. The averaged wave-induced steady force coefficients in irregular waves, $\overline{C_{XW}}$, $\overline{C_{YW}}$ and $\overline{C_{NW}}$ can be obtained by the short-term prediction based on C_{XW}, C_{YW} and C_{NW} in Eq.(2.18). Fig. 4.5 shows $\overline{C_{XW}}$ with different Froude numbers, F_n=0.15 and 0.0, and $\overline{C_{YW}}$ and $\overline{C_{NW}}$ for KVLCC2 model. In the figure, $\chi = 0°$ means heading waves, $\chi = 0°$ the beam waves and $\chi = 0°$ the following waves when the ship advances to the direction of $\psi = 0°$. The database is made based on the results of $\overline{C_{XW}}$, $\overline{C_{YW}}$ and $\overline{C_{NW}}$ for the interpolation in the maneuvering simulations.

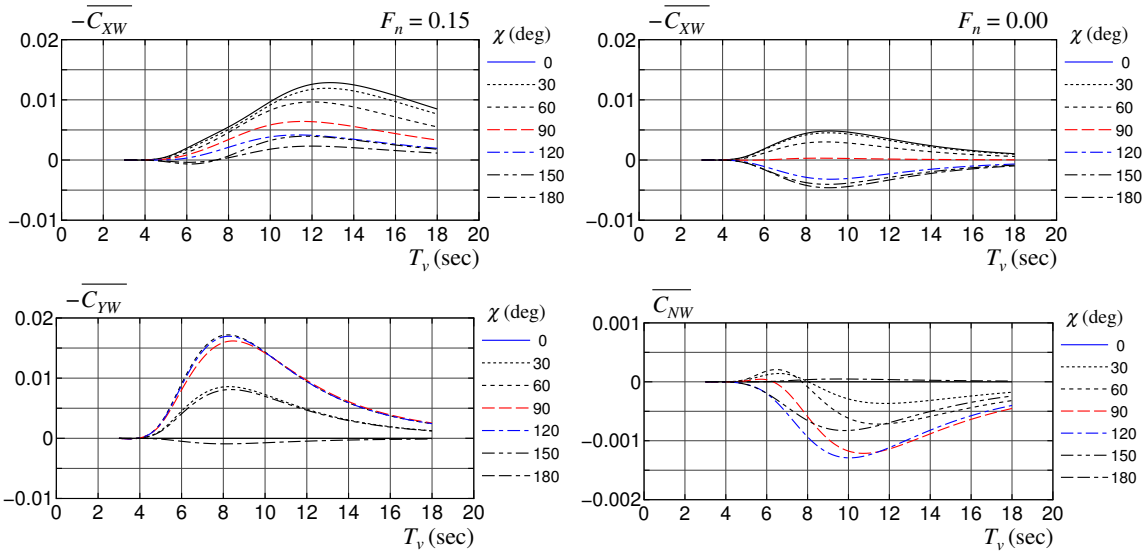

Figure 4.5: Averaged wave-induced steady force coefficients in irregular waves

4.2.5 Turning in waves

The comparisons of turning trajectories with $\delta = -35°$ and $35°$ in irregular waves are shown in Fig. 4.6. In U_0=13.0kn, the simulated trajectory agrees well with the experiment. However, the difference between simulation and experiment becomes large with decreasing the approach speed. Subsequently, the ship drifting amount becomes large with decreasing the approach speed since the effect of the wave-induced steady forces becomes relatively large for the slow ship even though the wave condition is the same. The ship drifting direction appears the

direction to the coordinate $(x_0/L,\ y_0/L)$=(-1,0) for three approach speeds, and is different from the wave direction. The turning trajectories in irregular waves and the wave effect are captured roughly with the present method, although the accuracy of simulation results are worse with decreasing the approach speed. In addition to the usual A_D and D_T, also we

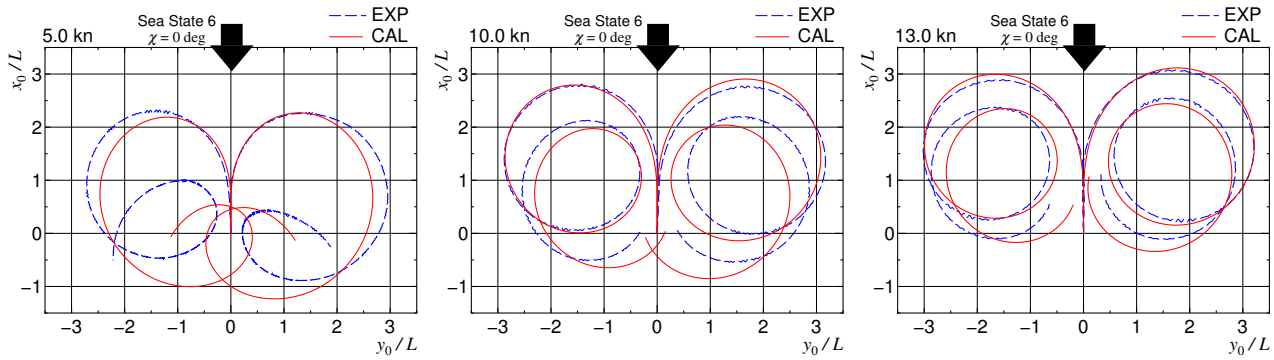

Figure 4.6: Comparison of turning trajectories in irregular waves ($\delta = \pm 35°$)

defined new turning indices in waves A_{D2} and D_{T2} as follows: A_{D2} is the advance when the heading angle reaches 450(=90+360)deg, and D_{T2} the tactical diameter when the heading angle reaches 540(=180+360)deg as shown in Fig. 4.7. Note that A_{D1} and D_{T1} are completely the same as the usual advance A_D and the tactical diameter D_T. The comparison of A_{D1}, D_{T1}, A_{D2} and D_{T2}. A_{D2} becomes small with decreasing the approach speed since the ship drifts due to waves as shown in Fig. 4.8. D_{T2} also becomes small with decreasing the approach speed and the ship drifts laterally toward the position of $(x_0/L,\ y_0/L)$=(-1,0). The simulated results agree with the experimental results roughly.

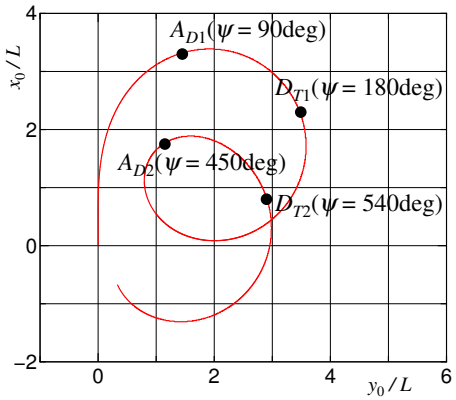

Figure 4.7: Definition of advance and tactical diameter

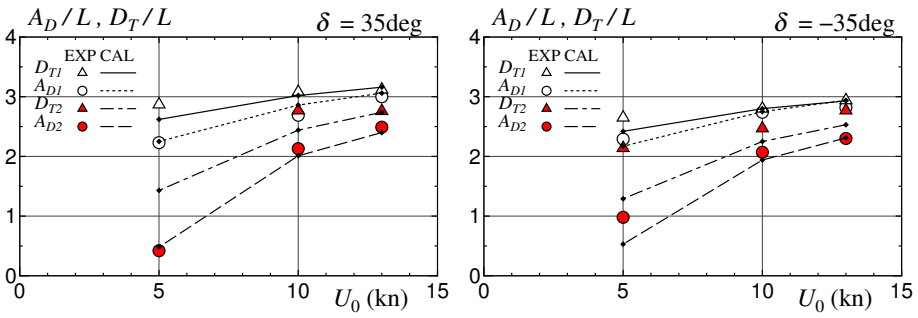

Figure 4.8: Comparison of turning trajectories in irregular waves ($\delta = \pm 35°$)

4.2.6 Zig-zag maneuvers in waves

The comparisons of time histories of ψ and δ for 10/10 and $-10/-10$ zig-zag maneuvers in irregular waves are shown in Fig. 4.9.

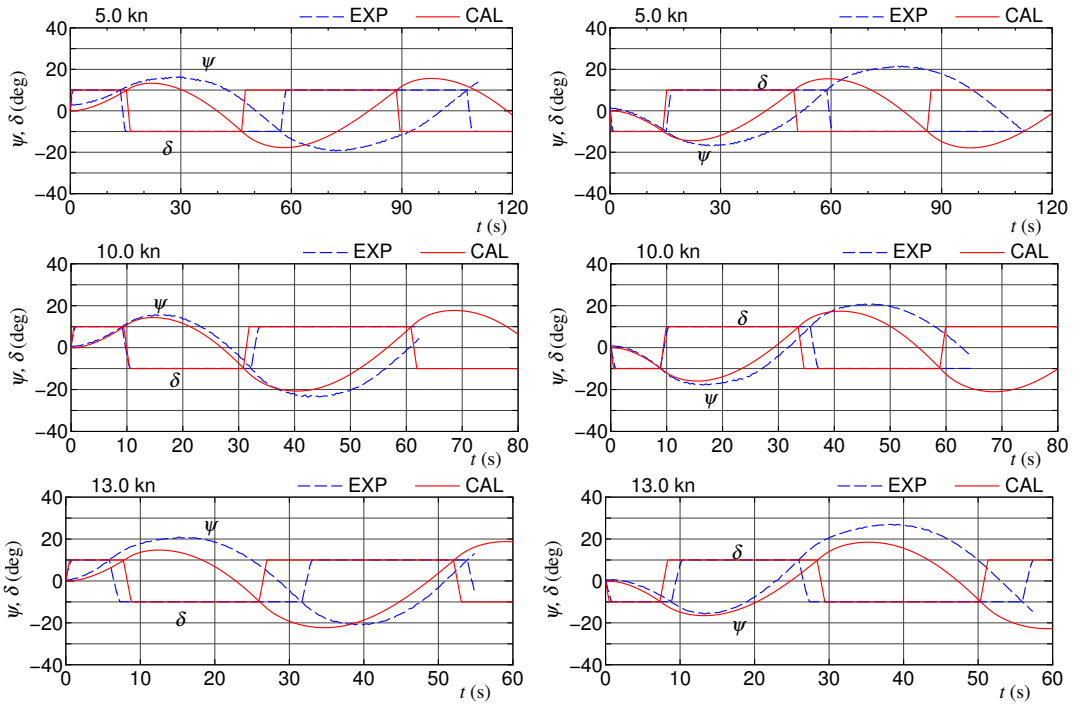

Figure 4.9: Comparison of time histories of the heading angle (ψ) and rudder angle (δ) in still water (left: $10°/10°$ zig-zag, right: $-10°/-10°$ zig-zag)

The comparison of overshoot angles (OSA) in irregular waves is shown in Table 4.7. The difference between simulation and experiment becomes large compared with the results in still water. Steering timing in the simulations is different from that in the experiments. This is due to the poor estimation accuracy of the added resistance in waves. OSAs in irregular waves are

the same order of magnitude of OSAs in still water. We see that the course stability in waves does not change so much for $\chi = 0°$ case. However, steering timing is different in still water and irregular waves for cases of U_0=10kn and 5kn. This may be caused by the effect of the propeller load increase in irregular waves for keeping the same approach speed.

Table 4.7: A comparison of overshoot angle in still water

	10/10 zig-zag		-10/-10 zig-zag	
	1st OSA (°)	2nd OSA (°)	1st OSA (°)	2nd OSA (°)
EXP (5.0kn)	6.1	9.3	6.7	11.4
CAL (5.0kn)	3.3	7.8	4.4	5.5
EXP (10.0kn)	5.6	13.3	7.8	10.8
CAL (10.0kn)	4.3	10.7	6.0	7.4
EXP (13.0kn)	10.9	10.9	5.6	15.8
CAL (13.0kn)	4.7	12.3	6.6	8.5

4.3 Conclusions

This chapter presents a maneuvering simulation method in irregular waves. The maneuvering simulation method was based on the MMG model as explained in Chapter 2. The present method is evaluated by the simulations on turning and zig-zag maneuvers in irregular waves using a KVLCC2 model, and the simulated results are compared with the model test results. Chapter 2 partly answers the first question in Section 1.3;

What are the practical simulation models to evaluate the ship maneuvers in adverse weather conditions?

From the comparison results, it was confirmed that the present method can capture the maneuvering motions in irregular waves with the sufficient accuracy for practical purposes although it still needs improvement. Furthermore, based on the present method, studies on the ship maneuvering in adverse weather conditions can be performed using a large tanker in fullscale.

Chapter 5

Effect of Load Condition on Ship Maneuverability

Chapter 1 has discussed the importance of loading conditions effects on ship maneuverability. Subsequently, Chapter 2 introduced a maneuvering simulation method based on MMG model. For the simulations, KVLCC2 is selected as a reference ship which has been presented in Chapter 3. Next in Chapter 4, a free running model test was carried out and the maneuvering simulation method was evaluated. Since the loading conditions influence the ship maneuverability, this chapter further discusses its effect on maneuvering motions such as turning and zig-zag maneuvers in both still water and adverse weather conditions. Section 5.1 provides some data related to the loading conditions used in this study. Section 5.2 outlines the simulation procedures with respect to the load conditions. Section 5.3 simulates turning and zig-zag maneuvers in still water, and uses the criterion to measure a difference of course stability due to the load conditions. Section 5.4 analyses the performance of ship maneuvering in wind and waves, and discusses the results of the simulations from a navigation safety point of view. In the end, Section 5.5 remarks the conclusions of this chapter.

5.1 Ship particulars in loading conditions

The VLCC in full loaded even keel condition is referred to as DF, and the normal ballast in trim by the stern condition is referred to as NB [47]. Table 5.1 shows the principal particulars of the ship in two loading conditions (DF and NB). A ship in DF is same as the ship particulars were defined in Section 3.1 and 3.2. The rudder, main engine, and propeller are same as previously presented in Section 3.3. In the table, d_a denotes the draft at after perpendicular, *df* denotes the draft at fore perpendicular of the ship.

Table 5.1: Principal particulars of KVLCC2 tanker

items	**value**	
L (m)	320.0	
B (m)	58.0	
D (m)	30.0	
C_b	0.81 (in DF)	
Load Condition	**DF**	**NB**
d_a (m)	20.80	15.12
d_f (m)	20.80	11.28
d (m)	20.80	13.2
∇ (m^3)	312,622	182,439
S (m^2)	27,467	21,700
x_G (m)	11.2	8.873
A_X (m^2)	1,161	1,712
A_Y (m^2)	4,258	6.724

5.2 Outline of simulations

Maneuvering simulations are carried out in DF and NB. The following parameters and treatments are as follows:

- The engine and propeller used in this study as described in Table 3.3. The torque limit lines for DF and NB are obtained by the torque limit model as previously mentioned in Section 2.5. Fig. 5.1 shows the torque limit lines for two loading conditions (DF and NB).
- Hydrodynamic force coefficients were obtained from the model experiment based on MMG

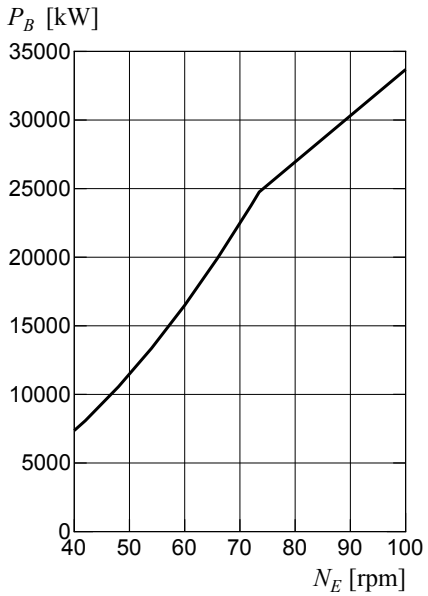

Figure 5.1: Torque limit lines

model procedures [37]. Table 5.2 shows the hydrodynamic force coefficients used in the simulations. The notations as shown in Table 5.2 follow to the definition in Ref. [37].

Table 5.2: Hydrodynamic force coefficients used in simulations

Symbol	**DF**	**NB**	**Symbol**	**DF**	**NB**
X'_{vv}	-0.0397	-0.0470	m'_x	0.0189	0.0111
X'_{vr}	0.5181	0.4409	m'_y	0.2405	0.1429
X'_{rr}	0.0211	0.0320	J'_z	0.0135	0.0076
X'_{vvvv}	0.7707	0.3669	t_P	0.149	0.200
Y'_v	-0.3145	-0.3016	t_R	0.387	0.306
Y'_R	-0.2326	-0.2047	a_H	0.312	0.292
Y'_{vvv}	-1.6074	-1.0433	x'_H	-0.464	-0.412
Y'_{vvr}	0.3794	0.6101	C_1	8.0	6.0
Y'_{vrr}	-0.3907	-0.3536	$C_2(\beta_P > 0)$	1.4	1.45
Y'_{rrr}	0.0078	0.0249	$C_2(\beta_P < 0)$	1.1	1.30
N'_v	-0.1366	-0.0655	$\gamma_R(\beta_R < 0)$	0.395	0.397
N'_R	-0.0586	-0.0517	$\gamma_R(\beta_R > 0)$	0.640	0.578
N'_{vvv}	-0.0298	-0.0429	ℓ'_R	-0.71	-0.71
N'_{vvr}	-0.2942	-0.2815	ε	1.09	1.37
N'_{vrr}	0.0553	0.0632	κ	0.499	0.39
N'_{rrr}	-0.0132	-0.0163	f_α	2.747	2.747

- In the simulation, the propeller revolution (n_P) both of DF and NB is set same as 1.2 rps (= 72 rpm), then the initial approach speed U_0 both of those can be obtained in steady state conditions. The initial approach speed in fullscale for DF is 15.5 knots and NB is 18.1 knots, the rudder steering rate is 2.34°/s in fullscale, and the radius of yaw gyration

is $0.25L$. Propeller revolution (n_P) is assumed to be kept the revolution at U_0 constant in a case without torque-rich.

5.2.1 Free running model tests

The free running model tests were conducted to confirm the maneuvering simulation results of the ship in DF and NB condition in the National Research Institute of Fisheries Engineering (NRIFE) Square Tank in Japan (length: 60 m, width: 25 m, depth: 3.2 m) by using a scaled ship model (length: 2.901 m, scale ratio 110).

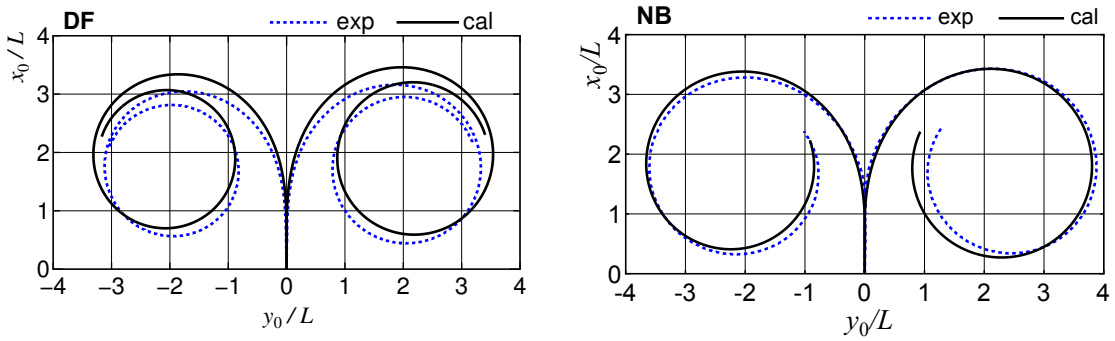

Figure 5.2: Comparison of ship trajectories between experiment and calculation for DF and NB in still water with $\delta = 35°$

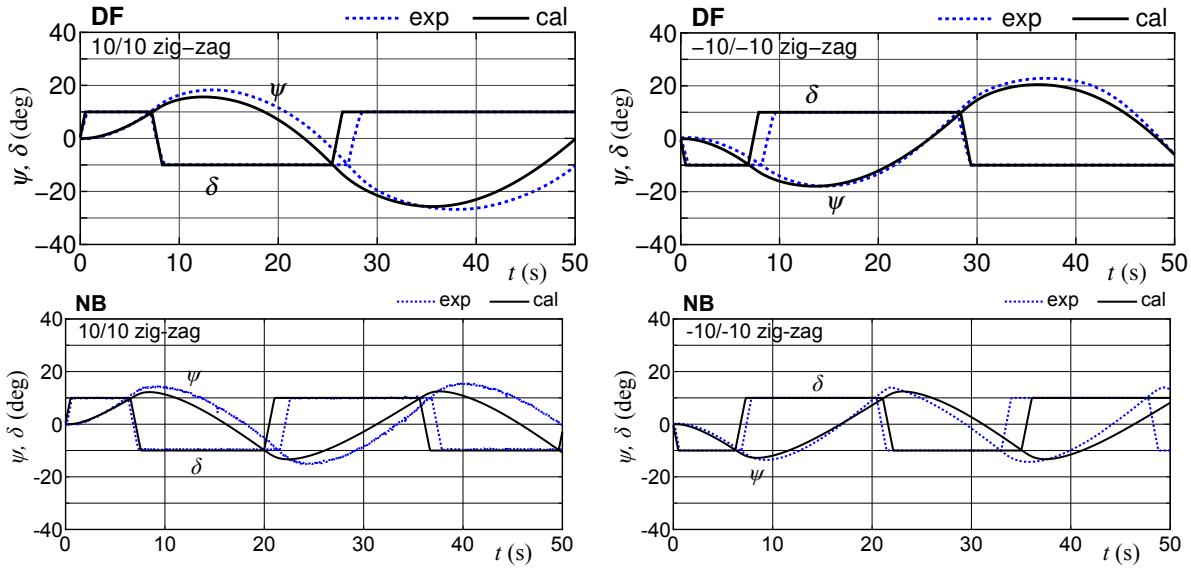

Figure 5.3: Comparison of time histories of the heading angle (ψ) and rudder angle (δ) between experiment and calculation for DF and NB in still water (right: 10/10 zig-zag, left: $-10/-10$ zig-zag)

The comparison of maneuvering simulation results and free running model test as presented in Chapter 4 and follow to the work of Yasukawa et al. [35, 37]. In the test, the approach speed U_0 for DF is 0.76 m/s (15.5 kn in fullscale), and NB is 0.785 m/s (16 kn in fullscale). The propeller revolution (n_P) were set as 17.2 rps (1.6 rps in fullscale) for DF and 16.1 rps (1.5 rps in fullscale) for NB. A comparison of the simulation (cal) and experiment (exp) both of DF and NB during turning in still water with a rudder angle of $\pm 35^\circ$ as shown in Fig. 5.2. The turning simulation results agree well with the free-running model test results, although the simulation results slightly smaller than the experiment results. Fig. 5.3 shows a comparison of the simulation and experiment for time histories of heading angle ψ and rudder angle δ in $10/10$ and $-10/-10$ zig-zag maneuvers for both of DF and NB in still water. The simulation results roughly agree with the free-running test results. The steering timing in the experiment was slightly slower than those of simulation results. However, the differences in overshoot angle between simulations and experiments are small. From those results, it indicated that NB has a larger turning radius than DF, as well as the course keeping performance of NB improved when compared to that of DF.

5.2.2 Wave-induced steady force coefficients

A database of wave-induced steady forces in irregular waves was made based on both results of DF and NB for the interpolation in the maneuvering simulations, and this was predicted with the same procedures as those used in Section 4.2.4. The wave-induced steady forces in irregular waves were obtained by performing short-term predictions based on the wave-induced steady forces in regular waves, which were calculated by zero-speed 3D panel method (3DPM) for the steady lateral force and yaw moment and the strip theory-based Kochin-function method (SKFM) for added resistance [41]. Fig. 5.4 shows surge force ($\overline{C_{XW}}$), lateral force ($\overline{C_{YW}}$) and yaw moment ($\overline{C_{NW}}$) corresponds to 15.5 knot ($F_n = 0.14$). These are non-dimensionalized by $\rho H_{1/3}^2 gL$ for forces and $\rho H_{1/3}^2 gL^2$ for moment, where $H_{1/3}$ is the significant wave height. In the Fig. 5.4, χ_0 denotes wave directions and T_v denotes the averaged wave period. The absolute values of wave-induced steady forces in NB become smaller than those in DF as a whole.

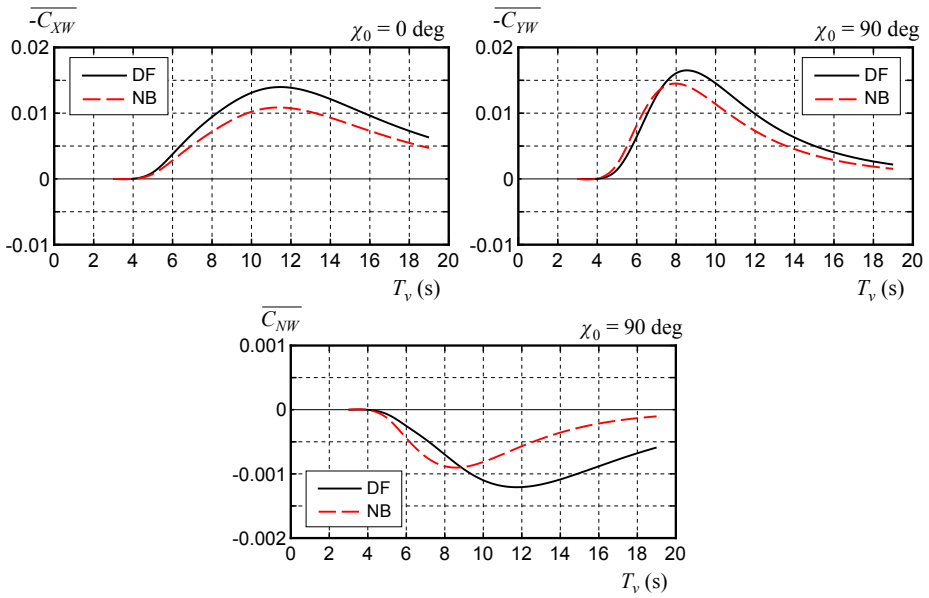

Figure 5.4: Averaged wave-induced steady force coefficients in irregular waves for DF and NB at $V_s = 15.5$ knot

5.2.3 Aerodynamic force coefficients

Aerodynamic coefficients (C_{XA}, C_{YA}, C_{NA}) for DF and NB were predicted by using a method proposed by Fujiwara [8].

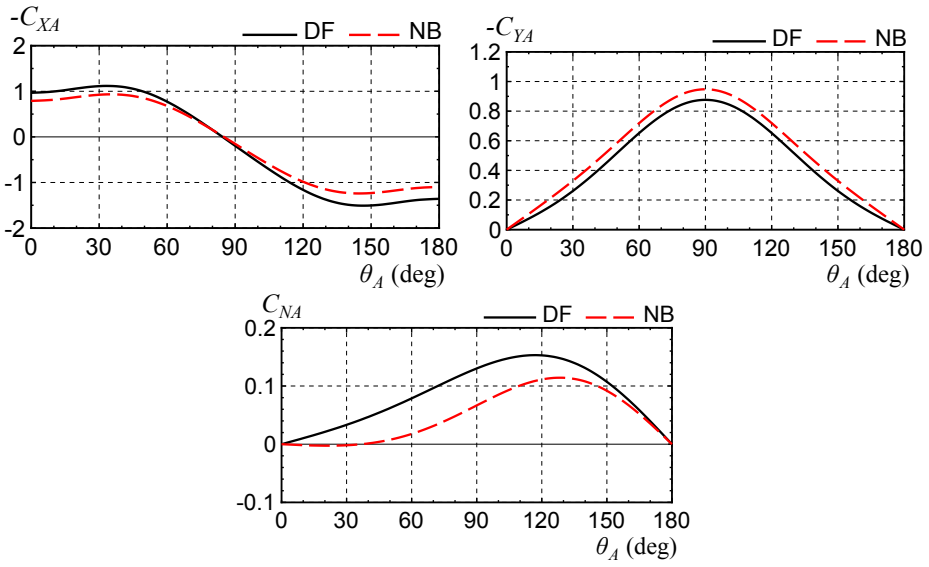

Figure 5.5: Aerodynamic force coefficients for DF and NB

Fig. 5.5 shows the coefficients which are non-dimensionalized by $0.5\rho_a A_X {V_A}^2$ for the surge force, $0.5\rho_a A_Y {V_A}^2$ for the lateral force, and $0.5\rho_a A_Y {V_A}^2 L$ for the yaw moment, respectively.

ρ_a is the air density and V_A is the relative wind velocity. These coefficients based on the front/profile wind pressure area of the target ship versus those of the relative wind direction θ_A. The absolute value of lateral wind force coefficients (C_{YA}) in NB generally becomes large than that in DF.

5.2.4 Beaufort scale

The environmental parameters were set based on the Beaufort scale. Table 5.3 shows the wind power class of the Beaufort scale (BF) used in the simulation under adverse conditions. From the table, the absolute wind speed (denoted as U_W), the significant wave height (denoted as $H_{1/3}$), the averaged wave period (denoted as T_v). The wind and waves were assumed to be constant with respect to time, and the wind direction (θ_W) was the same as the wave direction (χ).

Table 5.3: Wind and wave conditions in the simulations

BF	U_W (m/s)	$H_{1/3}$ (m)	T_v (s)
7	15.6	4.0	7.7
8	19.0	5.5	9.1
9	22.7	7.0	10.2
10	26.5	9.0	11.6

5.3 Maneuvering in still water

5.3.1 Turning

Fig. 5.6 shows a comparison of turning trajectories between DF and NB with a given rudder angle of $\pm 35^\circ$ in fullscale. Table 5.4 shows a comparison of turning indexes, advances (A_D), and tactical diameters (D_T). The turning radius increases in NB when compared with that of DF, and A_D and D_T increased 0.1% and 15.2% respectively, as the averaged value of port and starboard turning. The turning indexes (A_D, D_T) in NB condition satisfied the IMO maneuvering criteria [15, 16], although they increase when compared with that of DF condition. It should be noted that the IMO criteria for ship maneuverability are only applicable to the full-load and even-keel condition as the fundamental condition for the assessment. The turning performance of NB was not at a potentially problematic level in the safe navigation viewpoint.

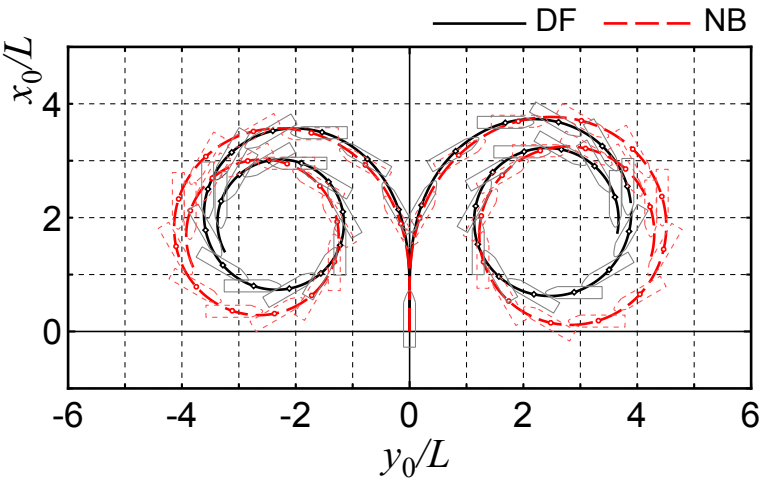

Figure 5.6: A comparison of the turning trajectories in still water ($\delta = \pm 35°$)

Table 5.4: A comparison of turning indexes

	$\delta = 35°$		$\delta = -35°$	
	A_D/L	D_T/L	A_D/L	D_T/L
DF	3.67	3.83	3.50	3.54
NB	3.69	4.43	3.49	4.06
IMO criteria	4.50	5.00	4.50	5.00

Fig. 5.7 shows a comparison of the time history of the rudder normal force coefficient ($F_N{}'$) during turning. $F_N{}'$ is nondimensionalized by $0.5\rho LdU^2$. $F_N{}'$ in NB is larger than that in DF, although the turning circle is larger in NB than DF, as shown in Fig. 5.6.

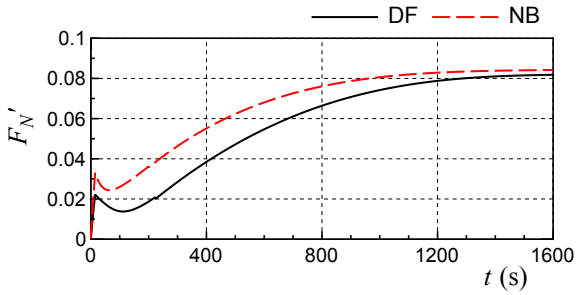

Figure 5.7: Comparison of time history of rudder normal force coefficient ($F_N{}'$) during turning in still water ($\delta = 35°$)

Generally, a larger rudder force makes a smaller turning circle. Therefore, the reason why the turning circle is larger in NB than DF is not caused by the rudder force. This may be caused by a difference in course stability in DF and NB, and it is expected that the course stability in NB is better than that in DF.

5.3.2 Course stability

To observe a difference of course stability in DF and NB, the course stability criterion C in still water is compared. The criterion C is expressed as follows:

$$C = Y_v^{G\prime} N_r^{G\prime} - [Y_r^{G\prime} - (m' + m'_x)] N_v^{G\prime} > 0 \tag{5.1}$$

Here, the derivatives correspond to the center of gravity as converted from midship point (see Appendix A.1). The ship stable when $C > 0$ and unstable when $C < 0$. $Y_v^{G\prime}$, $Y_r^{G\prime}$, $N_v^{G\prime}$ and $N_r^{G\prime}$ denote the non-dimensionalized linear of the hydrodynamic forces on maneuvering without steering effects shown in Table 5.5. m' and m'_x are the non-dimensionalized mass and added mass as mentioned in Table 5.2, respectively. The details of course stability derivation are explained in Appendix A.2.

Table 5.5: Comparison linier derivatives on maneuvering and C without propeller and steering effects

Index	**DF**	**NB**
$Y_v^{G\prime}$	-0.3145	-0.3016
$Y_r^{G\prime}$	0.0718	0.0735
$N_v^{G\prime}$	-0.1256	-0.0571
$N_r^{G\prime}$	-0.0461	-0.0444
C	-0.02	0.00

As the results, the C in DF is -0.02 and C in NB is 0.00. Namely, the ship in DF is unstable for course-keeping, and the ship in NB is neutral. Thus, it is confirmed that better turning performance in DF comes from the bad course stability. Furthermore, since the effect propeller and rudder are taken into account on the course stability correspond to derivatives in Appendix A.3, the criterion C which represents a course stability includes steering effects can be expressed as,

$$C = Y_v^{G*\prime} N_r^{G*\prime} - [Y_r^{G*\prime} - (m' + m'_x)] N_v^{G*\prime} > 0 \tag{5.2}$$

where,

$$\left.\begin{aligned} k_Y &= (1+a_H)\tfrac{A_R}{Ld} f_\alpha \\ k_N &= -(x'_R + a_H x'_H)\tfrac{A_R}{Ld} f_\alpha \\ Y_v^{G*\prime} &= Y_v^{G\prime} - k_Y u'_R \gamma_R \\ Y_r^{G*\prime} &= Y_r^{G\prime} - k_Y u'_R \gamma_R \ell'_R \\ N_v^{G*\prime} &= N_v^{G\prime} + k_N u'_R \gamma_R \\ N_r^{G*\prime} &= N_r^{G\prime} + k_N u'_R \gamma_R \ell'_R \end{aligned}\right\} \tag{5.3}$$

Here, the non-dimensionalized linear of the hydrodynamic forces on maneuvering includes the steering effects denoted as $Y_v^{G*\prime}$, $Y_r^{G*\prime}$, $N_v^{G*\prime}$ and $N_r^{G*\prime}$. Those values are shown in Table 5.6. The interaction coefficients values among hull, propeller and rudder are taken from Table 5.2. a_H denotes the rudder force increase factor, x'_R denotes the non-dimensionalized longitudinal coordinate of rudder position (normaly, $x'_R \simeq -0.5$). x'_H denotes the non-dimensionalized longitudinal coordinate of acting point of the additional lateral force component induced by steering. f_α denotes rudder lift gradient coefficient, it was estimated using Fujii's formula $(= (6.13\Lambda)/(\Lambda + 2.25))$[7]. u'_R denotes the non-dimensionalized longitudinal rudder inflow velocity, since δ is small, the non-dimensionalized resultant rudder inflow velocity U'_R $(\simeq u'_R)$, u'_R was assumed as 1.0 for both of DF and NB. γ_R denotes flow straightening coefficient, and assumed in average value of $\gamma_R(\beta_R < 0)$ and $\gamma_R(\beta_R > 0)$. ℓ'_R denotes the non-dimensionalized effective longitudinal coordinate of rudder position.

Table 5.6: Comparison of linear derivatives on maneuvering and C (including effect of propeller and rudder

Index	**DF**	**NB**
$Y_v^{G*\prime}$	-0.3528	-0.3576
$Y_r^{G*\prime}$	0.0990	0.1132
$N_v^{G*\prime}$	-0.1068	-0.0303
$N_r^{G*\prime}$	-0.0594	-0.0635
C	0.00	0.02

The calculation result of C in DF is 0.00 (neutral) and NB is 0.02 (stable). The stability criterion improves since the course stability considers the steering effects. Thus, it confirms that ship in NB is more stable for course keeping and quicker to respond to the rudder in transient motion, even though steady turning performance is worse than in DF.

5.3.3 Zig-zag maneuvers

Fig. 5.8 shows the time histories of heading angle ψ and rudder angle δ in $10/10$ and $-10/-10$ zig-zag maneuvers in still water. Additionally, Fig. 5.9 shows the time histories of ψ and δ during $20/20$ and $-20/-20$ zig-zag maneuvers. At the same time, a comparison of time histories of the ship speed (u), yaw rate (r), hull drift angle (β) and rudder normal force (F_N) during zig-zag maneuvers are shown in Fig. 5.8 and Fig. 5.9. The steering timing of NB is faster in all cases than that of DF, which means that a VLCC has a quick response when the ship is sailing in the ballast load condition. Tables 5.7 and 5.8 present the comparison of overshoot angle (OSA) during the zig-zag maneuvers. The OSA of NB is smaller than that of DF, and the course stability evidently improved. The averaged value of 1st OSAs in the port and starboard side decreases approximately by 60% in NB, and the averaged value of second OSAs also decreases approximately 73%. Thus, the zig-zag maneuvers in ballast condition have a good performance, and the IMO maneuvering criteria [15, 16] are fulfilled in all cases. This is caused by better course stability in NB, as mentioned in Section 5.3.2.

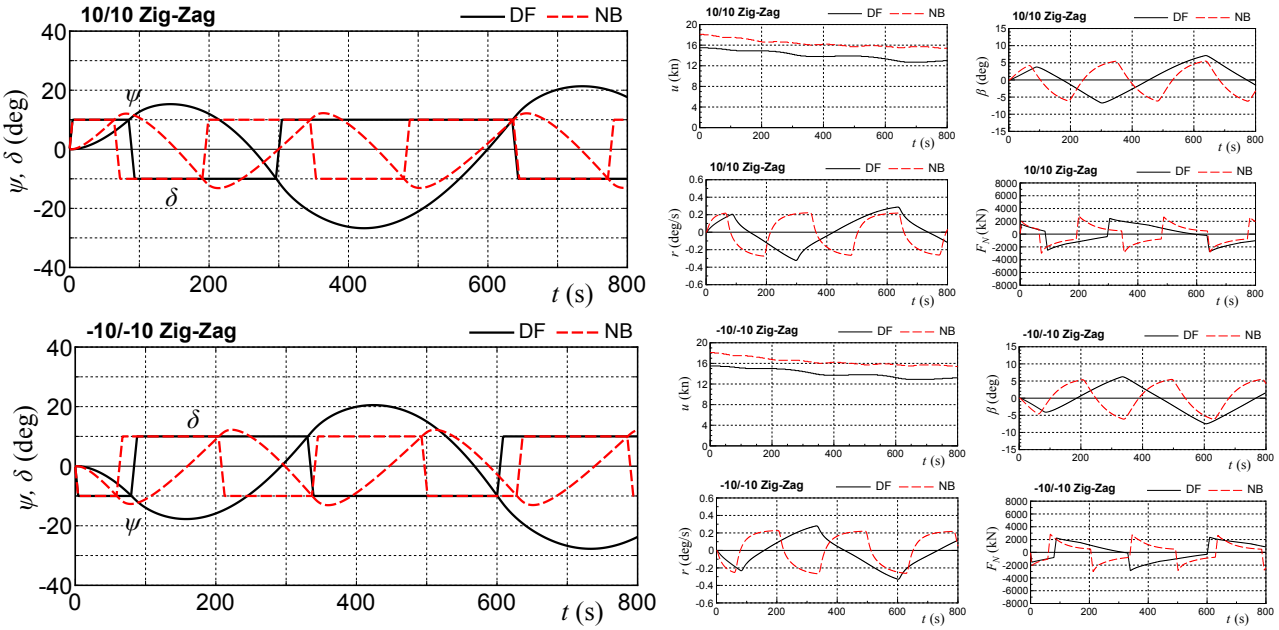

Figure 5.8: Comparison of time histories of the heading angle (ψ) and rudder angle (δ) in still water (left: 10/10 zig-zag, right: -10/-10 zig-zag)

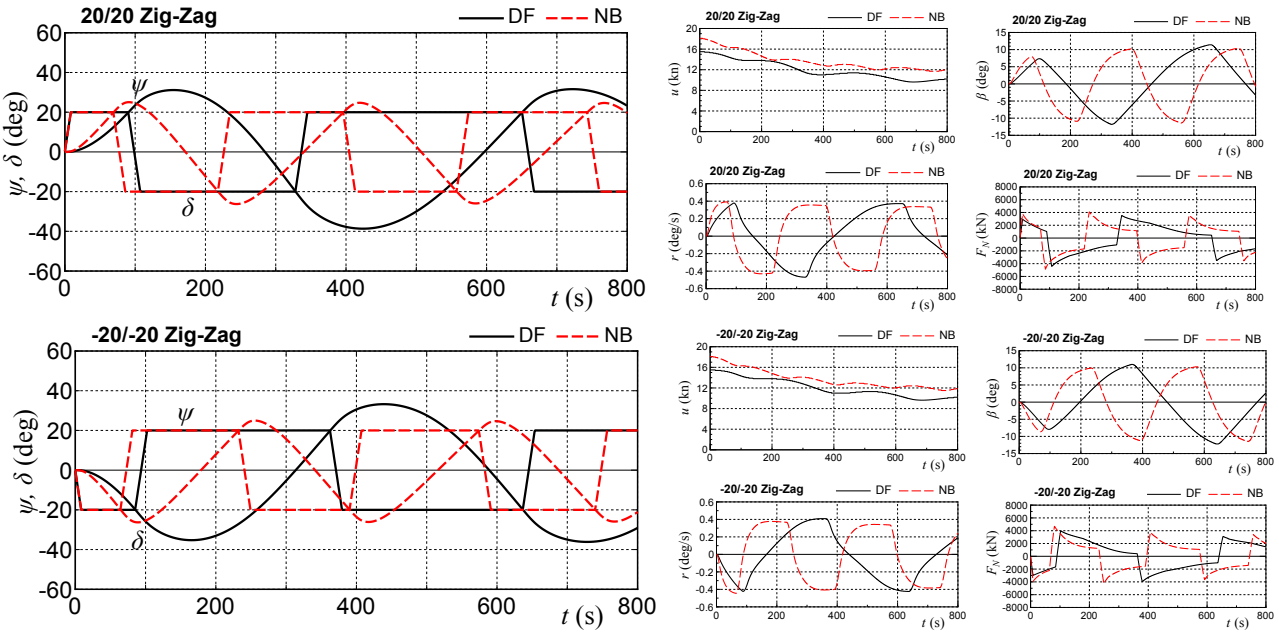

Figure 5.9: Comparison of time histories of the heading angle (ψ) and rudder angle (δ) in still water (top: 20/20 zig-zag, bottom: -20/-20 zig-zag)

Table 5.7: Comparison of the overshoot angle of 10/10 and -10/-10 zig-zag maneuvers in still water

	10/10 zig-zag		-10/-10 zig-zag	
	1st OSA (°)	2nd OSA (°)	1st OSA (°)	2nd OSA (°)
DF	5.3	16.7	7.8	10.5
NB	2.1	3.1	2.7	2.2
IMO criteria	20.0	40.0	20.0	40.0

Table 5.8: Comparison of the overshoot angle of 20/20 and -20/-20 zig-zag maneuvers in still water

	20/20 zig-zag		-20/-20 zig-zag	
	1st OSA (°)	2nd OSA (°)	1st OSA (°)	2nd OSA (°)
DF	11.2	18.7	15.3	13.2
NB	5.1	6.3	6.3	4.9
IMO criteria	25.0	–	25.0	–

5.4 Maneuvering in adverse conditions

5.4.1 Straight moving conditions in adverse weather conditions

A ship traveling with a propeller revolution in the design speed under wind and waves is considered using the auto-pilot. In the auto-pilot, the PD control is applied with a proportional gain corresponding to 5.0 and a differential gain corresponding to 20.0 s. Fig. 5.10 shows the longitudinal component of the ship speed (denoted as u), hull drift angle (denoted as β), and check helm (denoted as δ) in the steady state sailing condition under wind and waves. In the figure, for purposes of distinction, additional lines are placed to connect the calculation results.

A significant decrease in speed occurred with the increase in the BF scale. The ship speed decrease for NB was slightly smaller than that for DF with respect to the head waves. In BF10, the smallest u is about 4.1 knots ($\chi_0 = 15°$) in DF and about 5.2 knots ($\chi_0 = 30°$) in NB. The β and the absolute value of δ increase with increases in the BF scale. With respect to BF10, The largest β both of DF and NB occurs approximately at $\chi_0 = 45°$, and the smallest δ occurs about at $\chi_0 = 75°$ in DF and about at $\chi_0 = 105°$ in NB. The maximum β is about 7.3° in DF and about 16.2° in NB. The minimum δ is about $-10.3°$ in DF and $-3.6°$ in NB. The check helm of NB is smaller than that of DF. Thus, the steady-state sailing conditions in adverse weather conditions are quite different between DF and NB: the absolute value of δ becomes small, and β becomes large in NB when compared with DF.

Fig. 5.11 depicts a schematic showing the lateral force components, such as the rudder force, hull lateral force, wind lateral force, and wave-induced steady lateral force acting on the ship in DF and NB ($\chi_0 = 45°, 90°$, and 135°). The largest external force (the sum of the wind lateral

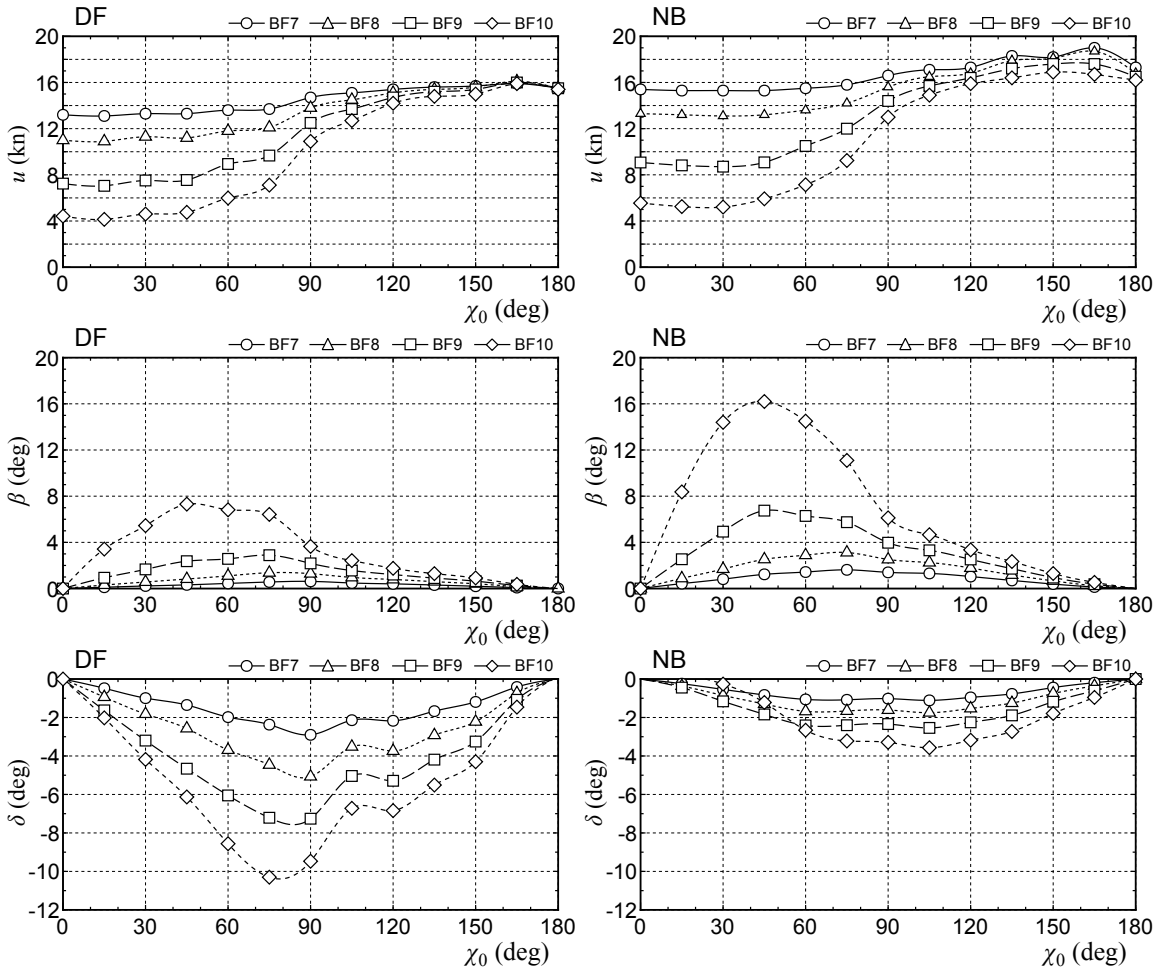

Figure 5.10: Comparison of ship speed (u), drift angle (β) and check helm (δ) in wind and waves

force and wave-induced steady lateral force) is induced in beam wind and waves ($\chi_0 = 90°$) for both DF and NB. Although the order of magnitude of the external force is roughly the same between DF and NB in any wind (wave) directions, the significant difference appears at the longitudinal acting point of the hull lateral force. The acting point of the hull lateral force for DF (approximately 135 m in the x-coordinate) is close to the fore perpendicular (FP), and the acting point for NB (approximately 70 m in the x-coordinate) is close to midship. The abovementioned difference comes from a difference of the hydrodynamic force characteristic represented as linear derivatives on maneuvering, such as $Y_v^{G*\prime}$ and $N_v^{G*\prime}$, as mentioned in Table 5.6. The absolute value of $N_v^{G*\prime}$ in NB is significantly smaller than that in DF, although the absolute value of $Y_v^{G*\prime}$ is almost the same between DF and NB. As a result, the acting point of the hull lateral force in NB moves toward the midship direction. In NB, larger lateral force is required to counterbalance the yaw moment due to the external force because the acting point

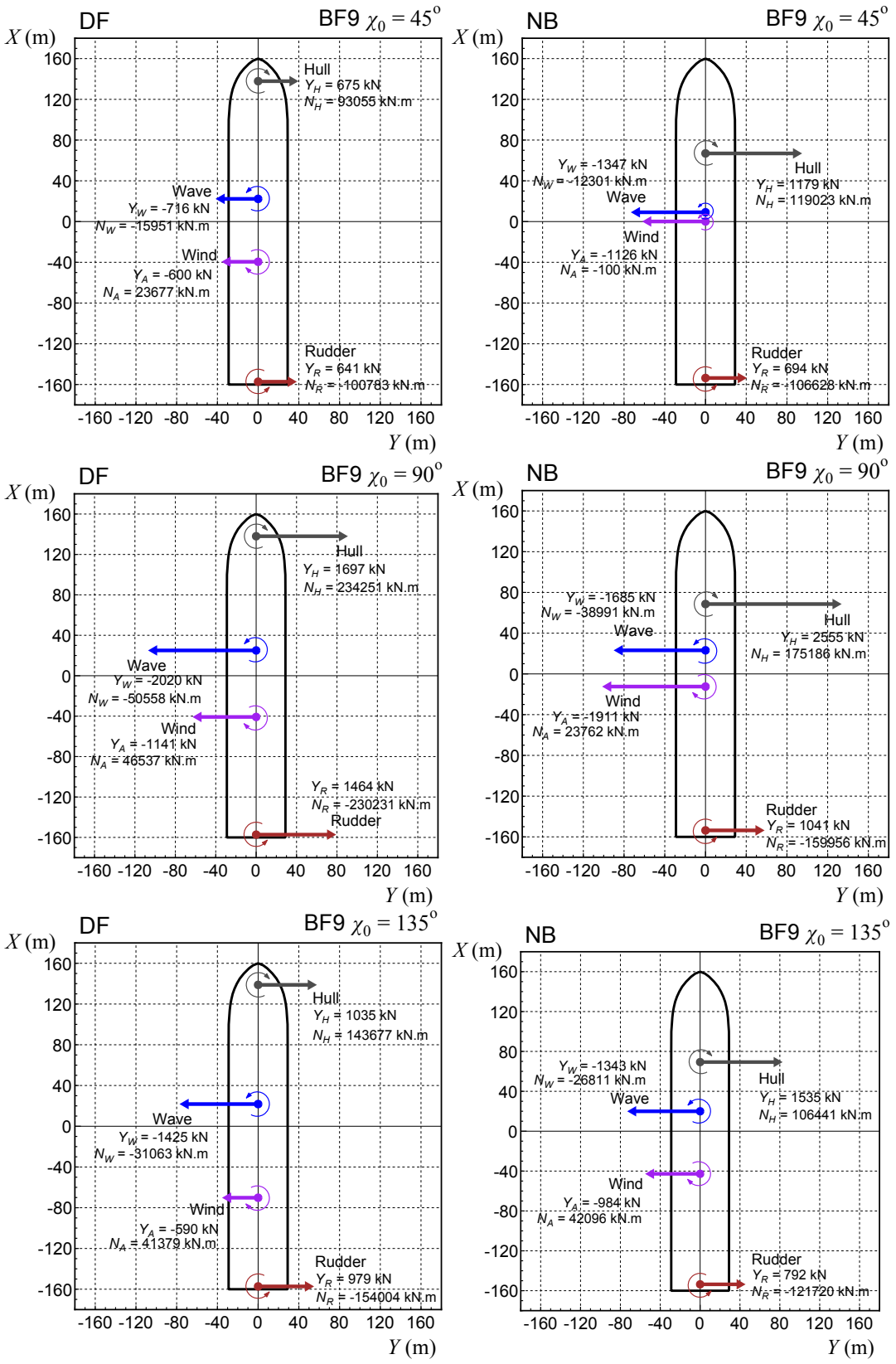

Figure 5.11: Force application point in Beaufort 9 ($\chi_0 = 45°, 90°$, and $135°$)

of the hull lateral force that is located near a more midship position and the moment lever is smaller than DF. For producing a large lateral force, the hull drift angle should be large. Meanwhile, in DF, a large hull drift angle is not necessary, as is NB, because the acting point of the hull lateral force is located near FP and the moment lever is relatively large. When the large lateral force is produced by taking the large drift angle like NB, the required rudder force to counterbalance the external force can be small. This is the reason why the absolute value of the check helm becomes small in NB.

5.4.2 Turning in adverse weather conditions

Turning simulations were performed in adverse weather conditions such as BF7 and BF9. It was assumed that the ship initially advances along x_0-axis. Fig. 5.12 show a comparison of turning trajectories in wind and waves of $\chi = 0°$ and $180°$ with $\delta = 35°$. Fig. 5.13 show a comparison of turning trajectories in wind and waves of $\chi = 90°$ with $\delta = \pm 35°$. An approach speed used in the simulation is obtained from the steady state speed as shown in Fig. 5.10. It is obvious that ship drifting becomes large with increasing BF scale. The ship drifting direction during the turning (drift turning direction) changes with changing wind (wave) directions. Also, the drifting displacement in NB is larger than that of DF in any wind (wave) direction. However, an uncontrollable situation does not occur in both DF and NB in the simulations.

Fig. 5.14 shows a definition of the angles of drift turning direction denoted as β_0, relative drift direction in turning to the wind (wave) directions, denoted as $\alpha_0 (\equiv \beta_0 - \chi)$, and displacement of the drift in turning denoted as D_d. β_0 can be obtained as the angle between the x_0-axis and the drift turning direction. D_d is the distance between the edges of turning circles (taken from the second edge of the circle to the third edge), and it was measured perpendicular to the line of drift turning direction.

Fig. 5.15 shows a comparison of β_0, α_0, and ${D_d}'(= D_d/L)$ in BF7 and BF9 with $\delta = \pm 35°$. The β_0 linearly increases with χ for both DF and NB. The values of α_0 in DF and NB tend to be constant for both cases (BF7 and BF9). The order of magnitude of α_0 is $20° - 27°$ in NB and approximately $30°$ in DF in BF7 and BF9 for $\delta = 35°$. The α_0 becomes small in NB

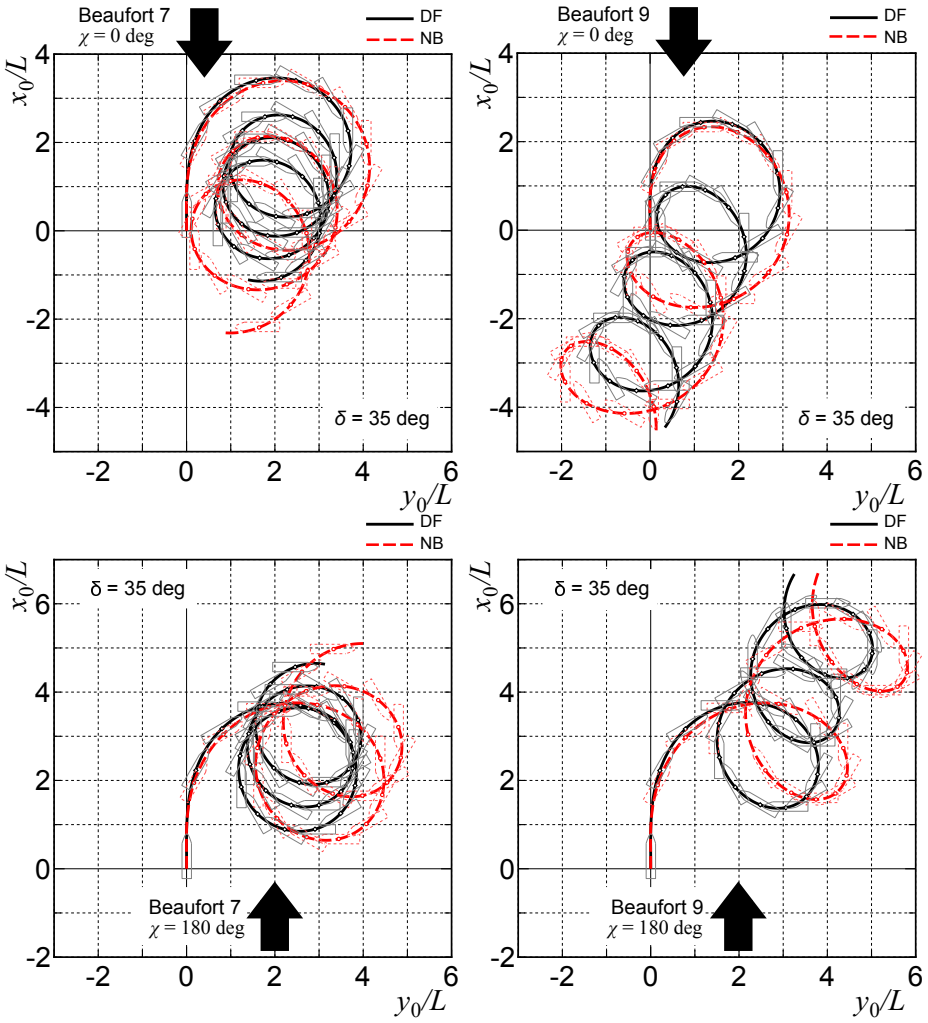

Figure 5.12: Comparison of turning trajectories in wind and waves $\chi = 0°$ for BF7 and BF9 ($\delta = 35°$)

compared with DF. The discrepancy of α_0 between DF and NB becomes small with increasing the BF scale. The $D_d{}'$ is almost the constant for any wind (wave) directions, although there is a tendency that $D_d{}'$ gradually decreases with an increase of wind (wave) directions. $D_d{}'$ in NB is larger than that of DF in all cases, and $D_d{}'$ significantly increases in larger BF scale like BF9. The ship's mass in NB is obviously smaller than that in DF, although the external forces due to wind and waves are almost the same between DF and NB. Therefore, the external forces due to wind and waves per ship's mass are larger in NB. The ship in NB with a light displacement easily drifts away because of wind and waves. Because of the effect of the ship drifting in adverse weather, the turning indexes (A_D,D_T) also change with the magnitude and the direction of the external forces.

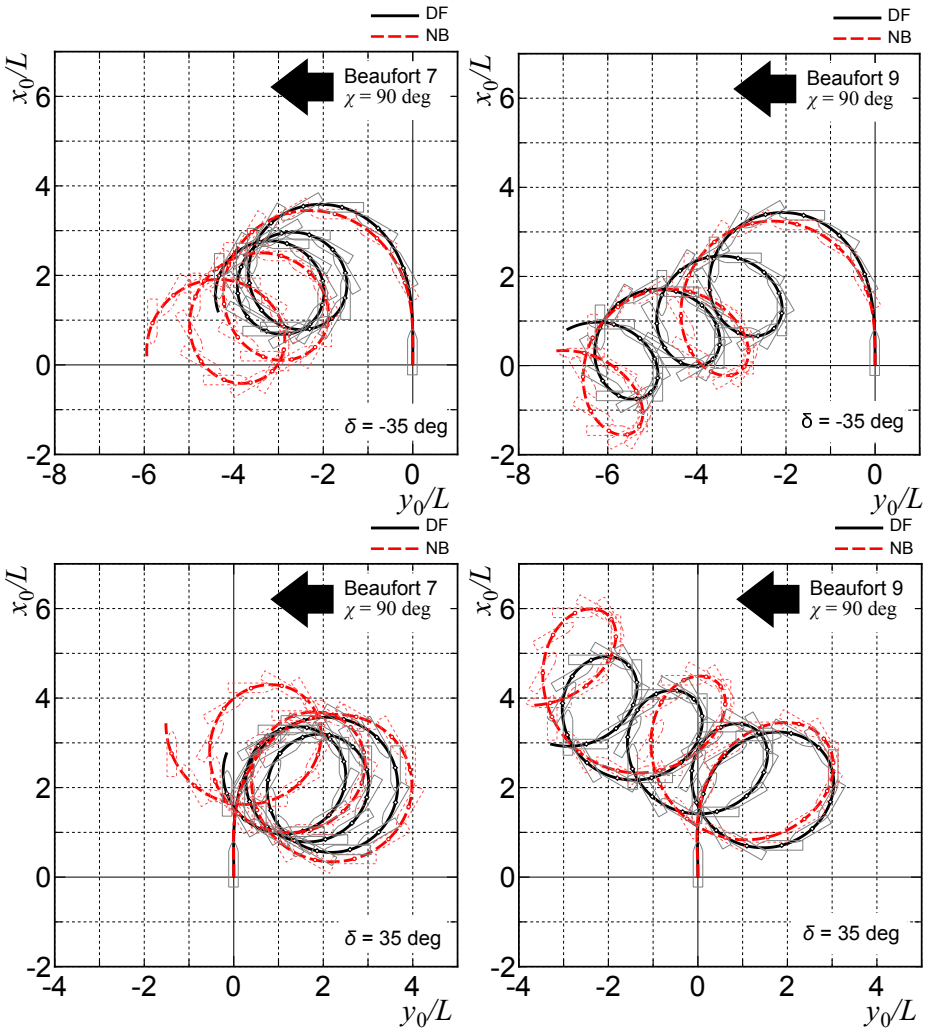

Figure 5.13: Comparison of turning trajectories in wind and waves $\chi = 90°$ for BF7 and BF9 ($\delta = \pm 35°$

Fig. 5.16 shows a comparison of the turning indexes (A_D,D_T) in adverse weather conditions. Note that "SW" in the horizontal axis of the figure denotes the still water. In $\chi = 0°$, A_D and D_T become significantly small for both DF and NB with increasing BF scale. This is because the rudder force increase comes from a significant speed drop in adverse weather. When the speed drop occurs under the condition of constant propeller revolution, the propeller load increases and the rudder force increases.

Fig. 5.17 shows a comparison of time history of rudder normal force coefficient ($F_N{}'$) during turning with $\delta = 35°$ in SW, BF7 and BF9 ($\chi = 0°$) for both DF and NB. $F_N{}'$ in BF7 and BF9 is larger than that in SW at about t=100s just after the steering action finished. Also, we can observe that peaks of $F_N{}'$ periodically appear at the speed drop range during turning in wind

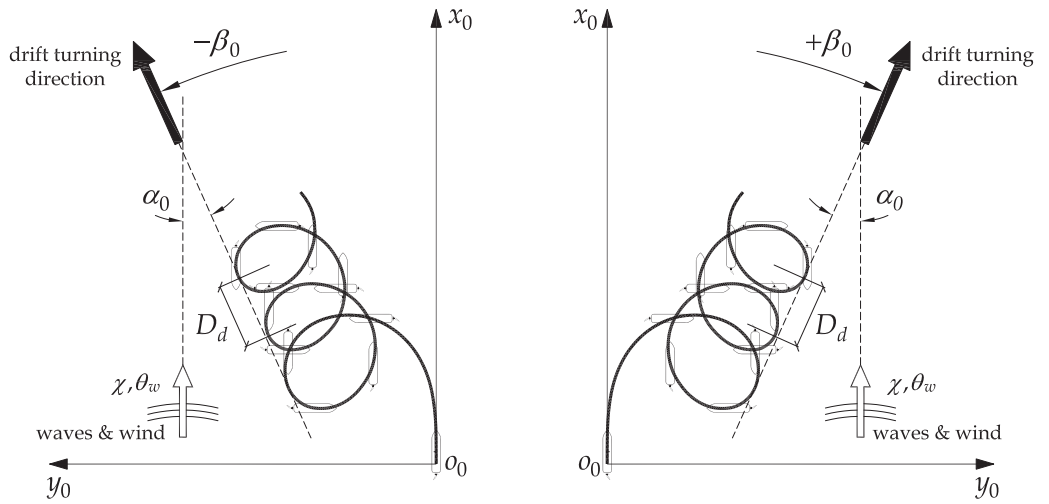

Figure 5.14: A definition of angles of drift turning direction β_0, relative drift direction in turning to wave directions α_0, and displacement of drift in turning α_0 (left: $\delta = -35°$, right: $\delta = 35°$)

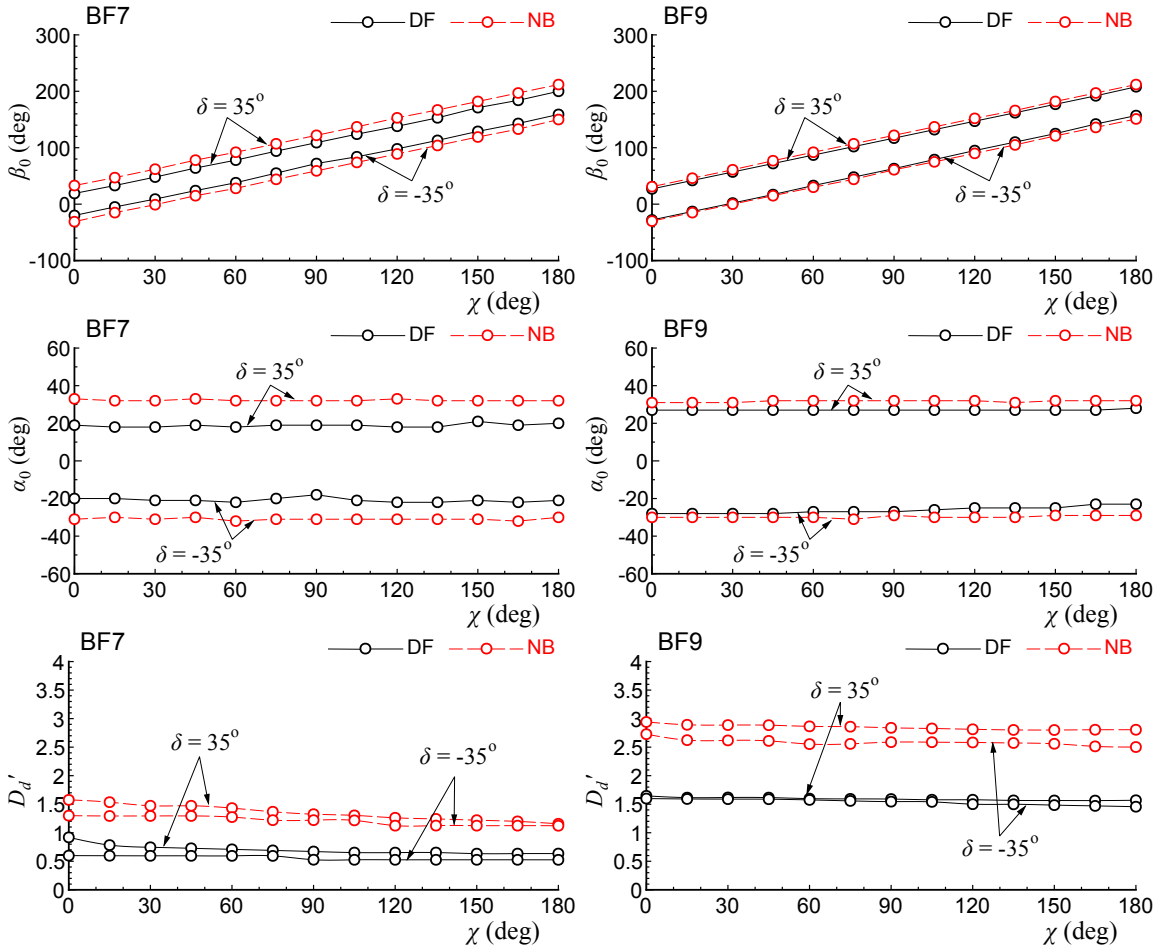

Figure 5.15: Comparison of β_0, α_0 and D_d' for DF and NB in BF7 and BF9

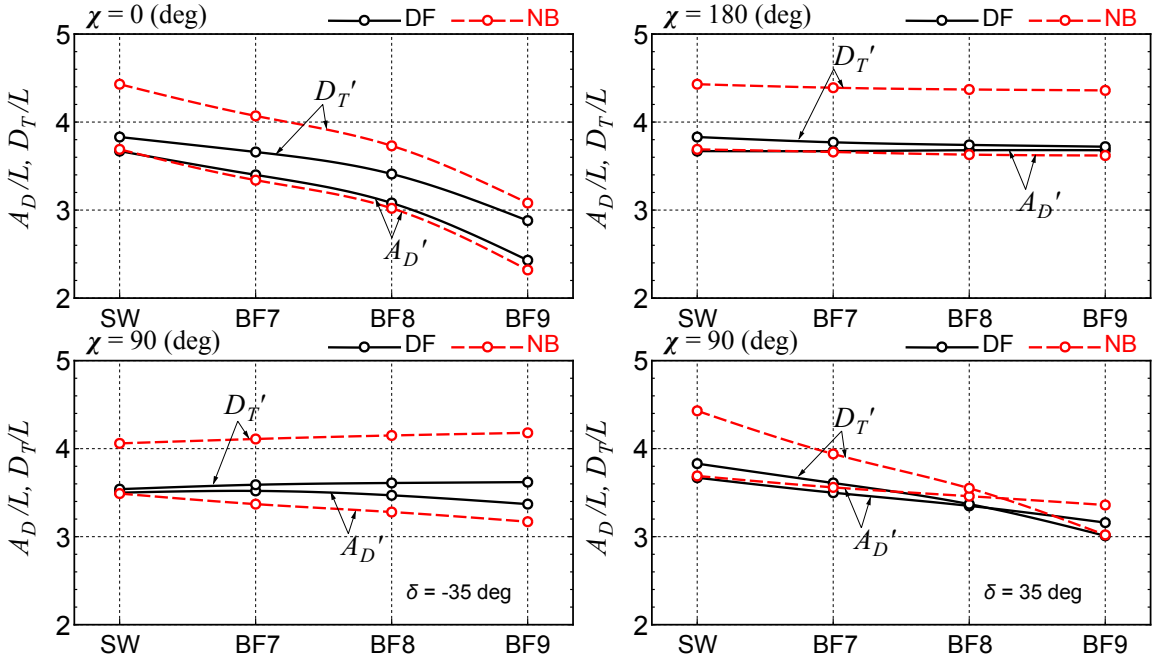

Figure 5.16: Comparison of turning indexes A_D and D_T in wind and waves ($\delta = \pm 35°$)

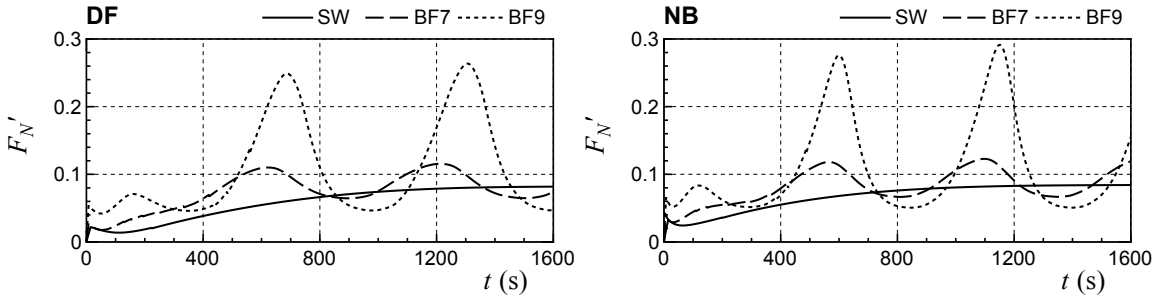

Figure 5.17: Comparison of time history of rudder normal force coefficient ($F_N{}'$) during turning with $\delta = 35°$ in still water (SW), BF7 and BF9 ($\chi = 0°$)

and waves. In $\chi = 180°$, A_D and D_T are almost constant in both DF and NB since the ship speed is almost the same in still water. In $\chi = 90°$, the change of A_D and D_T for increasing BF scale is quite different in between $\delta = 35°$ and $\delta = -35°$. In the case of $\delta = 35°$, A_D and D_T become small for both DF and NB with increasing BF scale, and, conversely, in the case of $\delta = -35°$, A_D decreases slightly and D_T increases slightly with increasing BF scale. At the beginning of the turning with $\delta = 35°$, the relative wind (wave) direction changes from the beam wind (wave) direction to the head wind (wave) direction (namely, $\chi_0 = 90°$ to $0°$). Roughly speaking, this situation is similar to the turning situation in $\chi = 0°$. On the contrary, in the case of $\delta = -35°$, the relative wind (wave) direction changes from beam wind (wave) direction

to following wind (wave) direction ($\chi_0 = 90°$ to $180°$). This situation is similar to the turning situation in $\chi = 180°$. In the change of A_D and D_T with changing BF scale, NB is remarkable compared with DF in all cases. This may be because a ship in NB with a light displacement easily drifts and follows the wind (wave) directions. However, the effect of external forces by the wind and waves on the turning indexes is qualitatively the same in DF and NB.

5.4.3 Zig-zag maneuvers in adverse weather conditions

Zig-zag maneuvering simulations were performed for DF and NB to capture the effect of the load condition in adverse weather. It also is assumed that the ship initially advances along the x_0-axis. The direction of the wind and waves changed to $\chi = 0°, 90°$, and $180°$. Fig. 6.7 shows time histories of ψ and δ in 10/10 zig-zag maneuver in $\chi = 0°$ and $180°$, and Fig. 5.19 shows time histories of ψ and δ in 10/10 and $-10/-10$ zig-zag maneuvers in $\chi = 90°$. The behaviors in time of ψ and δ are quite different between DF and NB. The overshoot angle in DF becomes large, and steering response is delayed, because the ship's mass in DF is larger, and the course stability is potentially worse, as mentioned in Section 5.3.2.

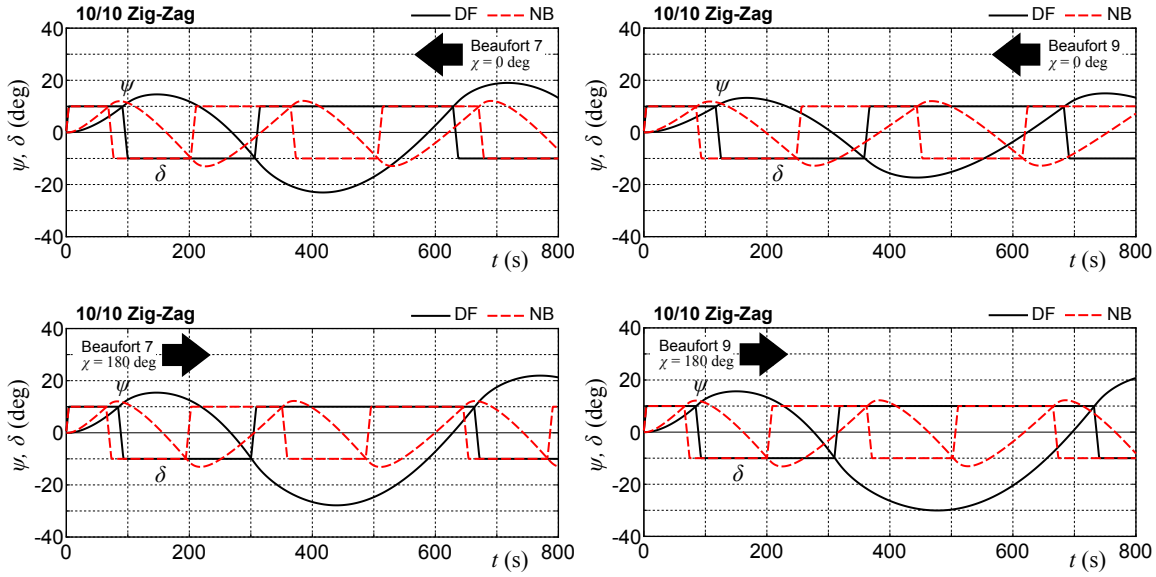

Figure 5.18: Comparison of time histories of the heading angle (ψ) and rudder angle (δ) for DF and NB in BF7 and BF9 ($\chi = 0°$ and $180°$)

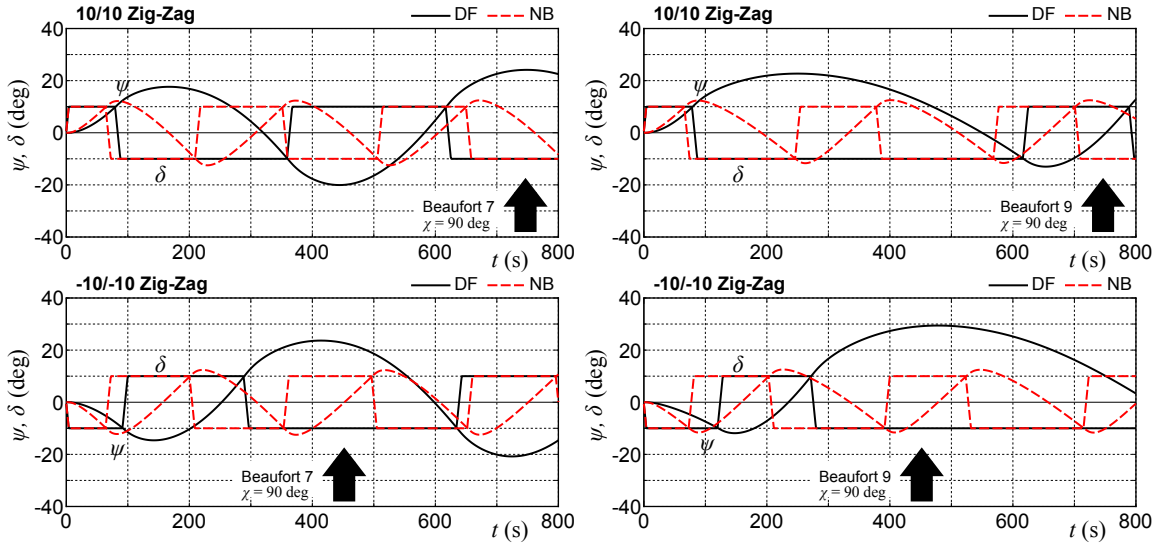

Figure 5.19: Comparison of time histories of the heading angle (ψ) and rudder angle (δ) for DF and NB in BF7 and BF9 ($\chi = 90°$)

Next, zig-zag maneuvering simulations were performed in still water (SW) and adverse weather conditions (BF9) to capture the effect of the adverse weather. Fig. 5.20 shows a comparison of time histories of heading angle ψ and rudder angle δ of a 10/10 zig-zag maneuver in $\chi = 0°, \chi = 90°$, and $\chi = 180°$, and $-10/-10$ zig-zag maneuver in $\chi = 90°$ for DF.

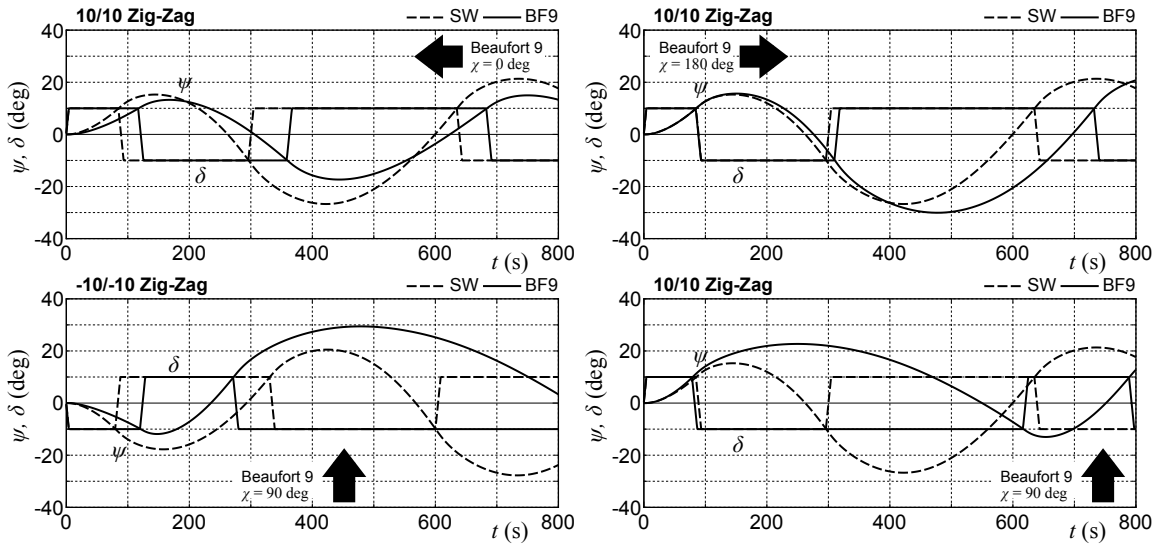

Figure 5.20: Comparison of time histories of heading angle (ψ) and rudder angle (δ) for DF in still water (SW) and BF9

In $\chi = 0°$, peak absolute values of ψ in BF9 become smaller than those in SW. In approaching conditions, a significant speed drop occurs, because the resistance increase induced by the disturbance comes from the heading wind (waves) direction. When the speed drop occurs under

the condition of constant propeller revolution, the propeller load increases, and the rudder force increases. However, in $\chi = 180°$, no remarkable difference is observed between BF9 and SW in the peak absolute values of ψ. In the following disturbance condition, the resistance increase is small. As a result, a significant speed drop does not occur. In a 10/10 zig-zag maneuver of $\chi = 90°$, the absolute value of the first peak of ψ in BF9 is larger than that in SW, and it takes time to change ψ to the minus value. Nevertheless, the absolute value of the second peak of ψ is smaller, and the response becomes faster. However, in $-10/-10$ zig-zag maneuver of $\chi = 90°$, the first peak of ψ is smaller, and the response becomes faster. The second peak is larger, and it takes time to change the sign of ψ. Thus, an interesting behavior appears in $\chi = 90°$. It should be noted that similar behaviors have been indicated by Yasukawa [33] in free-running model test results for an S-175 container ship model in regular beam waves. The reason for the behavior in zig-zag maneuvers of $\chi = 90°$ is discussed below.

Fig. 5.21 shows the comparison of OSAs for DF and NB in BF7 and BF9. From the figure, the following tendency can be observed:

- The first OSA becomes larger in $\chi = 45° - 180°$, and the second OSA becomes smaller in $\chi = 0° - 165°$ than those in SW for 10/10 zig-zag maneuvers. The tendency becomes opposite for $-10/-10$ zig-zag maneuvers: the first OSA becomes smaller in $\chi = 0° - 165°$, and the second OSA becomes larger in $\chi = 45° - 180°$.
- In $\chi = 0°$, the first and second OSAs become smaller than those in SW.
- In $\chi = 180°$, the first and second OSAs are almost the same or become larger than those in SW.

Basically, this tendency is the same between DF and NB, although DF is more significant. Further, this tendency becomes remarkable at a larger BF scale. The phenomena in $\chi = 0°$ and $\chi = 180°$ are deeply related to the rudder force mentioned in the previous subsection. In beam wind and wave conditions, such as $\chi = 90° - 120°$, the order of magnitude of the check helm becomes important. Here, consider the $-10/-10$ zig-zag maneuver of the ship of DF sailing in $\chi = 90°$. In BF9, the required check helm of the ship (δ_c) approximately

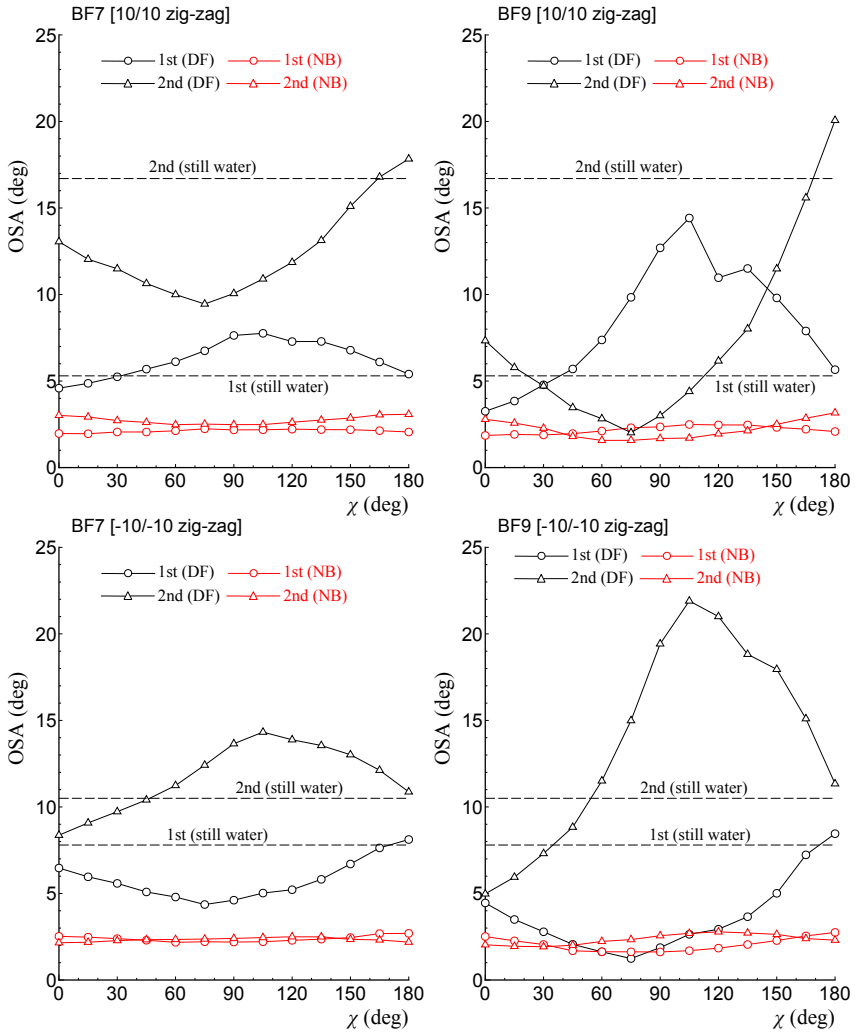

Figure 5.21: Comparison of OSAs of 10/10 and −10/ − 10 zig-zag manuevers for DF and NB in BF7 and BF9

−8°, as shown in Fig. 5.10. Then, the given rudder angle in the zig-zag maneuver (δ_z) is −10° for the second-time steering, because the rudder angle in the second time steering is important when discussing the first OSA. As a result, effective rudder angle δ_e ($\equiv \delta_z - \delta_c$) becomes approximately $\delta_e = 10 - 8 = 2°$, and it is too small to overcome the external forces due to wind and waves for safe sailing. In this condition, the ship gradually responds to the rudder with slower steering timing. For the second OSA, on the contrary, the effective rudder angle is approximately $\delta_e = 10 + 8 = 18°$, and the order of magnitude increases. As a result, the second OSA significantly decreases compared with the first OSA. Additionally, the OSAs of NB are significantly smaller than those of DF because the ship in NB has a better course stability in still water. In addition, the ship in NB has a quicker response in zig-zag maneuvers

to the rudder, because the effective rudder angle is relatively large (approximately $\delta_e = 7°$) for the first OSA. As a result, the produced OSAs in NB become smaller than those in DF.

5.5 Concluding remarks

This chapter has analyzed the effect of load conditions of a VLCC on maneuvering in still water and adverse conditions by using an MMG-based simulation method [37]. The maneuvering simulations were performed to the conventional VLCC in DF and NB conditions. Conclusions are summarized as follows to answer the research question in Section 1.3: ***How does the effect of loading conditions on ship maneuvering performance?***

- As NB is better in course stability than DF, the turning performance of NB in still water becomes worse than that of DF. Although the turning performance is worsened in NB, the turning indexes (A_D,D_T) are still in compliance to the IMO maneuvering criteria [15, 16].
- The averaged 1st and 2nd overshoot angle (OSA) of NB for zig-zag maneuvers in still water decreased since the dynamic course stability increased, the overshoot angle satisfied the IMO maneuvering criteria [15, 16].
- The steady-state sailing condition in adverse weather conditions is quite different between DF and NB. In NB, the absolute value of the check helm becomes small and the hull drift angle becomes large. This mainly comes from the difference in the dynamic course stability between DF and NB.
- Turning in adverse weather conditions, the relative drift direction of the ship in turning to the wave direction α_0 is almost the constant for any wave and wind directions. The order of magnitude is $20° - 30°$ in NB and DF in the case with a rudder angle of 35°, although α_0 in DF is slightly smaller than that in NB. The drifting displacement in turning D_d is almost the constant for any wind (wave) directions. D_d in NB is remarkably larger than that of DF at the same BF scale, because the external forces due to wind and waves per

the ship mass are larger in NB. D_d significantly increases with an increasing BF scale. Advance A_D and tactical diameter D_T become significantly small with an increasing BF scale in head wind and waves when approaching, although A_D and D_T are almost constant in following wind and waves. In beam wind and waves, the tendency depends on the plus and minus of the rudder angle δ. The effect of external forces owing to the wind and waves on the turning indexes is qualitatively the same in DF and NB.

- Zig-zag maneuvers in adverse weather conditions, the first and second OSAs in $\chi = 0°$ (heading) become smaller than those in still water (SW), and those in $\chi = 180°$ (following) are almost the same or become larger than those in SW. In the case of 10/10 zig-zag maneuvers of the ship in beam wind and waves, the first OSA increases compared with the value in SW because of the effective rudder angle decreases; the second OSA decreases because the effective rudder angle increases. This tendency becomes opposite for $-10/-10$ zig-zag maneuvers. The effective rudder angle changes owing to the order of magnitude of the check helm in adverse weather conditions. Basically, these tendencies are the same between DF and NB, although DF is more significant

With the results of this chapter, it is now possible to consider a study regarding the reduction of main engine output and its effect on ship maneuvering performance. Based on the results correspond to the conventional VLCC in full load condition, a small main engine output due to advances in energy-saving technology will be discussed in further studies (Chapter 6).

Chapter 6

Impacts of minimum power on ship maneuvering performance

The loading conditions affect the ship maneuverability as discussed in Chapter 5. However, the situation where the ship uncontrollable in all cases did not occur. Therefore, it is possible to propose a significant reduction in engine output which aims to improve EEDI. In this chapter, the engine output of a VLCC (KVLCC2) in full load condition as described in Chapter 3 is reduced due to the progress of the energy-saving. Next, a maneuvering simulation method based on MMG model [37] correspond to Chapter 2 is used to investigate the maneuverability of the VLCC in still water and adverse weather conditions. It may be noted that the prediction accuracy of the simulation method was sufficient for practical use as explained in Chapter 4. A VLCC with 30% reduced EEDI (Energy Efficiency Design Index) is proposed instead of a conventional VLCC by employing energy efficiency devices, a large-diameter, and low-revolution propeller. The VLCC with 30% reduced EEDI is referred to as Step3, and the conventional VLCC is referred to as Step0 [38, 46]. The engine output of Step3 is inevitably smaller than that of Step0. Thus, this study performs the maneuvering simulations for Step0 and Ship3 in still water and adverse weather conditions. The impacts of the minimum power on maneuverability will be discussed based on the calculation results from a navigation safety perspective.

6.1 EEDI improvement

This section presents the improvement of EEDI (or the propulsive performance) based on the KVLCC2 by employing the following technologies:

- a low-revolution engine and large-diameter propeller,
- a low-output engine with electronic control,
- energy-saving devices, such as Pre-Swirl Fin and Rudder Bulb Fin, to improve self-propulsion factors, and
- low frictional resistance paint and air lubrication technology to reduce hull frictional resistance.

Further, it was assumed that there were no changes in the main particulars and the hull form of the ship except for the propeller characteristics.

In the study, Step0 corresponds to a conventional VLCC that was the base ship and Step3 corresponds to a VLCC with 30% reduced EEDI. Table 6.1 shows a summary of EEDI, the main engine output, the propeller revolution, and other details for Step0 and Step3.

Table 6.1: Basic concept involved in reducing EEDI

	Step0	Step3
EEDI	2.67	1.85
MCR (kW)	25,600	21,200
N_{MCR} (rpm)	76.0	61.4
Engine control	Mechanical	Electronic
Propeller diameter	Original	Large
Energy-saving devices	non	PSF + RBF
Others		ACS + LFRP(-10%)
		others (-5%)

PSF: Pre-Swirl Fin, RBF: Rudder Bulb Fin
ACS: Air Circulation System, LFRP: Low Frictional Resistance Paint

Table 6.2 shows the estimated self-propulsion factors and roughness allowance ΔC_f in addition to the designed propeller particulars. In the table, D_P denotes the propeller diameter, p denotes

the propeller pitch ratio, A_e/A_d denotes the expanded area ratio, Z denotes the number of blades, t_P denotes the thrust deduction factor, w_P denotes the wake fraction, and η_R denotes the relative rotative efficiency. The propeller was designed such that it could achieve a ship speed of 15.5 knots in the normal output (NOR) with 15 % sea margin based on the existing propeller diagram. Changes in the self-propulsion factors due to the installation of energy-saving devices were determined based on prior experience of the authors of the present study. Moreover, ΔC_f was reduced to account for the reduction in hull frictional resistance due to air bubbles.

Table 6.2: Designed propeller particulars, estimated self-propulsion factors, and ΔC_f

	Step0	Step3
D_P (m)	9.86	10.60
p	0.673	0.674
A_e/A_d	0.384	0.380
Z	4	4
$1-t_P$	0.851	0.821
$1-w_P$	0.626	0.484
η_R	1.020	1.020
ΔC_f	0.00025	0.00015

A wave-making resistance coefficient curve (C_{ws}) based on wetted surface area shown in Fig. 6.1. The horizontal axis corresponds to the Froude number F_{nwl} based on the length waterline L_{wl}. The Hughes formula was used to predict the frictional resistance coefficient, and the form factor K was assumed as 0.40. Thus, the wave resistance coefficient and the form factor were same for Step0 and Step3 given that the hull form was the same.

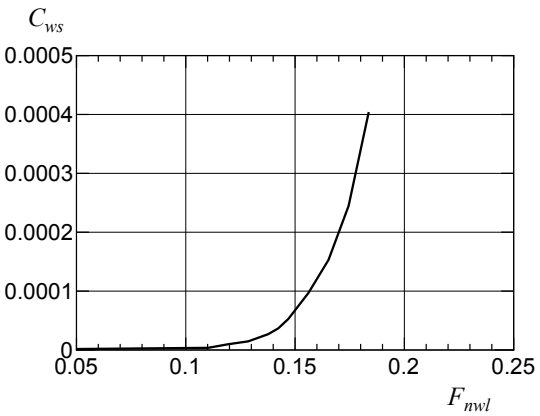

Figure 6.1: Wave-making resistance coefficient curve

Fig. 6.2 shows the BHP curves of Step0 and Step3 versus the ship speed. The transmission efficiency was assumed as 0.97. A significant reduction in the engine output of Step3 was observed due to the improvements in the EEDI.

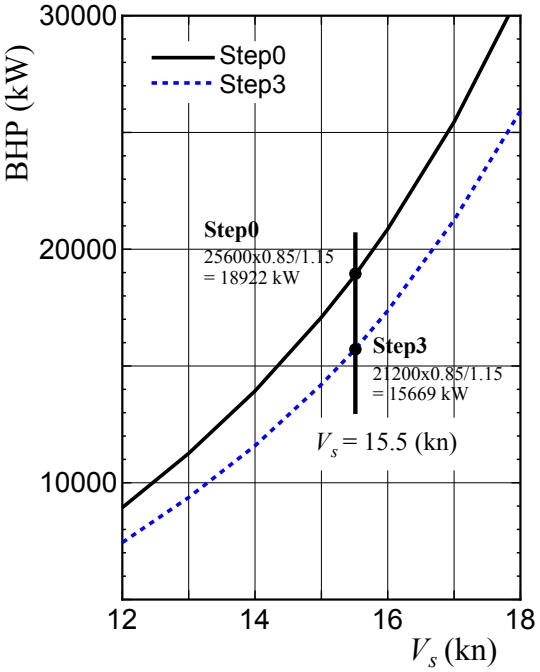

Figure 6.2: Estimated BHP curves

6.2 Outline of the maneuvering simulation

Maneuvering simulations are carried out in Step0 and Step3 [38, 46]. The detailed treatments of the simulations are described as follows:

- The maneuvering simulation used in this study based on the MMG model as explained in Chapter 2.
- Wave-induced steady forces in irregular waves (denoted as subcript W), and the wind forces (denoted as subcript A) are predicted with the same conditions as those in Section 5.2.2 and Section 5.2.3 correspond to the full load condition.
- The engine and propeller particulars according to Section 6.1 together with the torque limit model as mentioned in Section 2.5. Fig. 6.3 shows the torque limit lines for Step0 and Step3.

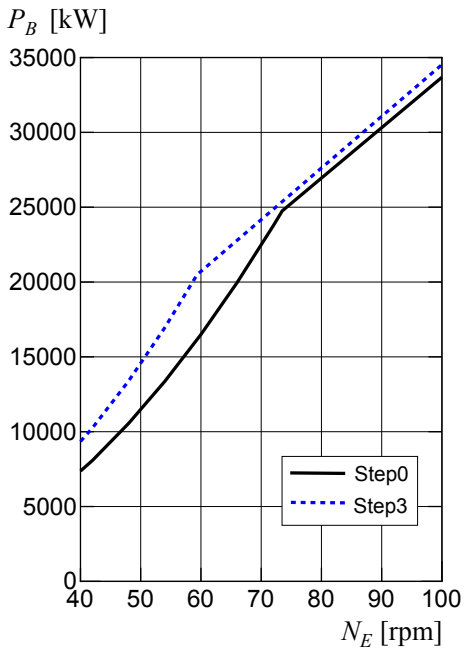

Figure 6.3: Torque limit lines for Step0 and Step3

- Hydrodynamic force coefficients on maneuvering examined in a previous study Ref. [38, 46] are used to perform maneuvering simulations for both Step0 and Step3.
- In this study, the environmental parameters in wind and wave conditions are set based on the Beaufort scale (BF) 7 to 9 as shown in Table 5.3

In the simulation, The initial approach speed U_0 corresponded to 15.5 knots (full load and even keel condition) for Step0 and Step3. The rudder steering rate is 2.34°/s in fullscale, and the radius of yaw gyration is $0.25L$.

6.3 Maneuvering in still water

6.3.1 Turning

A comparison of turning trajectories between Step0 and Step3 with $\delta = \pm 35°$ as shown in Fig. 6.4. Table 6.3 shows a comparison of turning indexes, advances (A_D), and tactical diameters (D_T). The turning radius increases in Step3 when compared with that of Step0, and A_D and D_T increased 14% and 12%, respectively, as the averaged value of port and starboard turning.

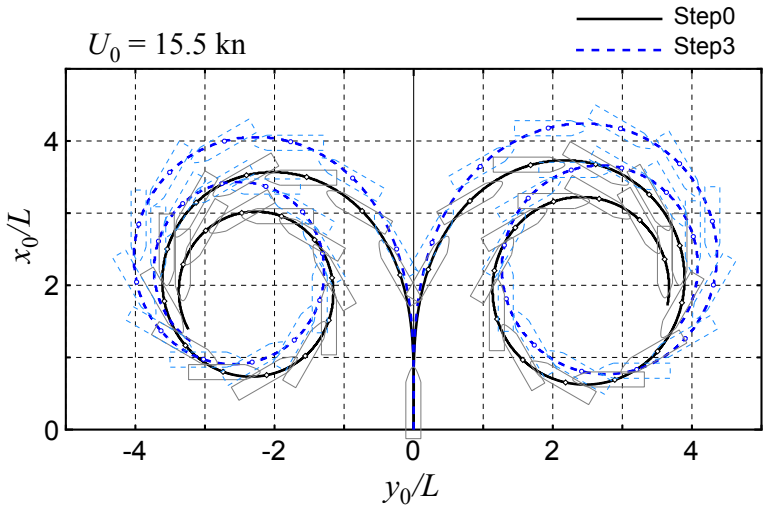

Figure 6.4: A comparison of the turning trajectories in still water (δ=±35 deg)

Table 6.3: A comparison of turning indexes

	$\delta = 35°$		$\delta = -35°$	
	A_D/L	D_T/L	A_D/L	D_T/L
Step0	3.67	3.83	3.50	3.54
Step3	4.18	4.29	3.99	3.95
IMO criterion	4.50	5.00	4.50	5.00

Fig. 6.5 shows a comparison of the time histories of the ship speed (u), yaw rate (r), hull drift angle (β), rudder normal force F_N and propeller thrust T during turning with $\delta = 35°$. In the figure, u slightly increases in Step3 since the ship resistance decreases due to the effect of energy efficiency devices. With the engine output reduced, the propeller thrust (T) in Step3 is smaller than those of Step0. As a result, the rudder normal force (F_N) of Step3 become decreases, and this is the reason for the deterioration in the turning performance. The time history of F_N in

Step3 was smaller than that in Step0 at the peak that appeared immediately after steering and the steady turning condition; this is due to the low propeller load that resulted from the small engine output. Although the turning performance worsened in Step3, the turning indexes (A_D, D_T) still satisfied the IMO maneuvering criteria [15] as shown in Table 6.3. Thus, the turning performance of Step3 still at a safe condition level.

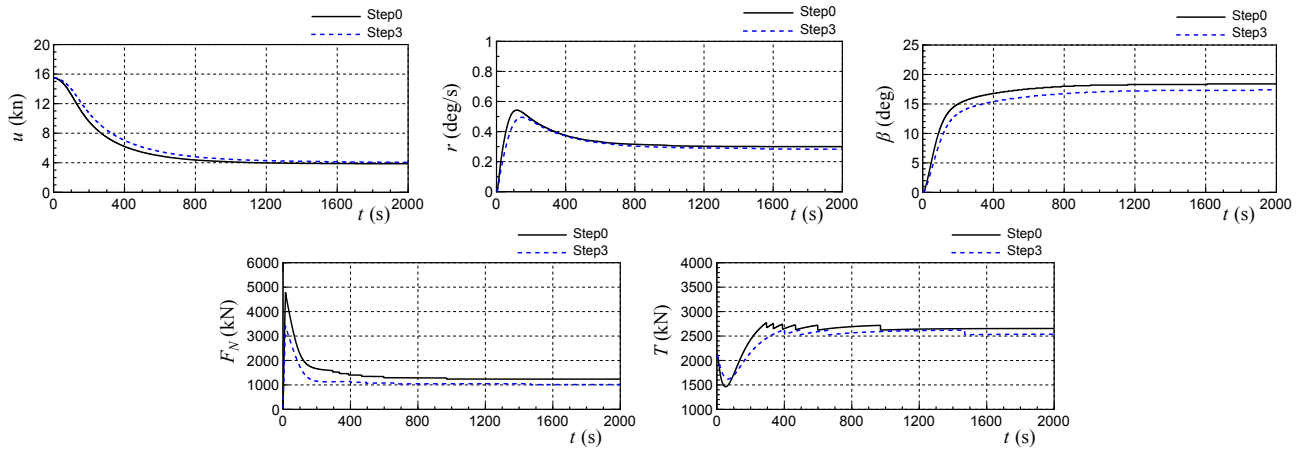

Figure 6.5: Comparison of time histories of ship speed u, yaw rate r, drift angle β, rudder normal force F_N and propeller thrust T during turning in still water ($\delta = 35°$)

6.3.2 Zig-zag maneuvers

Fig. 6.6 shows the time histories of heading angle ψ and rudder angle δ in $10/10$ and $-10/-10$ zig-zag maneuvers in still water. Additionally, Figure 6.7 shows the time histories of ψ and δ during $20/20$ and $-20/-20$ zig-zag maneuvers. A comparison of time histories of the ship speed (u), yaw rate (r), hull drift angle (β) and rudder normal force (F_N) during zig-zag maneuvers shown in Fig. 6.6 and Fig. 6.7. The steering timing of Step3 was slower than that of Step0, and this implied that the response of Step3 had worsened. Tables 6.4 and 6.5 show the comparison of overshoot angle (OSA) during the zig-zag maneuvers. The OSA of Step3 is larger than that of Step0, and the course stability evidently worsened. The averaged value of the 1st OSA in the port and starboard side increased by 23 % in Step3, and the averaged value of 2nd OSA also increased by 43%. However, the zig-zag maneuvering performance is not at a potentially problematic level since the IMO maneuvering criterion [15] is fulfilled in Step3.

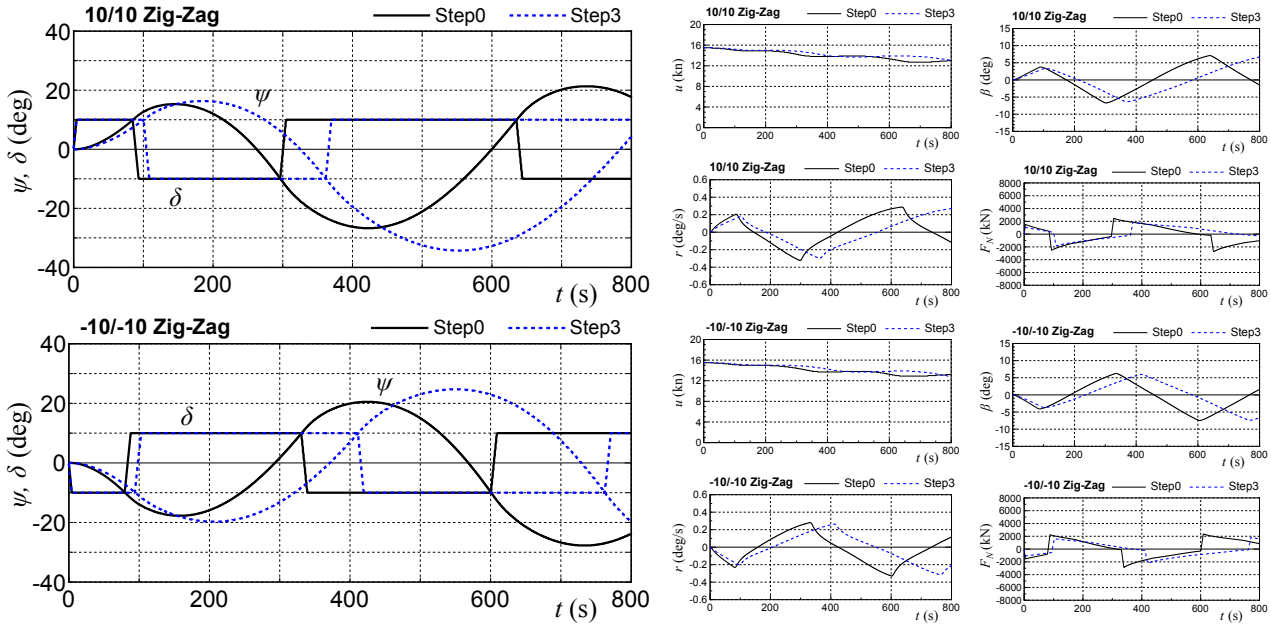

Figure 6.6: Comparison of time histories of the heading angle (ψ) and rudder angle (δ) in still water (left: 10/10 zig-zag, right: -10/-10 zig-zag)

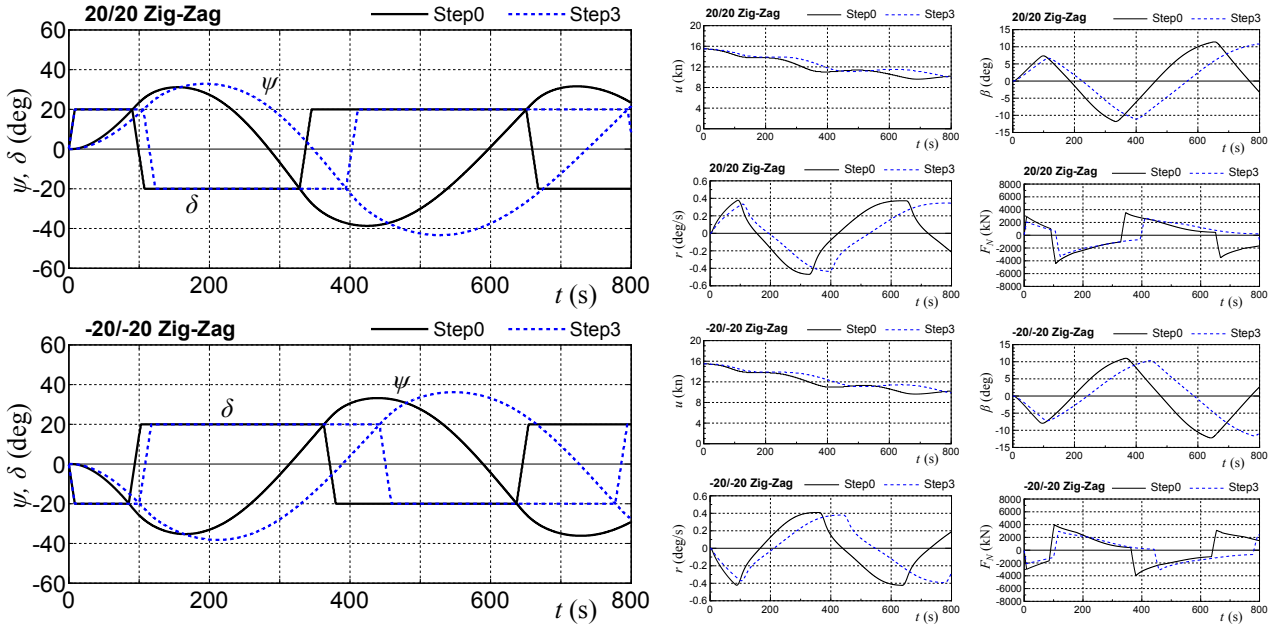

Figure 6.7: Comparison of time histories of the heading angle (ψ) and rudder angle (δ) in still water (left: 20/20 zig-zag, right: -20/-20 zig-zag)

Table 6.4: Comparison of the overshoot angle of 10/10 and -10/-10 zig-zag maneuvers in still water

	10/10 zig-zag		-10/-10 zig-zag	
	1st OSA (°)	2nd OSA (°)	1st OSA (°)	2nd OSA (°)
Step0	5.3	16.7	7.8	10.5
Step3	6.3	24.3	9.7	14.7
IMO criterion	20.0	40.0	20.0	40.0

Table 6.5: Comparison of the overshoot angle of 20/20 and -20/-20 zig-zag maneuvers in still water

	20/20 zig-zag		-20/-20 zig-zag	
	1st OSA (°)	2nd OSA (°)	1st OSA (°)	2nd OSA (°)
Step0	11.2	18.7	15.3	13.2
Step3	12.9	23.4	18.2	16.2
IMO criterion	25.0	–	25.0	–

6.4 Maneuvering in adverse conditions

6.4.1 Steady state sailing conditions

In this section, the autopilot condition is set the same as those in previous Section 5.4.1. The ship course was set to be $\psi = 0°$. Fig. 6.8 shows the longitudinal component of the ship speed (denoted as u), hull drift angle (denoted as β), and check helm (denoted as δ) in the steady state sailing condition under wind and waves.

As expected, a significant decrease in speed occurred with the increase in the BF scale. The speed decrease for Step3 was slightly larger than that for Step0 with respect to head waves. With respect to the head waves of BF9, u was less than 8 knots in both Step0 and Step3, and the propeller revolution (n_P) decreased due to the restriction placed by the torque limit as shown in Fig. 6.3. Thus, the torque limit line model employed in this study worked well with the propeller revolution control. The β and the absolute value of δ increased with the increase in the BF scale. With respect to BF9, the maximum β approximately 2.9° in Step0 and approximately 3.2° in Step3, and the minimum δ approximately $-7.3°$ in Step0 and approximately $-10.6°$ in Step3. The maximum β and the absolute value of minimum δ were slightly larger in Step3. The largest β occurred at approximately $\chi = 75°$, and the smallest δ occurred at approximately $\chi = 90°$. This tendency was the same for both Step0 and Step3.

The drift angle and check helm were not very large in both Step0 and Step3, and the ship speeds reached approximately 6 knots in head wind and waves until BF9, even though the torque-rich occurs.

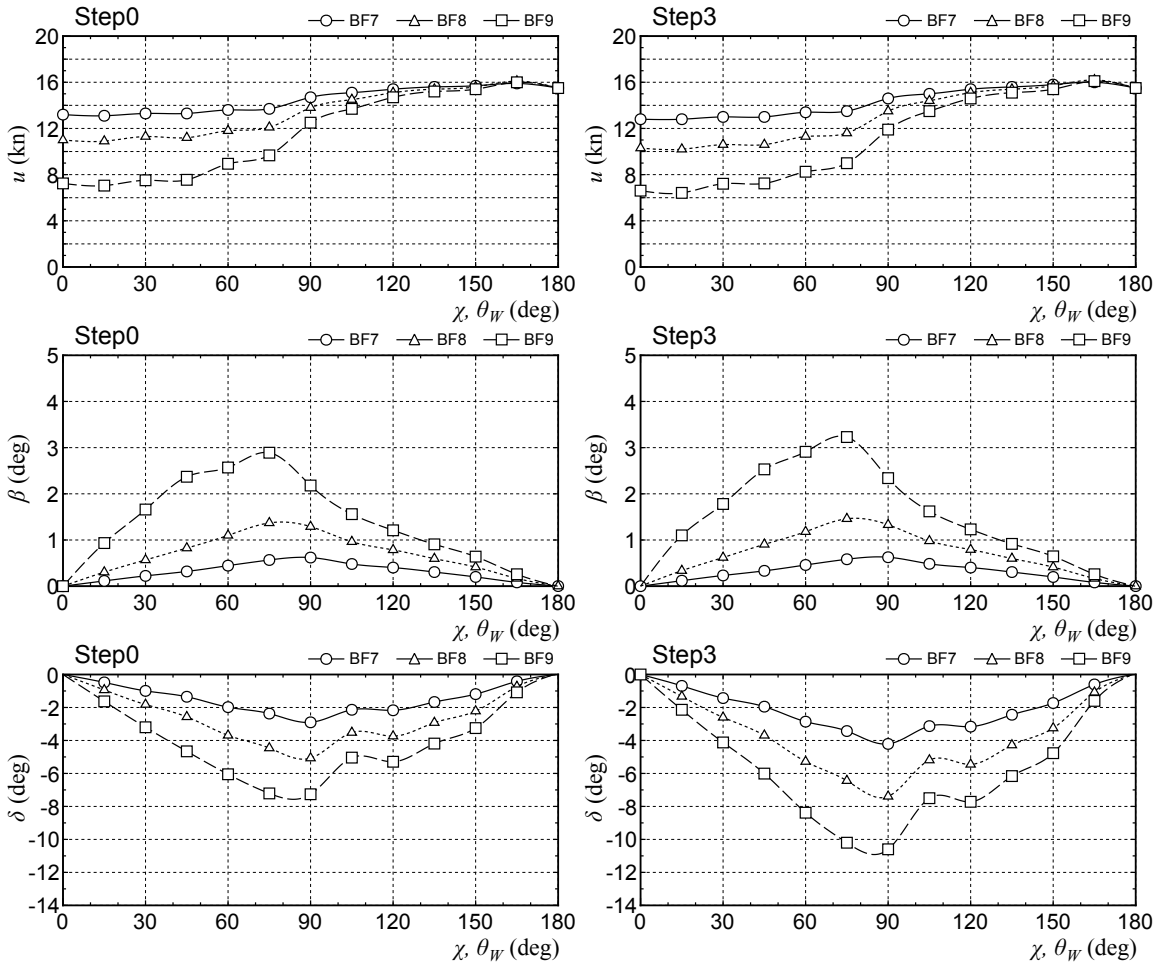

Figure 6.8: Comparison of ship speed (u), drift angle (β) and check helm (δ) in wind and waves

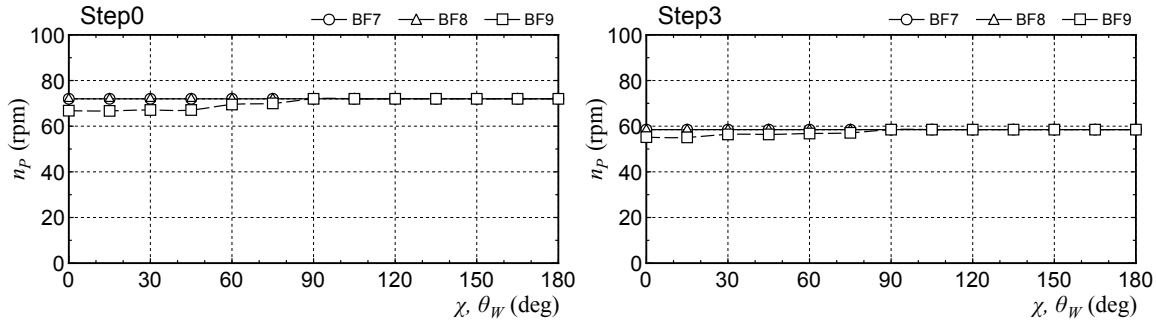

Figure 6.9: Comparison of propeller revolution (n_P) in wind and waves

6.4.2 Course changing ability

Course changing simulations are carried out by steering the rudder angle $\delta = 20°$ in wind and waves. Fig. 6.10 shows a comparison of ship trajectories in BF7, BF8 and BF9. The direction of the wind and waves changed to $\chi = 0°$, $30°$ and $60°$. The steady state speed is shown in

Fig. 6.8 is used as an approach speed in the simulation. A course change with a significant speed decrease is observed in BF9 since the situations involved the bow wind and waves. Fig. 6.11 shows a comparison of the non-dimensional values of advance A_D and transfer T_R in the course changing with respect to the BF scale for the three different wave (wind) directions. It should be noted that "SW" shown in the horizontal axis of the figure denotes the still water. The results of A_D and T_R are smaller in Step0 when compared to those in Step3. Thus, Step0 indicated better maneuverability than Step3. This was because Step0 had a better turning performance in still water when compared with that of Step3 as discussed in Section 6.3.1. However, the difference between the trajectories (or A_D and T_R) for Step0 and Step3 clearly decreased when the BF scale is large.

Fig. 6.12 shows time histories of the rudder normal force (F_N), the lateral force acting on the ship by the wind and waves ($Y_A + Y_W$), and the ratio ($F_N/(Y_A + Y_W)$) during course changing. Specifically, $F_N/(Y_A + Y_W)$ denotes a ratio of the rudder normal force to the lateral force acting on the ship hull due to external disturbances such as wind and waves. A greater value of $F_N/(Y_A + Y_W)$ indicates higher rudder effectiveness with respect to external disturbances. Additionally, F_N of Step0 exceeded that of Step3 for both BF7 and BF9, and this tendency was the same as the result in still water as shown in Fig. 6.5. The difference of $Y_A + Y_W$ between Step0 and Step3 was small since the wind forces and the wave-induced steady forces were the same for both Step0 and Step3 in principle. As a result, $F_N/(Y_A + Y_W)$ of Step0 exceeded that of Step3, and this tendency became significant in BF7. In contrast, with respect to BF9, the difference of $F_N/(Y_A + Y_W)$ between Step0 and Step3 decreased. This is because $Y_A + Y_W$ showed a more significant increase in BF9 than the others. Thus, it could be interpreted that the difference in the rudder force between Step0 and Step3 decreased due to the presence of large external lateral forces in terms of the strong wind and waves such as BF9. Thus, the course changing performance of Step3 became similar to that of Step0 with respect to strong external disturbances, although the turning performance of Step3 is worse in still water.

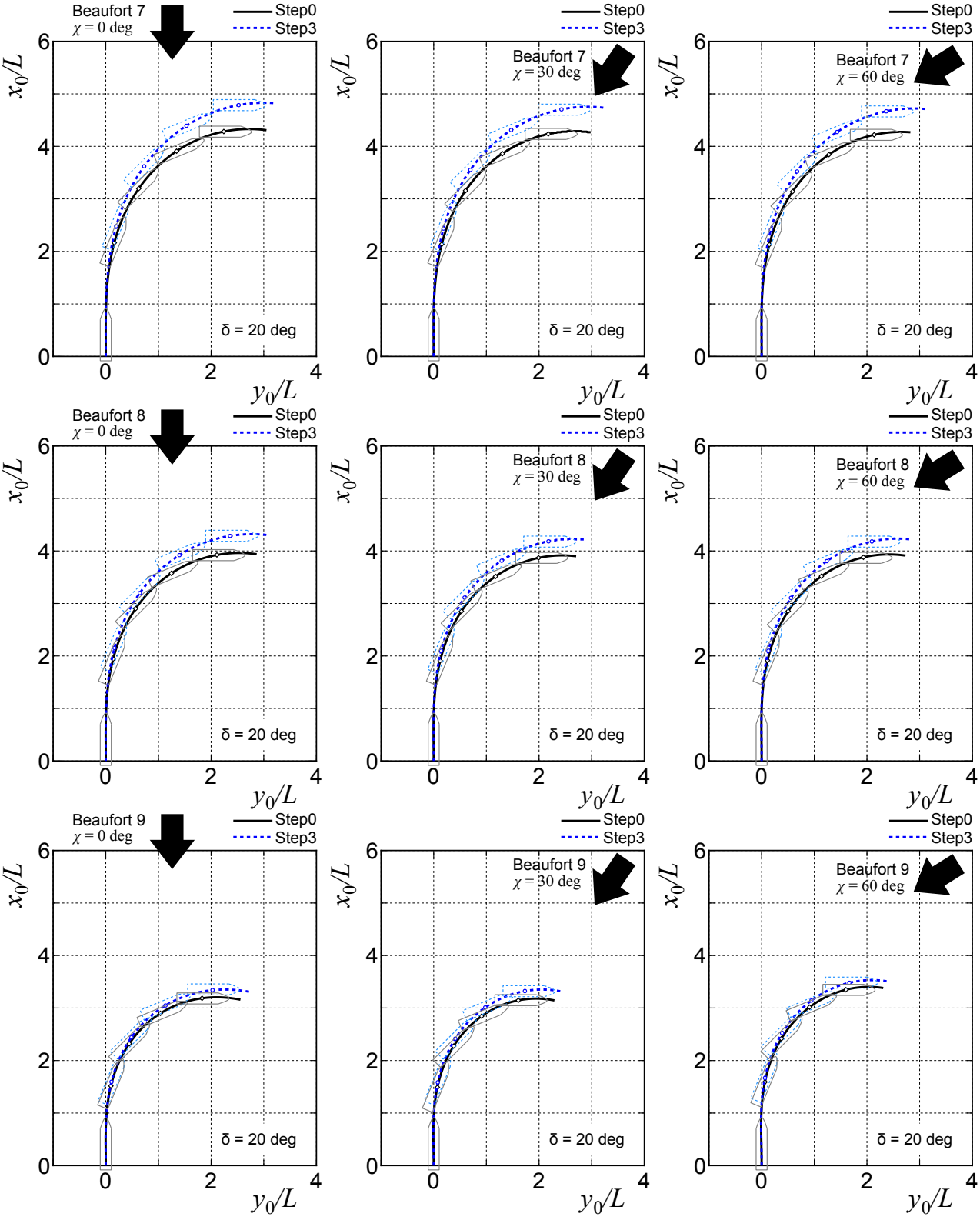

Figure 6.10: Comparison of ship trajectories for course changing in wind and waves

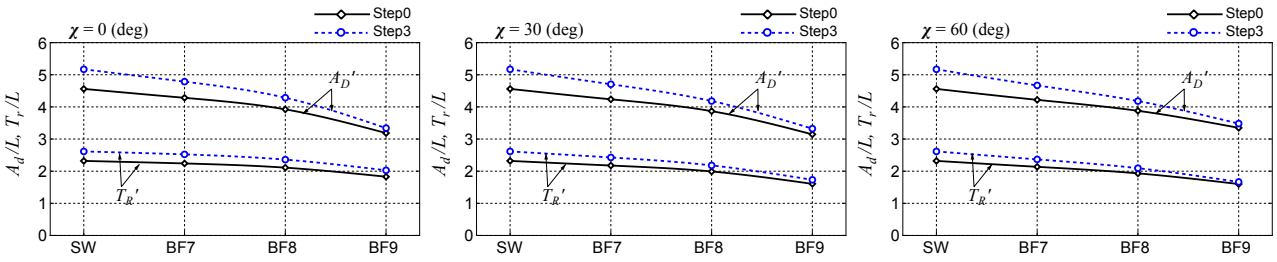

Figure 6.11: Comparison of A_D and T_R in wind and waves ($\delta = 20\,\mathrm{deg}$)

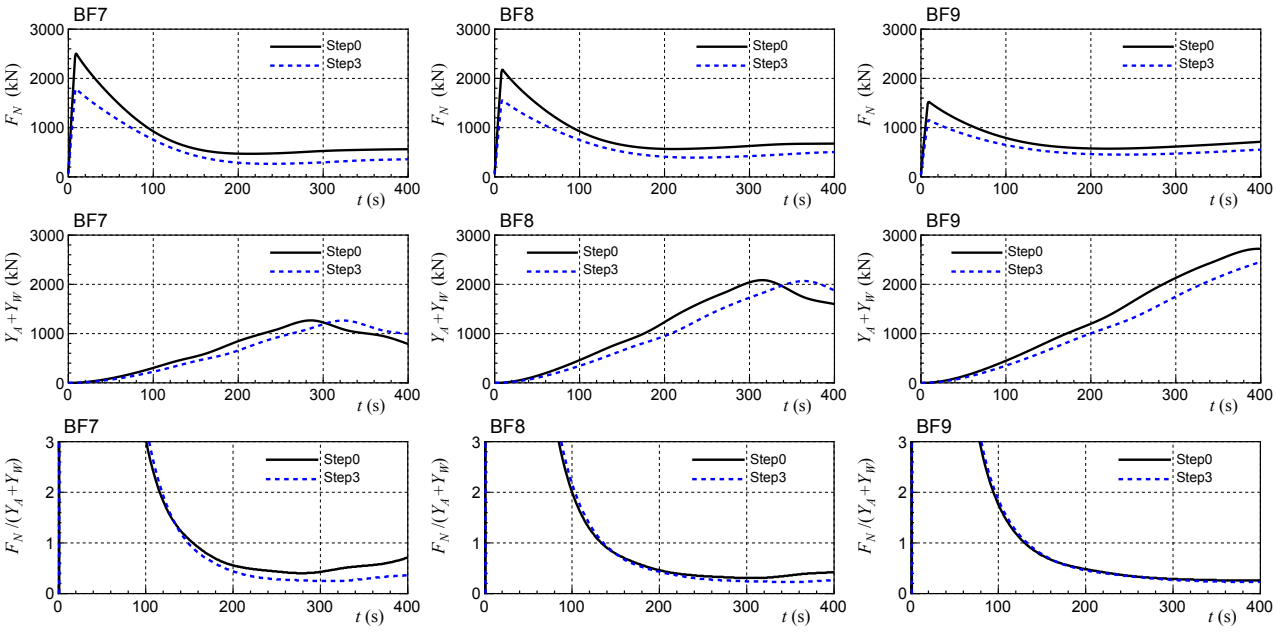

Figure 6.12: A comparison of the rudder normal force (F_N), lateral force due to wind and waves ($Y_A + Y_W$), and ratio of F_N to $Y_A + Y_W$ during course changing ($\chi = 0$, $\delta = 20\,\mathrm{deg}$)

6.5 Concluding remarks

This chapter applied an MMG-based maneuvering simulation method (Chapter 2) to investigate the maneuverability of a VLCC in still water and adverse weather conditions. A conventional VLCC in full load condition (Chapter 5) has been replaced by proposing a VLCC with 30% reduced EEDI together with energy efficiency devices and a propeller with a large-diameter and low-revolution. The engine output of the VLCC with 30% reduced EEDI (Step3) evidently reduced when compared with that of a conventional VLCC (Step0). The presented results show the impacts of minimum power on the maneuverability of the ships in still water and adverse weather conditions, and answer the third question in Section 1.3:

How does the engine output effect on ship maneuvering performance?

Conclusions of this chapter are drawn as follows:

- In Step3, both the turning radius and the overshoot angles of the zig-zag maneuver in still water increase with improved EEDI when compared with those of Step0. By reducing the engine output, the rudder normal force decreased due to the low propeller load. Although the maneuverability worsened in Step3, the turning indexes and the overshoot angles satisfied the IMO maneuvering criteria[15, 16].

- The steady state sailing performance of Step3 in adverse weather conditions is worse than that of Step0. Specifically, speed drop, hull drift angle, and check helm of Step3 are slightly large.

- The course changing ability of Step3 also worsened in adverse weather conditions. However, the difference in the trajectories of Step0 and Step3 clearly reduced when the BF scale is large. This is because the difference of the rudder force between Step0 and Step3 decreased due to the presence of large external lateral forces in the strong wind and waves. Hence, the course changing performance of Step3 was at a similar level to that of Step0 in the presence of strong external disturbances.

In Chapter 6, the effect of engine output are primarily analyzed on ship maneuverability. In the simulations, problems that not comply with the IMO maneuvering criteria does not occur even though the engine output reduced in Step3. This is because the subject ship (Step0) initially possessed good maneuverability as discussed in Chapter 5, and there is a sufficient margin for the IMO criteria. However, there could be a possibility in which the maneuverability worsened until an unacceptable level is reached in terms of navigational safety by reducing the rudder force due to a small main engine output. Therefore, further research is suggested to improve the performance of maneuverability in Step3. The attachment of a high lift rudder considerably is an effective way to improve the ship maneuvering performance. Moreover, some aspects should be considered to choose a proper rudder such as the high lift rudder force, the rudder impacts on the resistance and maneuvering ability, and the efficiency of the rudder in related with the rudder construction and the maintenance cost. Thus, the high lift rudder is proposed for improving the maneuverability of the VLCC with a 30% reduction in EEDI (equivalent 19% reduced-engine output), and to be discussed in Chapter 7.

Chapter 7

Improvement of Maneuverability of a Large Tanker by a High Lift Rudder

As reviewed in Chapter 6, the reduction of engine output of a VLCC generates in decreasing the rudder force due to low propeller load. This condition has consequences in which maneuverability worsened in still water and adverse weather conditions. Therefore, it is necessary to advance the maneuvering performance of a VLCC with low powered engine output. This chapter involved performing an improvement in the maneuverability of a VLCC with small engine output under a condition with 30% reduced EEDI (Step3) by attaching a high lift rudder as an extension of a previous study in Chapter 6. Thus far, extant studies did not investigate the effect of a high lift rudder on the maneuverability of a ship in adverse weather conditions with respect to small engine output. In this Chapter, the discussion of the impact of a high lift rudder on maneuverability refers to the work of Zaky et. al [48], and it is systematically explained as follows; Section 7.1 proposes a new design of high lift rudder with a fishtail section and end plates to increase the rudder force under a restriction that minimized the rudder resistance increase. The new rudder is termed as a HL rudder and the original mariner rudder is termed as a MN rudder. Section 7.2 describes the captive model test by using a scaled ship model (model length: 2.909 m) to capture the propulsive performance and rudder force characteristics of a ship with MN and HL rudders. The incorporation of the test results into

the MMG simulation model (Chapter 2) led to the performance of maneuvering simulations in still water and adverse weather conditions for a VLCC with a HL rudder (Step3_{HL}) and MN rudder (Step3_{MN}). Section 7.3 presents the maneuvering simulations in both still water and adverse weather for a VLCC in Step3 with a MN rudder and HL rudder. For the purposes of comparison, maneuvering simulations are also performed for Step0 with a MN rudder. It should be noted that the prediction accuracy of the simulation method was confirmed by performing a comparison with free-running test results [37, 35]. At last, Section 7.4 draws the conclusions of this chapter.

7.1 Design of a high lift rudder

A rudder design necessitates the consideration of certain aspects such as working conditions, parameters (area, thickness, span, and aspect ratio), sectional shape, structural arrangement, and hydrodynamic interactions (among hull, propeller, and rudder). Significantly, the selection of the parameters and sectional shape impact ship maneuverability [3]. Existing studies [22, 25, 24] indicate that a special rudder with a fishtail section produced a larger rudder force and smaller turning indexes when compared to those of a mariner rudder. A rounded leading edge and a fishtail trailing edge were employed as the sectional shape of the present HL rudder. Additionally, slipstream guide plates fitted to top and bottom of the rudder are used. The plates increased the lift gradient, and it was experimentally investigated by Tachi and Endo [28]. Fig. 7.1 shows the profiles of MN and HL rudders in a fullscale. Table 7.1 shows the principal particulars of MN and HL rudders. In the table, H_R denotes span of the rudder, B_R denotes averaged chord of the rudder, Λ denotes the aspect ratio, A_R denotes rudder area including the horn, and $A_R/(Ld)$ denotes rudder area ratio. The rudder area of the HL rudder is approximately 30% less than that of MN rudder. Its aim involves reducing the rudder resistance of the HL rudder. With a reduction in the rudder area of HL rudder, it is expected to minimize the rudder torque, although the rudder torque in HL rudder may be increased due to fishtail section and end plates effect. Additionally, thinner thickness with a taper was employed in the HL rudder to reduce the rudder resistance since a thinner profile generally exhibits a better propulsive performance when compared to a thicker profile. Fig. 7.2 shows photographs of two

rudders for the ship model used in the tank tests. The MN rudder incorporates a rudder horn that provides housing for a pintle to support the rudder, and otherwise, the HL rudder does not possess a horn.

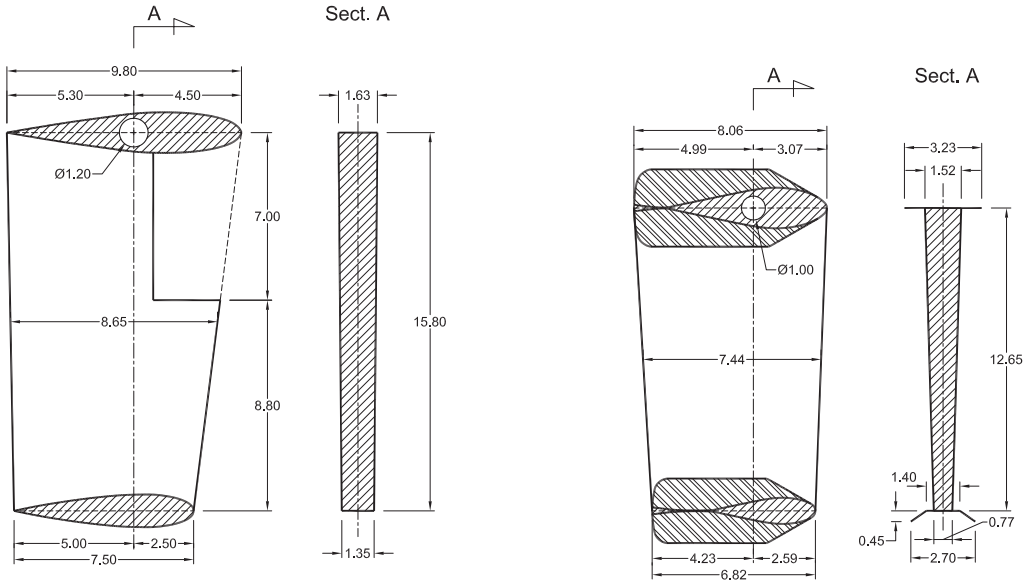

Figure 7.1: Rudder profiles (left: MN rudder, right: HL rudder), units in meter

Table 7.1: Principal particulars of two rudders

	MN rudder	HL rudder	remarks
H_R (m)	15.80	12.65	
B_R (m)	8.65	7.44	including the horn part for MN rudder
Λ	1.83	1.70	including the horn part for MN rudder
A_R (m^2)	136.67	94.12	including the horn area for MN rudder
$A_R/(Ld)$	1/48.7	1/70.7	

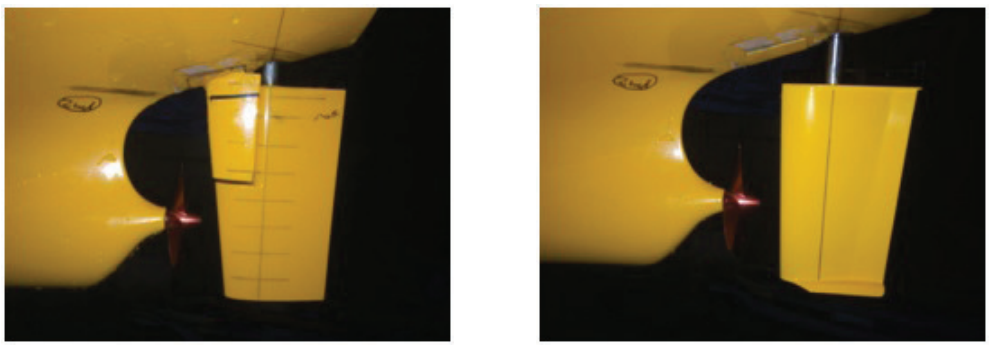

Figure 7.2: Layout of the rudder (left: MN rudder, right: HL rudder)

7.2 Tank Test

In order to capture the propulsive performance and rudder force characteristics of the ship with MN and HL rudders, tank tests were performed in the Hiroshima University Towing Tank (length: 100 m, width: 8 m, depth: 3.5 m) by using a scaled ship model (model length: 2.901 m, scale ratio 1/110) as shown in Fig. 7.3.

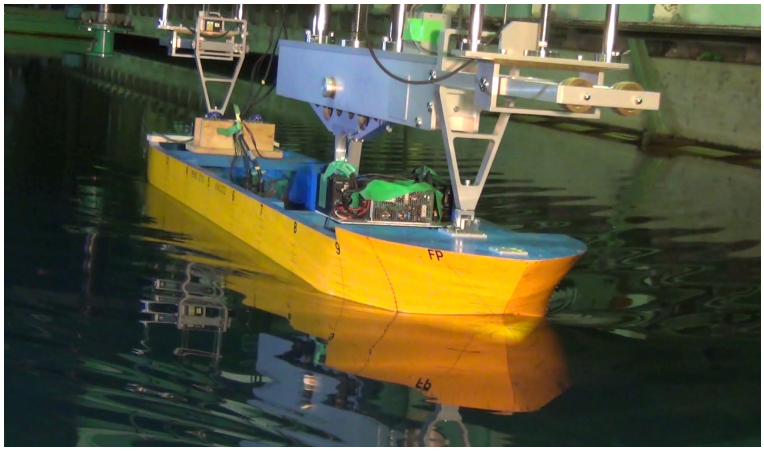

Figure 7.3: Self propulsion test

7.2.1 Propulsive performance

Self-propulsion tests were conducted for a ship model with MN and HL rudders after completing propeller open test using a stock propeller model with 90 mm in the diameter and resistance tests by using the same ship model without a rudder. Therefore, the effect of rudder difference was captured by the difference in the self-propulsion factors such as thrust deduction factors (t_P), wake fraction (w), and relative rotative efficiency (η_R). Subsequently, the hull efficiency (η_H) was predicted by $(1-t_P)/(1-w_s)$ of the full-scale ship where w_s denotes the wake fraction in full-scale.

Table 7.2: Self-propulsion factors and hull efficiency at $V_s = 15.5$ kn

	$1-t_P$	$1-w_s$	η_R	η_H
MN rudder	0.694	0.534	1.018	1.300
HL rudder	0.727	0.552	1.014	1.316

Fig. 7.4 shows the self-propulsion factors and the hull efficiency. The horizontal axis corresponds

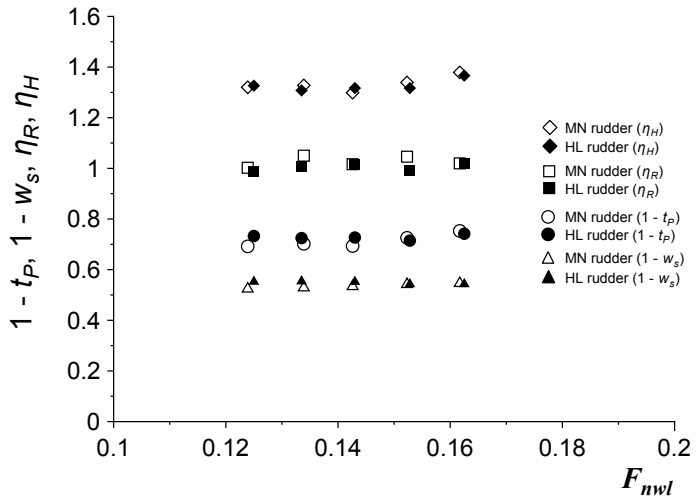

Figure 7.4: Self-propulsion test results

to the Froude number F_{nwl} based on the length waterline L_{wl}. Table 7.2 shows a comparison of the self-propulsion factors between MN and HL rudders at a service speed (V_s) of 15.5 knots (equivalent to $F_{nwl} = 0.141$). The ratio of wake fraction in fullscale w_s to the model w is assumed as 0.85. A high lift rudder (HL rudder) was attached, and $(1 - t_P)$ increases to approximately 5% when compared to that of the MN rudder, $(1-w_s)$ increases by approximately 4%, η_R decreases by approximately 1%, and η_H increases by approximately 1%. The difference is small. The designed HL rudder is significantly reasonable to minimize the increase in rudder resistance.

7.2.2 Characteristics of Rudder forces

Additionally, 'the rudder force test in straight moving' was performed to capture rudder force characteristics. In the test, the lateral force (Y) and yawing moment around the midship (N_m) acting on a ship hull and rudder normal force (F_N) were measured when a ship moved in a straight manner while maintaining a certain rudder angle δ. In the test, the rudder angle (δ) was changed from $-35°$ to $35°$ with an interval corresponding to $5°$. Fig. 7.5 shows the rudder force test results for both MN and HL rudders under a propeller loading condition with $n_P = 17.2$ rps and ship model speed $U = 0.76$ m/s (equivalent to 15.5 kn in fullscale). This condition is termed as the model point. The forces (Y and F_N) and moment (N_m) are non-dimensionalized

by $(1/2)\rho LdU^2$ and $(1/2)\rho L^2dU^2$, respectively, where ρ denotes water density. The absolute values of Y', N'_m, and F'_N increase linearly with increases in δ in the range of $-20°$ to $20°$. Inclinations of Y', N'_m, and F'_N relative to the δ for the HL rudder increase when compared to those for the MN rudder. Thus, Y' and N'_m are expressed as follows:

$$\left.\begin{aligned} Y' &= Y'_\delta\delta \\ N'_m &= N'_\delta\delta \end{aligned}\right\} \tag{7.1}$$

where Y'_δ denotes rudder force derivative, and N'_δ denotes turning moment derivative. Table 7.3 shows the derivatives determined based on the measured data in the range of $-20°$ to $20°$. When compared to the absolute value of the MN rudder, the absolute value of Y'_δ increases by 10% in HL rudder, and the absolute value of N'_δ increases by approximately 8%. Thus, a rudder force increase of 8-10% was confirmed with respect to the HL rudder as expected.

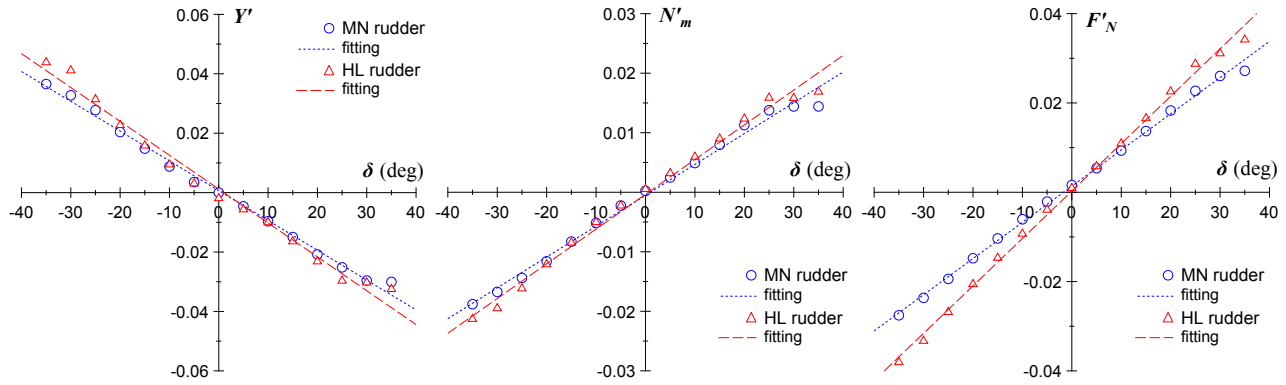

Figure 7.5: Lateral force coefficient acting on a ship hull (Y'), yawing moment coefficient around the midship (N'_m) and rudder normal force coefficient (F'_N) in the rudder force test versus rudder angle δ

Table 7.3: Rudder force and moment coefficients

	MN rudder	HL rudder
Y'_δ	-0.0571	-0.0626
N'_δ	0.0315	0.0339

In contrast, F'_N at the same δ increase by approximately 30% with respect to the HL rudder, and the increase ratio is significantly different from the results of Y' and N'_m. In order to clarify the reason, the measured data were analyzed based on the MMG model [37]. According to the

MMG model, Y' and N'_m are expressed as follows:

$$\left.\begin{aligned} Y' &= -(1+a_H)F'_N\cos\delta \\ N'_m &= -(x'_R+a_H x'_H)F'_N\cos\delta \end{aligned}\right\} \tag{7.2}$$

where a_H denotes the rudder force increase factor, x'_R denotes the non-dimensionalized longitudinal coordinate of rudder position (normaly, $x'_R \simeq -0.5$), and x'_H denotes the non-dimensionalized longitudinal coordinate of the acting point of the additional lateral force component induced by steering. $(1+a_H)$ is determined as an inclination of Y' relative to $-F'_N\cos\delta$, and $(x'_R+a_H x'_H)$ is also determined as an inclination of N' relative to $-F'_N\cos\delta$ as shown in Fig. 7.6. Table 7.4 shows $(1+a_H)$ and $(x'_R+a_H x'_H)$ of the MN and HL rudders. Furthermore, $(1+a_H)$ decreases by approximately 16% in HL rudder and the absolute value of $(x'_R+a_H x'_H)$ decreases by approximately 17% when compared to those of the MN rudder. The effective rudder force in HL rudder is reduced by approximately 16-17% due to the hull-rudder interaction effect although the absolute value of F'_N increases by approximately 30%. Hence, the increase ratio of the effective rudder force with respect to the HL rudder actually approximately corresponds to 1.09 ($\simeq 1.30\times(1-0.16)$). The order of magnitude approximately coincides with the increase ratio of Y'_δ or N'_δ as previously mentioned. This potentially because the HL rudder is incorporated with the horn although MN rudder is not as shown in Fig. 7.1. Therefore, the lift force acting on the horn part is not considered for F'_N of MN rudder. Conversely, $(1+a_H)$ or $(x'_R+a_H x'_H)$ increases with the additional lift force.

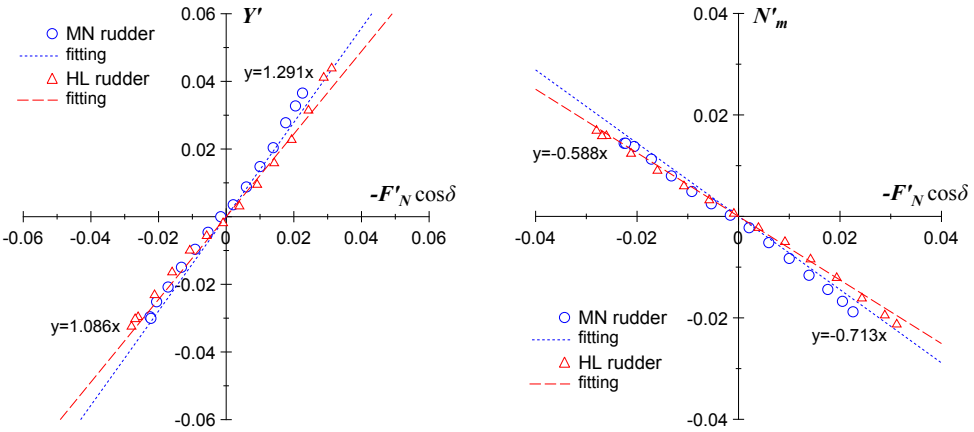

Figure 7.6: Analysis results with respect to the hull and rudder interaction coefficients

Table 7.4: Hull and rudder interaction coefficients

	MN rudder	HL rudder
$1 + a_H$	1.291	1.086
$x'_R + a_H x'_H$	-0.713	-0.588

7.2.3 Course stability

To observe a difference of course stability of the ship with MN and HL rudders, the course stability criterion C in still water is compared. The criterion C is expressed as follows:

$$C = Y_v^{G*\prime} N_r^{G*\prime} - [Y_r^{G*\prime} - (m' + m'_x)] N_v^{G*\prime} \tag{7.3}$$

The ship becomes stable when $C > 0$ and unstable when $C < 0$. Here, $Y_v^{G*\prime}$, $Y_r^{G*\prime}$, $N_v^{G*\prime}$ and $N_r^{G*\prime}$ denote the non-dimensionalized linear hydrodynamic derivatives on maneuvering, and m' and m'_x are the non-dimensionalized mass and added mass, respectively. The derivatives correspond to the center of gravity as converted from a midship point and include the effect of propeller and rudder, and are expressed as follows:

$$\left.\begin{aligned} Y_v^{G*\prime} &= Y_v{}' - k_Y u'_R \gamma_R \\ Y_r^{G*\prime} &= Y_r{}' - Y_v{}' x'_G - k_Y u'_R \gamma_R \ell'_R \\ N_v^{G*\prime} &= N_v{}' - Y_v{}' x'_G + k_N u'_R \gamma_R \\ N_r^{G*\prime} &= N_r{}' - Y_r{}' x'_G - (N_v{}' - Y_v{}' x'_G) x'_G + k_N u'_R \gamma_R \ell'_R \end{aligned}\right\} \tag{7.4}$$

$$\left.\begin{aligned} k_Y &= -Y'_\delta / u'^2_R \\ k_N &= N'_\delta / u'^2_R \end{aligned}\right\} \tag{7.5}$$

where u'_R is non-dimensionalized longitudinal inflow velocity component to the rudder, and assumed to be 1.0. γ_R is the flow straightening coefficient, and ℓ'_R is non-dimensional effective longitudinal coordinate of rudder position in formula of the effective inflow angle to rudder in maneuvering motions. The last term of Eq.(7.4) represents the rudder effect. The difference

between MN and HL rudders in the linear derivatives appears as a change of k_Y and k_N. As shown in Eq.(7.5), k_Y and k_N are equivalent to the rudder force and moment coefficients (Y'_δ, N'_δ). Table 7.5 shows the calculation results of k_Y and k_N, the linear derivatives and C for a ship with MN and HL rudders. The hydrodynamic derivatives and parameters required for the calculation of C except Y'_δ and N'_δ have been shown in Ref. [37]. Y'_δ and N'_δ were indicated in Table 7.3. The C in MN rudder (Step3_{MN}) is -0.002 and HL rudder (Step3_{HL}) is -0.001. Thus, it confirmed that the ship with HL rudder is slightly more stable for course keeping. However, the difference is small.

Table 7.5: Hydrodynamic coefficients and C

	MN rudder	HL rudder
k_Y	0.057	0.063
k_N	0.032	0.034
$Y_v^{G*\prime}$	-0.345	-0.347
$Y_r^{G*\prime}$	0.115	0.117
$N_v^{G*\prime}$	-0.110	-0.108
$N_r^{G*\prime}$	-0.059	-0.060
C	-0.002	-0.001

7.3 Maneuvering simulations

7.3.1 Simulation outlines

In the maneuvering simulations of fullscale ship with the HL rudder, the initial approach speed U_0 corresponds to 15.5 knots (navigation full condition), the rudder steering rate corresponds to 2.34°/s, and the radius of yaw gyration corresponds to $0.25L$. The engine and propeller used are the same as those in the ship with MN rudder together with the torque limit model, with referring to Step0 in Chapter 6. Propeller revolution n_P is assumed to be constant except a case over the restrictions placed by the torque limit. MMG model as explained in Chapter 2 is used for the maneuvering simulations. Wave drift forces and wind forces are predicted with the same conditions as those used in Chapter 6. The hydrodynamic treatments in the simulations are summarized as follows:

- A 30% increase in the rudder normal force (F_N) is used for the simulations based on the test result indicated in Section 7.2.
- Given the a_H and x'_H, the measured values as shown in Table 7.4 are used
- With the exception of F_N, a_H, and x'_H, the hydrodynamic parameters used are the same as those of the ship in full load condition (DF) as presented in Table 5.2, and.
- The environmental parameters are set based on the Beaufort scale 7-9 as shown in Table 5.3.

7.3.2 Turning in still water

In the simulation, Step0 denotes a conventional VLCC, and Step3_{MN} and Step3_{HL} denote a VLCC with a MN rudder and a HL rudder, respectively, under a condition with 30% reduced EEDI.

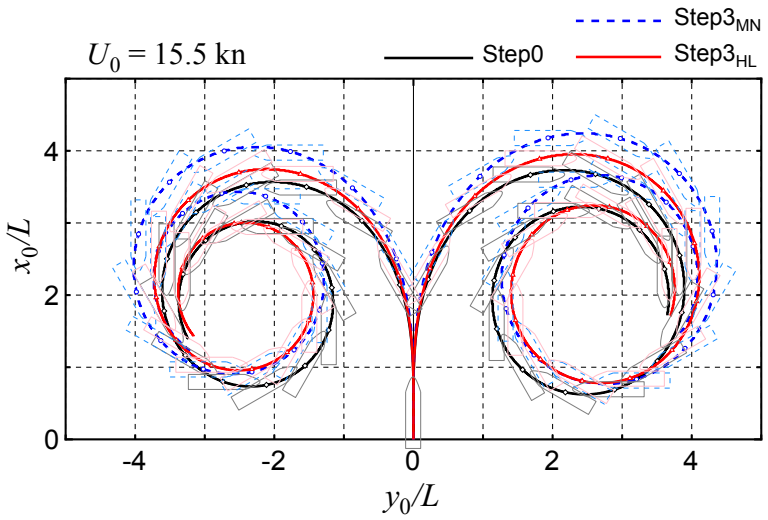

Figure 7.7: A comparison of turning trajectories in still water ($\delta = \pm 35°$)

Table 7.6: A comparison of turning indexes

	$\delta = 35°$		$\delta = -35°$	
	A_D/L	D_T/L	A_D/L	D_T/L
Step3_{MN}	4.18	4.29	3.99	3.95
Step3_{HL}	3.89	4.04	3.68	3.65
Step0	3.67	3.83	3.50	3.54
IMO criteria	4.50	5.00	4.50	5.00

Fig. 7.7 shows a comparison of turning trajectories between Step0, Step3_{MN}, and Step3_{HL} given a rudder angle of $\pm 35°$. Table 7.12 shows a comparison of turning indexes such as advances (A_D) and tactical diameters (D_T). When compared to Step0, the turning radius in Step3_{MN} increases, and A_D and D_T increase by 14% and 12%, respectively, and correspond to the averaged value of port and starboard turning.

The reduction in the rudder normal force (F_N) of Step3 causes the deterioration in the turning performance. This is due to the low propeller load that results from the small engine output. When compared to Step3_{MN}, the turning radius in Step3_{HL} decreases, and A_D and D_T decrease by approximately 7% as the average values of port and starboard turning, respectively. Thus, a significant improvement of the turning performance is confirmed by attaching the high lift rudder. The turning indexes (A_D, D_T) in Step3_{HL} satisfy the IMO maneuvering criteria [15, 16] with a sufficient margin although they slightly exceed those in Step0. The turning performance of Step3_{HL} is not at a potentially problematic level.

7.3.3 Zig-zag maneuvers in still water

Fig. 7.8 shows the time histories of heading angle ψ and rudder angle δ in 10/10 and $-10/-10$ zig-zag maneuvers in still water. Additionally, Fig. 7.9 shows the time histories of ψ and δ during 20/20 and $-20/-20$ zig-zag maneuvers. To confirm the effect of HL rudder during zig-zag maneuvers, a comparison of rudder normal force (F_N) between MN and HL rudders is also shown in Figs. 7.8 and 7.9. Step3_{HL} has the larger absolute values of F_N than Step3_{MN} at the time of rudder angle changes from port side to starboard side and vice versa, and is close to the Step0 in all cases. This indicates that HL rudder produces a larger lift force than MN rudder as expected.

Tables 7.7 and 7.8 depict a comparison of overshoot angle (OSA) during the zig-zag maneuvers. The OSAs of Step3_{MN} exceed those of Step0, and the course stability evidently worsens. The average value of the 1st OSA in 10/10 and -10/-10 zig-zag maneuvers increases by 23% in Step3_{MN}, and the average value of 2nd OSA also increases by 43%. The reduction in the rudder normal force (F_N) led to an increase in the OSAs as mentioned in Section 7.3.2. Conversely,

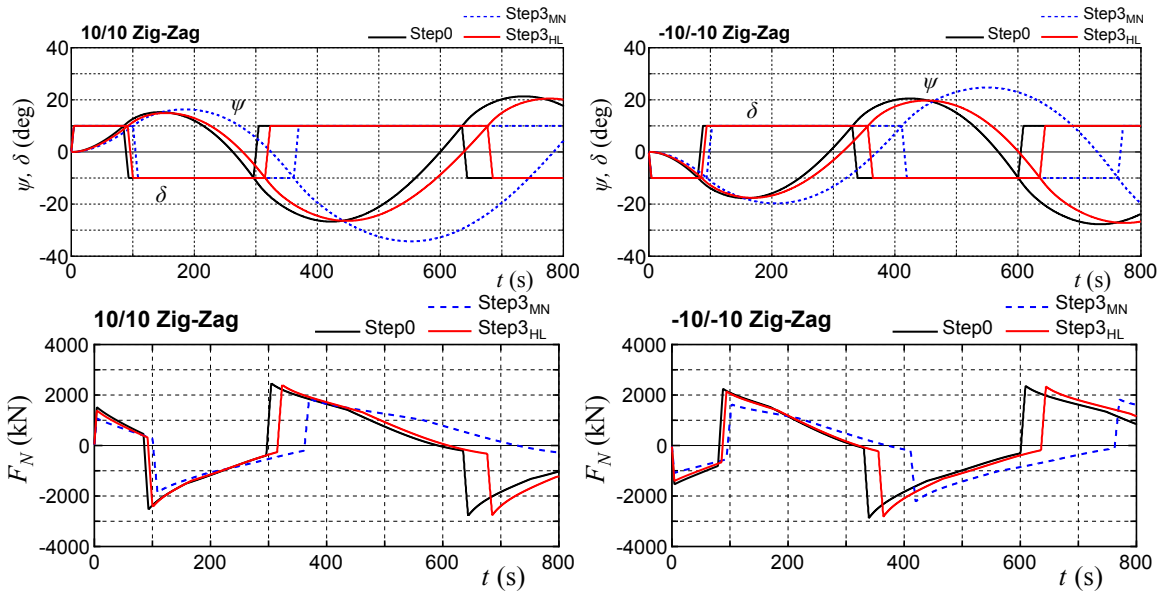

Figure 7.8: A comparison of time histories of heading angle (ψ), rudder angle (δ), and rudder normal force (F_N) in still water (left: 10/10 zig-zag, right: -10/-10 zig-zag)

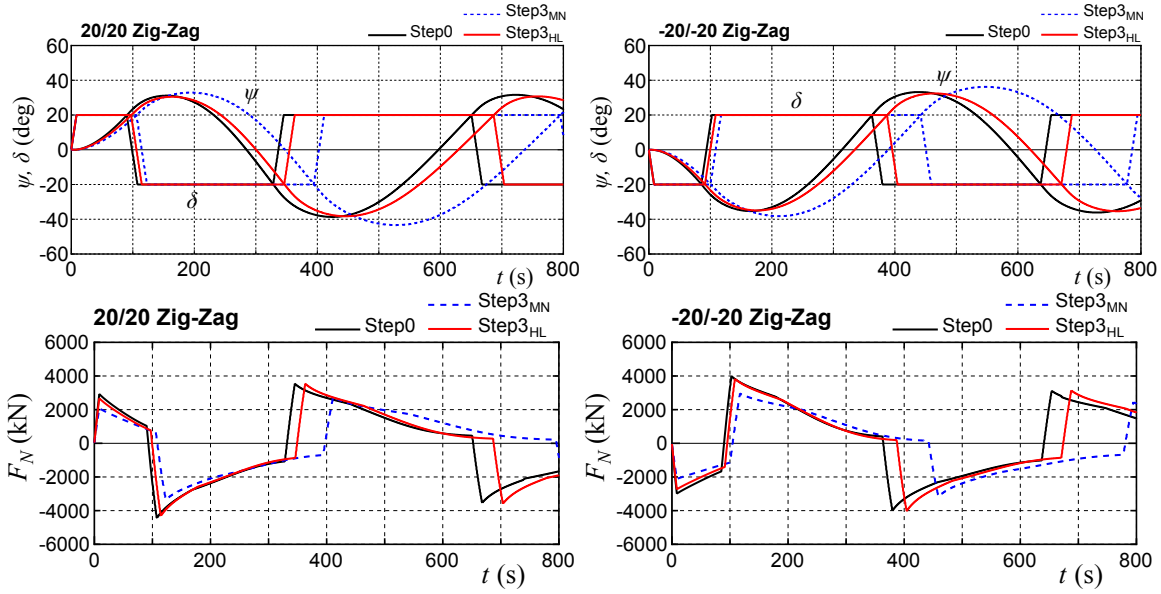

Figure 7.9: A comparison of time histories of heading angle (ψ), rudder angle (δ), and rudder normal force (F_N) in still water (left: 20/20 zig-zag, right: -20/-20 zig-zag)

the OSA in Step3_{HL} is smaller than that of Step3_{MN}. The average value of the 1st OSA in 10/10 and -10/-10 zig-zag maneuvers decreases by 22% in Step3_{HL}, and the average value of 2nd OSA also decreases by 33%. The high lift rudder is useful in significantly reducing the OSAs in zig-zag maneuvers. It should be noted that the IMO maneuvering criterion [15, 16] is fulfilled in all the cases.

Table 7.7: A comparison of overshoot angle of 10/10 and -10/-10 zig-zag maneuvers in still water

	10/10 zig-zag		-10/-10 zig-zag	
	1st OSA (°)	2nd OSA (°)	1st OSA (°)	2nd OSA (°)
Step3_{MN}	6.3	24.3	9.7	14.7
Step3_{HL}	4.9	16.4	7.6	9.7
Step0	5.3	16.7	7.8	10.5
IMO criteria	20.0	40.0	20.0	40.0

Table 7.8: A comparison of overshoot angle of 20/20 and -20/-20 zig-zag maneuvers in still water

	20/20 zig-zag		-20/-20 zig-zag	
	1st OSA (°)	2nd OSA (°)	1st OSA (°)	2nd OSA (°)
Step3_{MN}	12.9	23.4	18.2	16.2
Step3_{HL}	10.5	18.3	14.9	12.4
Step0	11.2	18.7	15.3	13.2
IMO criteria	25.0	–	25.0	-

7.3.4 Steady state sailing conditions in adverse weather conditions

A ship traveling with a propeller revolution in the design speed is considered under wind and waves using the auto-pilot. In the auto-pilot, the PD control is applied with a proportional gain corresponding to 5.0 and a differential gain corresponding to 20.0 s. The adverse conditions in the simulation correspond to the environmental parameters (wind and waves) which were based on Beaufort scale as mentioned in Table 5.3.

Fig. 7.10 shows the longitudinal component of the ship speed (denoted as u), hull drift angle (denoted as β), and check helm (denoted as δ) in the steady state sailing condition under wind and waves for Step3_{MN} and Step3_{HL}. In the figure, additional lines are inserted to connect the calculation results for purposes of distinction. A significant decrease in speed occurs with an increase in the BF scale. The speed decreases in Step3_{HL} are almost the same as those in Step3_{MN}. In $\chi_0 = 0°$ of BF9, u is less than 8 knots for both, and the propeller revolution decreases due to the restrictions placed by the torque limit. The β and the absolute value of δ increase with increases in the BF scale. The largest β occurs approximately at $\chi_0 = 75°$, and the smallest δ occurs approximately at $\chi_0 = 90°$. This tendency is the same for both Step3_{MN} and Step3_{HL}. In BF9, the maximum β approximately corresponds to 3.2°, and is

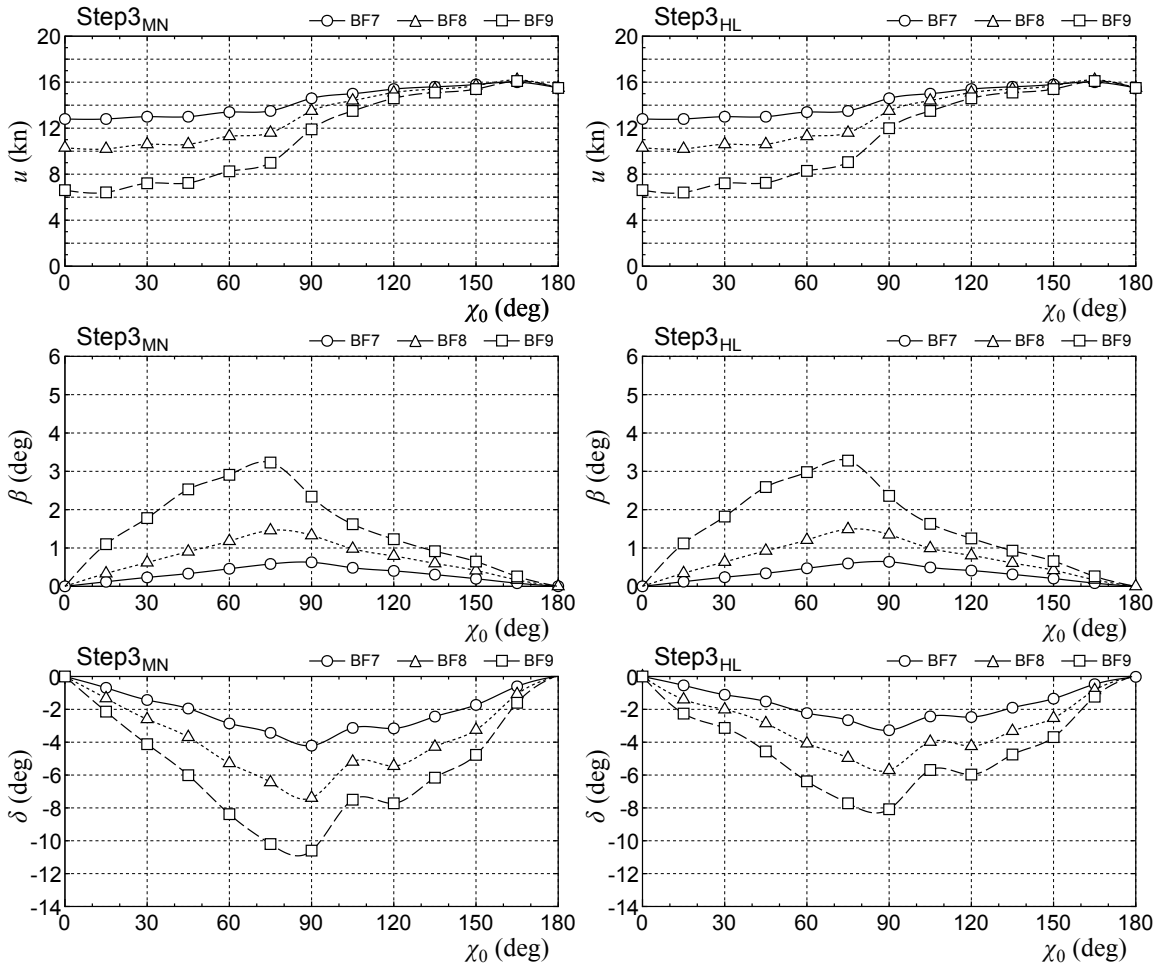

Figure 7.10: A comparison of ship speed (u), drift angle (β,) and check helm (δ) in wind and waves

almost identical in both Step3_{MN} and Step3_{HL}. The minimum δ approximately corresponds to $-8.1°$ in Step3_{HL} and $-10.6°$ in Step3_{MN}. Thus, the check helm of Step3_{HL} is smaller than that of Step3_{MN}. The HL rudder is effective in reducing the check helm in adverse weather conditions.

7.3.5 Course changing ability in adverse weather conditions

Course changing simulations are performed by steering the rudder angle, $\delta = 20°$, in wind and waves. Fig. 7.11 shows a comparison of ship trajectories in BF7, BF8 and BF9. The direction of the wind and waves changes to $\chi = 0°$, $30°$, and $60°$. The steady state speed is shown in Fig. 7.10 is used as an approach speed in the simulation. A course change with a significant speed decrease is observed in BF9 since the situations involved bow wind and waves.

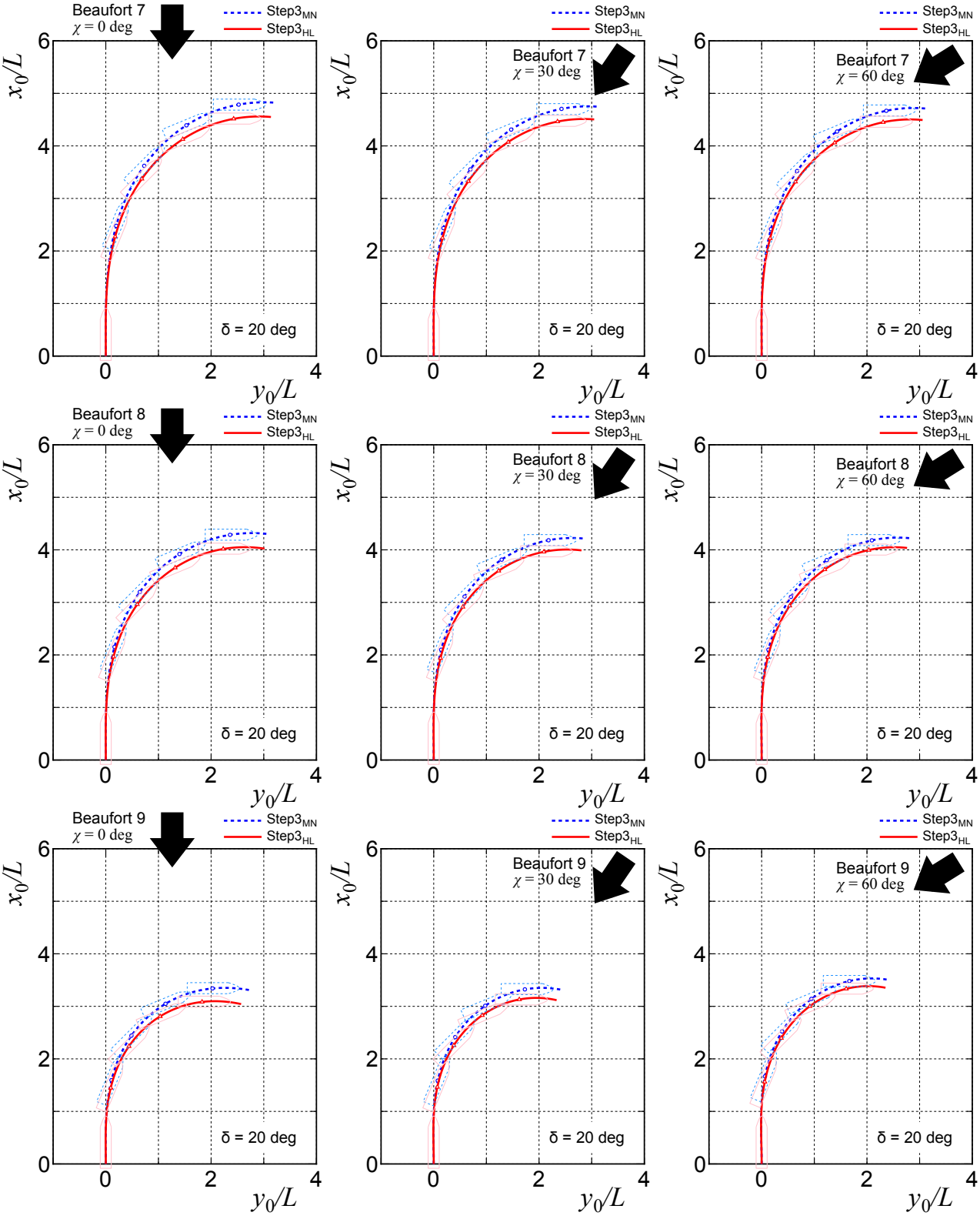

Figure 7.11: Comparison of ship trajectories for course changing in wind and waves

Fig. 7.12 shows a comparison of the non-dimensional values of advance A_D and transfer T_R in the course change with respect to the BF scale for the three different wave (wind) directions. It should be noted that "SW" shown in the horizontal axis of the figure denotes still water.

Additionally, A_D and T_R in Step3$_{\mathrm{HL}}$ are smaller than those in Step3$_{\mathrm{MN}}$. Thus, Step3$_{\mathrm{HL}}$ indicates better maneuverability when compared to Step3$_{\mathrm{MN}}$. This is because Step3$_{\mathrm{HL}}$ indicates a better turning performance in still water when compared to Step3$_{\mathrm{MN}}$ as discussed in Section 7.3.2.

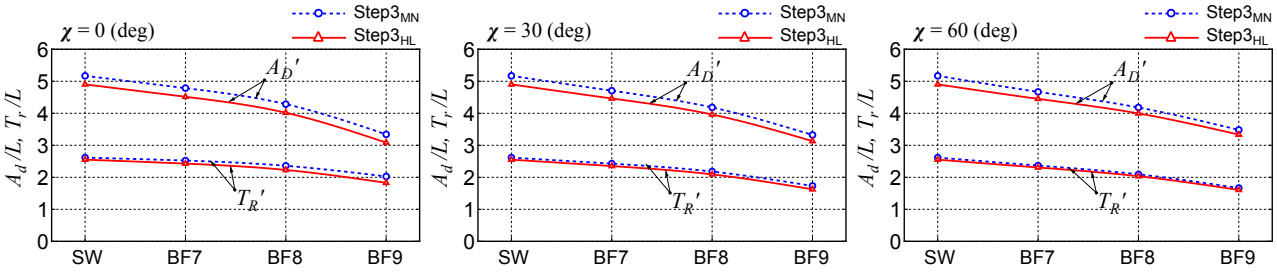

Figure 7.12: Comparison of A_D and T_R in wind and waves ($\delta = 20°$)

7.4 Conclusions

An improvement of maneuverability of a VLCC with small engine output under a condition with 30% reduced EEDI has been performed by attaching a high lift rudder. First, a high lift rudder (HL rudder) with fishtail section and end plates was newly designed to increase the rudder force under a restriction that involved minimizing the rudder resistance increase. The rudder area including horn was reduced by approximately 30% when compared to the original mariner rudder (MN rudder). The tank tests confirmed that the designed HL rudder increased the effective rudder force to approximately 10% with a few delivered power increases when compared to those of MN rudder. Subsequently, time-domain simulations based on the MMG model [37] were conducted for a fullscale ship with HL and MN rudders to investigate the effect of the high lift rudder on the maneuvering motions in still water as well as the steady state sailing condition and course changing ability in adverse weather conditions. The impacts of a high lift rudder on the maneuverability of a large tanker in still water and adverse weather conditions have been presented in this chapter. As summary, this chapter answers the fourth question in Section 1.3:

How does the high lift rudder effect of improving ship maneuverability under a small main engine output?

Conclusions of this chapter are drawn as follows:

1. Advance A_D and tactical diameter D_T decreased to approximately 7% as the averaged value of port and starboard turning with a rudder angle of $\pm 35^\circ$ in still water.

2. The averaged 1st overshoot angle (OSA) in 10/10 and -10/-10 zig-zag maneuvers decreased by 22%, and the averaged 2nd OSA also decreased by 33%.

3. The check helm reduced by approximately 25% in adverse weather conditions, and a better course changing ability was confirmed in all the wind and wave directions.

Thus, the results indicated that a high lift rudder is useful in improving the maneuverability of the VLCC with a 30% reduction in EEDI.

Chapter 8

Conclusions and Future Works

This thesis investigates the maneuvering performance of a large tanker in still water and adverse weather conditions. Several studies have been conducted through simulations in the previous chapters. As a concluding chapter, Section 8.1 summarizes the main findings and answers the research questions of this thesis. Section 8.2 discusses the remaining open issues and suggests the direction for future research.

8.1 Conclusions

In this thesis, the following main research question is addressed: ***How does the maneuverability of a large tanker in adverse weather conditions?*** To investigate the subject of this research, a simulation method for ship maneuvering in wind and waves has been introduced in Chapter 2. By using KVLCC2 as reference ship in Chapter 3, the present simulation method was evaluated with the model test results in Chapter 4. With the maneuvering simulation method, the effect of load conditions on the maneuvering performance of a VLCC was studied in Chapter 5. Since a VLCC in full load condition has a good maneuvering performance, the EEDI improvement through employing a small main engine output was proposed as described in Chapter 6. Further, to improve the maneuverability of a VLCC with a small main engine output under 30% reduction in EEDI, a high lift rudder with special shape was

attached as presented in Chapter 7. Following the main research question, the following four key research questions as mentioned in Section 1.3 are answered as follows:

Q1: ***What is the practical maneuvering simulation model to evaluate the ship maneuverability in adverse weather conditions?***

To resolve this question, a maneuvering simulation method should be built accurately considering the wind and waves. A simulation method in Chapter 2 was proposed to predict the maneuvering motions such as turning and zig-zag maneuvers in wind and waves. The validation study was carried out to confirm the present method as presented in Chapter 4 using a VLCC (KVLCC2) as described in Chapter 3. As the results, it was confirmed that the present method can capture the maneuvering motions in waves with the sufficient accuracy for practical purposes. Moreover, further research is required to investigate the performance of ship maneuvers in adverse weather conditions.

Q2: ***How does the effect of loading conditions on ship maneuvering performance?***

The effect of load conditions on maneuvering performance of a VLCC has been considered in design full (DF) and normal ballast (NB) as critical conditions when the ship is sailing in rough seas. By using the present maneuvering simulation method in Chapter 2 and its hydrodynamic characteristics based on MMG model, the maneuverability of a VLCC in two loading conditions (DF and NB) were investigated in still water and stormy conditions. The hydrodynamic characteristics of DF and NB were obtained from the model experiment based on MMG model. As discussed in Chapter 5, in still water, the turning performance of NB becomes worse than that of DF since ship in NB has a good course stability than DF. Zig-zag maneuvers performance of NB improved with the steering timing were faster than DF since the course stability increased. The turning indexes (A_D,D_T) and OSAs of DF and NB comply with the IMO maneuvering criteria. The steady-state sailing condition in adverse weather conditions is quite different between DF and NB: the absolute value of the check helm becomes small in NB, but the hull drift angle becomes large. The relative drift direction of the ship in turning to the wave direction is $20^\circ - 30^\circ$ in NB and DF with a rudder angle 35° and almost constant

for any wind (wave) directions. The drifting displacement in turning under NB becomes larger than that under DF at the same environmental condition. Advance A_D and tactical diameter D_T become significantly small with an increasing Beaufort scale in head wind and waves when approaching, although A_D and D_T are almost constant in following wind and waves. In beam wind and waves, the tendency depends on the plus and minus of the rudder angle. In zig-zag maneuvers, the first and second overshoot angles (OSAs) in head wind and waves become smaller than those in still water (SW), and those in following wind and waves are almost the same or become larger than those in SW. In the case of 10/10 zig-zag maneuvers of a ship in beam wind and waves, the first OSA increases compared with the value in SW, because the effective rudder angle decreases, and the second OSA decreases, because of the effective rudder angle increases. This tendency becomes opposite for $-10/-10$ zig-zag maneuvers. The effective rudder angle changes owing to the order of magnitude of the check helm in adverse weather conditions. These tendencies with respect to OSAs are the same in between DF and NB, although DF is more significant. However, the situation where the VLCC uncontrollable in DF did not occur.

Q3: ***How does the engine output effect on ship maneuvering performance?***

Further study has been performed for a VLCC in design full load condition by the employment of a small main engine output due to advances energy efficiency devices and a propeller with a large-diameter and low-revolution, as discussed in Chapter 6. The engine output of the VLCC with 30% reduced EEDI (Step3) evidently reduced when compared with that of a conventional VLCC (Step0). In still water, both the turning and zig-zag maneuvers in Step3 become worse compared to Step0. This was due to the rudder normal force decreased as a result of the engine output in Step3 reduced. The same tendency also occurs in adverse weather, the performance of Step3 in steady state sailing is worse than that of Step0, and the course changing ability also worsened. However, the discrepancy in the trajectories of Step0 and Step3 becomes small when wind and waves strong. The differences in the rudder forces between Step0 and Step3 decreased due to the presence of large external lateral forces in the high wind and waves. Thus, Step3 has a similar

level of course changing performance comparable to Step0 in the presence of the strong external disturbance.

Q4: ***How to improve the ship maneuverability under a small main engine output?***

The maneuverability of Step3 was worse than that of Step0 since the rudder force was reduced owing to the low propeller load, which resulted from the small engine output. However, problems that not comply with the IMO maneuvering criteria does not occur even though the engine output reduced in Step3. It was observed that Step3 satisfied IMO maneuvering criteria in the still water condition. In the next discussion in Chapter 7, a high lift rudder (HL rudder) has been proposed to improve the ship maneuvering performance in Step3. To minimize the rudder resistance, the rudder area of HL rudder was reduced by 30% when compared to the original mariner rudder (MN rudder). By attaching a HL rudder, both the turning radius and OSAs in still water decreased, the check helm reduced and a better course changing ability in adverse weather conditions. In general, the maneuvering performance of a VLCC with a 30% reduction in EEDI improved by attaching the HL rudder.

In summary, a brief answer to the main research question is made as the following:

A large tanker must be designed to sail safely and efficiently. A safe tanker means having a good course stability and well maneuvers in still water and adverse weather under any loading conditions. In this study, it was confirmed that a VLCC in ballast load condition is better in course stability than a VLCC in full load condition, the drifting displacement in ballast load is remarkably larger than that of full load at the same BF scale due to wind and waves per the ship mass are larger in ballast load, and the effective rudder angles changes owing to the order of magnitude of the check helm in adverse weather conditions. A tanker must be efficient that is proven by low fuel consumption to reduce CO_2 emissions with respect to the EEDI. To achieve an energy efficiency, a VLCC with a 30% reduction in EEDI is planned for the conventional VLCC in full load condition by the employment of a small main engine output owing to advances energy efficiency devices and a propeller with a large-diameter and low-rotation, etc. It was observed that the maneuverability of the VLCC with 30% reduced EEDI was worse than the conventional VLCC since the rudder force decreased due to the low propeller load. Furthermore, to improve the maneuverability of a VLCC with a small main engine output was performed by attaching a HL rudder. The results indicated that the designed HL rudder increased the effective rudder force and the HL rudder presented in this study is useful in improving maneuverability.

8.2 Future Works

Further investigations are required in the following sections. These further research directions are given in the perspectives of the degrees of freedom, the types of ships, the rudder area, and the speed effect in lateral force and yaw moment coefficients as follows:

- **Degrees of Freedom**

  As it may affect the speed and accuracy in the simulations, the required number of degrees of freedom should be considered according to the navigation conditions. For seagoing ships that frequently encounter severe wind and waves, a maneuvering simulation model with 6 Degree of Freedom (DOF) including surge, sway, yaw, heave, pitch and roll motions can give more reliable results rather than 3 DOF (surge, sway and yaw). Considering the impacts of sinkage and trim, further research with a 6 DOF can be more suitable for seagoing vessels.

- **Ship types**

  In this research, all investigations were conducted with respect to the large tanker. Thus, it is possible to directly apply the study to extend studies involving other ship types with different sizes to validate the accuracy of the present maneuvering simulation method. Hence, investigations involving other types of ships could be an interesting topic for further research.

- **Rudder area**

  HL rudder is useful in improving the ship maneuverability of a VLCC with a 30% reduction in EEDI. Although, the HL rudder does not possess a horn. As previously reviewed in Chapter 7, the effective rudder force of HL rudder increased by 10% compared to MN rudder. However, there is an open space between the bottom of the stern part and the HL rudder as drawn in Figure 7.2. Further investigations are suggested to modify the structure of the rudder by extending the rudder area of the HL rudder. Meantime, it should be kept in mind that the rudder resistance is maintained as minimum as possible. By adjusting its arrangement, it is expected to create more lift force in the HL rudder.

Additionally, Computational Fluid Dynamic (CFD) can be used to visualize the flow pattern as well as the hydrodynamic characteristics around the rudder.

- **Speed effect in lateral force and yaw moment coefficients**

  In this study, the ship speed effect on the steady lateral force and yaw moment coefficients in irregular waves ($\overline{C_{YW}}, \overline{C_{NW}}$) is negligible in view of the practical purposes. Meanwhile, the speed effect on steady lateral force and yaw moment coefficients is important for the accuracy of calculation to capture the maneuvering motions in irregular waves. Thus, the speed effect on those coefficients should be considered in the future research.

Appendix A

Appendices

A.1 Conversion of midship base and center of gravity derivatives

The non dimensionless of linear hydrodynamic derivatives of lateral force and turning moment acting on the ship hull in midship point can be written as follows:

$$\left.\begin{aligned} Y' &= Y'_v v' + Y'_r r' + Y'_\delta \delta \\ N' &= N'_v v' + N'_r r' + N'_\delta \delta \end{aligned}\right\} \tag{A.1}$$

Here, the forces Y and moment (N) are non-dimensionalized by $(1/2)\rho L d U^2$ and $(1/2)\rho L^2 d U^2$, respectively, where ρ denotes water density, L denotes ship length, d denotes ship draft, and U denotes ship speed. And if the lateral force and yaw moment correspond to the center of gravity, the notation G is attached in the equation above, it can be rewritten as

$$\left.\begin{aligned} Y'_G &= Y_v^{G'} v'_G + Y_r^{G'} r'_G + Y_\delta^{G'} \delta_G \\ N'_G &= N_v^{G'} v'_G + N_r^{G'} r'_G + N_\delta^{G'} \delta_G \end{aligned}\right\} \tag{A.2}$$

Then lateral velocity (v_G), yaw rate (r) and rudder angle (δ) component at the center of gravity are expressed as,

$$\left.\begin{aligned} v'_G &= v' + x'_G r' \\ r'_G &= r' \\ \delta_G &= \delta \end{aligned}\right\} \tag{A.3}$$

Substituting Eq.(A.3) into Eq.(A.2), then obtained

$$Y'_G = Y_v^{G'} v' + (Y_r^{G'} + Y_v^{G'} x'_G) r' + Y_\delta^{G'} \delta \tag{A.4}$$

$$N'_G = N_v^{G'} v' + (N_r^{G'} + N_v^{G'} x'_G) r' + N_\delta^{G'} \delta \tag{A.5}$$

Since Y in the midship and Y_G in the center of gravity are same, Eq.(A.4) can be expressed as,

$$Y' = Y_v^{G'} v' + (Y_r^{G'} + Y_v^{G'} x'_G) r' + Y_\delta^{G'} \delta \tag{A.6}$$

then obtained,

$$\left.\begin{aligned} Y'_v &= Y_v^{G'} \\ Y'_r &= Y_r^{G'} + Y_v^{G'} x'_G \\ Y'_\delta &= Y_\delta^{G'} \end{aligned}\right\} \tag{A.7}$$

On the other hand, there is relationship between N around the midship point and N_G around the center of gravity, $N = N_G + x_G Y$. Eq.(A.5) can be rewritten as

$$N' = (N_v^{G'} + Y'_v x'_G) v' + [N_r^{G'} + (N_v^{G'} + Y'_r) x'_G] r' + (N_\delta^{G'} + Y'_v x'_G) \delta \tag{A.8}$$

then obtained,

$$\left.\begin{aligned} N'_v &= N_v^{G\prime} + Y'_v x'_G \\ N'_r &= N_r^{G\prime} + (N_v^{G\prime} + Y'_r) x'_G \\ N'_\delta &= N_\delta^{G\prime} + Y'_v x'_G \end{aligned}\right\} \tag{A.9}$$

Combining Eq.(2.1) and the lateral force Y and yaw moment N in midship point relative to the center of gravity as expressed in Eq.(A.6) and (A.8), the following equation are obtained,

$$\left.\begin{aligned} (m' + m'_y)\dot{v}' + (m' + m'_x)u'r' + x'_G m'\dot{r}' = \\ Y_v^{G\prime} v' + (Y_r^{G\prime} + Y_v^{G\prime} x'_G) r' + Y_\delta^{G\prime}\delta \\ (I'_{zG} + x_G^{2\prime} m' + J'_z)\dot{r}' + x'_G m'\dot{v}'_m + x'_G m'u'r' = \\ (N_v^{G\prime} + Y'_v x'_G)v' + [N_r^{G\prime} + (N_v^{G\prime} + Y'_r)x'_G]r' + (N_\delta^{G\prime} + Y'_v x'_G)\delta \end{aligned}\right\} \tag{A.10}$$

Since both of sway and yaw relative to the center of gravity, then $x_G = 0$ and the maneuvering motion equations can be expressed as follows:

$$\left.\begin{aligned} (m' + m'_y)\dot{v}' + (m' + m'_x)u'r' &= Y_v^{G\prime} v' + Y_r^{G\prime} r' + Y_\delta^{G\prime}\delta \\ (I'_{zG} + J'_z)\dot{r}' &= N_v^{G\prime} v' + N_r^{G\prime} r' + N_\delta^{G\prime}\delta \end{aligned}\right\} \tag{A.11}$$

where,

$$\left.\begin{aligned} Y_v^{G\prime} &= Y'_v \\ Y_r^{G\prime} &= Y'_r - Y'_v x'_G \\ Y_\delta^{G\prime} &= Y'_\delta \\ N_v^{G\prime} &= N'_v - Y'_v x'_G \\ N_r^{G\prime} &= N'_r - Y'_r x'_G - (N'_v - Y'_v x'_G) x'_G \\ N_\delta^{G\prime} &= N'_\delta - Y'_v x'_G \end{aligned}\right\} \tag{A.12}$$

A.2 Dynamic course stability

From Eq.(A.11), we set $\delta = 0$ and the linear equation of ship maneuvering is the following:

$$\left.\begin{aligned} -Y_v^{G'}v' + (m' + m'_y)\dot{v}' - [Y_r^{G'} - (m' + m'_x)u']r' &= 0 \\ -N_v^{G'}v' - N_r^{G'}r' + (I'_{zG} + J'_z)\dot{r}' &= 0 \end{aligned}\right\} \tag{A.13}$$

Differentiating $\dot{v}_m$ and $\dot{r}$ in Eq.(A.13) by time then a linear differential equation is obtained as

$$\left.\begin{aligned} [(m' + m'_y)\tfrac{d}{dt} - Y_v^{G'}]v' - [Y_r^{G'} - (m' + m'_x)u']r' &= 0 \\ -N_v^{G'}v' + [(I'_{zG} + J'_z)\tfrac{d}{dt} - N_r^{G'}]r' &= 0 \end{aligned}\right\} \tag{A.14}$$

The general solution can be written:

$$\left.\begin{aligned} v' &= v'_1 e^{\sigma_1 t} + v'_2 e^{\sigma_2 t} \\ r' &= r'_1 e^{\sigma_1 t} + r'_2 e^{\sigma_2 t} \end{aligned}\right\} \tag{A.15}$$

Solving Eq.(A.14) for v and r by assuming A_1-A_3 and B_1-B_3, then obtained:

$$\left.\begin{aligned} (A_1\tfrac{d}{dt} + A_2)v' + (B_1)r' &= 0 \\ (A_3)v' + (B_2\tfrac{d}{dt} + B_3)r' &= 0 \end{aligned}\right\} \tag{A.16}$$

where,

$$\left.\begin{aligned} A_1 &= m' + m'_y \\ A_2 &= -Y_v^{G'} \\ A_3 &= -N_v^{G'} \\ B_1 &= -[Y_r^{G'} - (m' + m'_x)u'] \\ B_2 &= I'_{zG} + J'_z \\ B_3 &= -N_r^{G'} \end{aligned}\right\} \tag{A.17}$$

Eq.(A.16) can be rewritten in matrix form as follows,

$$\begin{vmatrix} (A_1\frac{d}{dt}+A_2) & B_1 \\ A_3 & (B_2\frac{d}{dt}+B_3) \end{vmatrix} \begin{vmatrix} v' \\ r' \end{vmatrix} = \begin{vmatrix} 0 \\ 0 \end{vmatrix} \tag{A.18}$$

Substituting Eq.(A.15) into the homogeneous differential Eq.(A.14), then obtained:

$$A\sigma^2 + B\sigma + C = 0 \tag{A.19}$$

where:

$$\left.\begin{aligned} A &= A_1B_3 \\ &= (m'+m'_y)(I'_{zG}+J'_z) \\ B &= A_1B_3 + A_2B_2 \\ &= -(m'+m'_y)N_r^{G'} - (I'_{zG}+J'_z)Y_v^{G'} \\ C &= A_2B_3 - A_3B_1 \\ &= Y_v^{G'}N_r^{G'} - [Y_r^{G'} - (m'+m'_x)u']N_v^{G'} \end{aligned}\right\} \tag{A.20}$$

Thus, the stability roots are

$$\sigma_{1,2} = \frac{-B \pm \sqrt{B^2-4AC}}{2A} \tag{A.21}$$

where the plus and minus signs of the radical refer to σ_1 and σ_1, respectively. If the real parts of σ_1 and σ_2 are negative, the solution v' and r' given by Eq.(A.15) will vanish with time and a new straight on course. In this case the ship is dynamically stable on course. On the other hand, if either σ_1 and σ_2 has a positive real part, an initial disturbance will lead to continuous increases of v' and r' (until the non linearity of the hydrodynamic reactions prevails) and the ship will be unstable in yaw. In Eq.(A.21), σ_2 is always negative and algebraically less than σ_1. Therefore, σ_1 is the critical root and is called the stability index. since $m'+m'_y$ and $I'_{zG}+J'_z$

are always large positive values, it can be concluded that:

$$A = (m' + m'_y)(I'_{zG} + J'_z) > 0 \tag{A.22}$$

and since both $(m' + m'_y)N_r^{G'}$ and $(I'_{zG} + J'_z)Y_v^{G'}$ are positive values, then B is always positive expressed as

$$B = -(m' + m'_y)N_r^{G'} - (I'_{zG} + J'_z)Y_v^{G'} > 0 \tag{A.23}$$

Moreover, since the product of $Y_v^{G'}$ and $N_r^{G'}$ are large absolute positive values, $Y_r^{G'} - (m' + m'_x)u'$ and N'_v are uncertain sign with small absolute values. Thus, the criterion for dynamic course stability is reduced to

$$C = Y_v^{G'}N_r^{G'} - [Y_r^{G'} - (m' + m'_x)u']N_v^{G'} > 0 \tag{A.24}$$

By eliminating u, the criterion C will be satisfied if

$$C = Y_v^{G'}N_r^{G'} > [Y_r^{G'} - (m' + m'_x)]N_v^{G'} \tag{A.25}$$

A.3 Effect of steering on course stability

The steering effect on the course stability was performed by considering the linearization of steering F_N in straight moving, note that $\sin\delta \simeq \delta$ and $\cos\delta \simeq 1$, the resultant rudder inflow velocity U_R is approximated to u_R and $\sin\alpha_R$ is approximated to α_R.

$$F_N = (1/2)\rho A_R u_R^2 f_\alpha \alpha_R \tag{A.26}$$

the angle α_R is expressed as

$$\alpha_R \simeq \delta - \frac{u_R}{v_R} \tag{A.27}$$

$$= \delta + \frac{U(v' + \ell'_R r')}{u_R}\gamma_R \tag{A.28}$$

where, $v_R = U\gamma_R(\beta - \ell'_R r')$ and $\beta \simeq -v'$. Substituting Eq.(A.28) into Eq.(A.26), the F_N can be expressed as

$$F_N = (1/2)\rho A_R u_R^2 f_\alpha \left[\delta + \frac{U(v' + \ell'_R r')}{u_R}\gamma_R\right] \tag{A.29}$$

Next, Eq.(A.29) non-dimensionalized by $(1/2)\rho LdU^2$ in both sides, then obtained

$$F'_N = \frac{A_R}{Ld} f_\alpha \left[u'^2_R \delta + u'_R \gamma_R (v' + \ell'_R r')\right] \tag{A.30}$$

where, $u'_R = u_R/U$. The dimensionless of lateral force and yaw moment by steering (Y'_R and N'_R) taken from MMG model [37] are expressed as

$$\left.\begin{aligned} Y'_R &= -(1 + a_H)F'_N \cos\delta \simeq -(1 + a_H)F'_N \\ N'_R &= -(x'_R + a_H x'_H)F'_N \cos\delta \simeq -(x'_R + a_H x'_H)F'_N \end{aligned}\right\} \tag{A.31}$$

Substituting Eq.(A.30) into Eq.(A.31). By considering the steering effect, the non dimensionless of lateral force and yaw moment (Y' and N') acting on the ship hull as mentioned in Eq.(A.11) can be expressed as

$$\left.\begin{aligned} Y' &= Y_v^{G'} v' + Y_r^{G'} r' - k_Y[u_R^2\delta + u'_R\gamma_R(v' + \ell'_R r')] \\ N' &= N_v^{G'} v' + N_r^{G'} r' + k_N[u_R^2\delta + u'_R\gamma_R(v' + \ell'_R r')] \end{aligned}\right\} \tag{A.32}$$

where,

$$\left.\begin{aligned} k_Y &= (1 + a_H)\frac{A_R}{Ld} f_\alpha \\ k_N &= -(x'_R + a_H x'_H)\frac{A_R}{Ld} f_\alpha \end{aligned}\right\} \tag{A.33}$$

Eq.(A.32) can be rewritten as

$$\left.\begin{aligned} Y' &= Y_v^{G*\prime} v' + Y_r^{G*\prime} r' + Y_\delta^{G\prime} \delta' \\ N' &= N_v^{G*\prime} v' + N_r^{G*\prime} r' + N_\delta^{G\prime} \delta' \end{aligned}\right\} \tag{A.34}$$

where,

$$\left.\begin{aligned} Y_v^{G*\prime} &= Y_v^{G\prime} - k_Y u'_R \gamma_R \\ Y_r^{G*\prime} &= Y_r^{G\prime} - k_Y u'_R \gamma_R \ell'_R \\ N_v^{G*\prime} &= N_v^{G\prime} + k_N u'_R \gamma_R \\ N_r^{G*\prime} &= N_r^{G\prime} + k_N u'_R \gamma_R \ell'_R \\ Y_\delta^{G\prime} &= -k_Y {u_R^2}' \\ N_\delta^{G\prime} &= k_N {u_R^2}' \end{aligned}\right\} \tag{A.35}$$

From Eq.(A.25), the criterion C which includes the effect of steering on course stability can be expressed as follows,

$$C = Y_v^{G*\prime} N_r^{G*\prime} - [Y_r^{G*\prime} - (m' + m'_x)] N_v^{G*\prime} > 0 \tag{A.36}$$

Bibliography

[1] Allianz Global Corporate and Specialty. Safety and Shipping Review 2017, *An annual review of trends and developments in ship losses and safety*, London, UK, May 2017.

[2] Australian Transport Safety Bureau. *ATSB Transport Safety Investigation Report, Marine Occurrence Investigation No. 243*, Independent Investigation Into the Grounding of The Panamian Registered Bulk Carrier Pasha Bulker on Nobbys Beach, Newcastle, New South Wales, Australia, June 2007.

[3] Bertram, V., Practical Ship Hydrodynamics. *Elsevier*, Oxford, UK, 2nd edition, 2012.

[4] Bingham, V. P. and Mackey, T. P., High-Performance Rudders-with Particular Reference to the Schilling Rudder. *Journal of Marine Technology*, SNAME, 24(4), pp.312-320, 1987.

[5] Brix, J., Manoeuvring Technical Manual. Seehafen Verlag, Hamburg, Germany, 1993.

[6] Eda, H., Falls, R., David, A, W., Ship Maneuvering Safety Studies, *SNAME Transactions*, Vol.87, pp. 229-250, 1979.

[7] Fujii, H., Tuda, T., Experimental Research on Rudder Performance (2), *J. Society of Naval Architects of Japan*, No.110, pp. 31-42, 1961. (in Japanese)

[8] Fujiwara, T., Ueno, M., and Nimura, T., Estimation of Wind Forces and Moments Acting on Ships, *J. Society of Naval Architects of Japan*, No.183 , pp.77-90, 1998. (in Japanese).

[9] Hasegawa, K., Kang, D. H., Sano, M., Nagarajan, V. and Yamaguchi, M., A Study on Improving the Course-Keeping of a Pure Car Carrier in Windy Conditions, *J. Marine Science and Technology*, Volume 11, Issue 2, pp.76-87, 2006.

[10] Hirano, M., Takashina, J., Takeshi, K. and Saruta, T., Ship Turning Trajectory in Regular Waves, *Trans. of West-Japan Society of Naval Architects*, No.60, pp.17-31, 1980.

[11] Hochkirch, K., and Bertram, V., Engineering options for more fuel efficient ships, *1st International Symposium on Fishing Vessel Energy Efficiency*, Vigo, Spain, 2010.

[12] IMO MEPC 62/24, Annex 19, Resolution MEPC.203(62), Amendments to the Annex of the Protocol of 1997 to amend the International Convention for the Prevention of Pollution from Ships, 1973, as Modified by the Protocol of 1978 relating thereto, 2011.

[13] IMO MEPC 63/23, Annex 8, Resolution MEPC.212(63), 2012 Guidelines on the Method of Calculation on the Attained Energy Efficiency Design Index (EEDI) for New Ships, 2012.

[14] IMO MEPC 65/22, Annex 16, Resolution MEPC.232(65), 2013 Interim Guideline For Determining Minimum Propulsion Power To Maintain the Manoeuvrability of Ships In Adverse Conditions, 2013.

[15] IMO MSC 76/23, Resolution MSC.137(76), Standards for Ship Manoeuvrability, Report of the Maritime Safety Committee on Its Seventy-Sixth Session-Annex 6, 2002.

[16] IMO MSC/Circ.1053, Explanatory Notes to the Standards for Ship Maneuverability, 2002.

[17] ISL Institute of Shipping Economics and Logistics, 2017. *Shipping Statistics and Market Review 2017*, Vol.61, No.3, Bremen, Germany, retrived from http://isl.org, 2017.

[18] Kashiwagi, M. et al., Hydrodynamics of Floating Bodies, *Seizan-Do Shoten*, ISBN4-425-71321-4, 2003. (in Japanese)

[19] Im, N., Kweon, S., and Kim, S. E., The Study On The Effect of Loading Condition On Ship Manoeuvrability, *Journal of The Society of Naval Architecture of Korea*, Vol. 42, pp. 105-112, 2005. (in Korean)

[20] Kijima, K., Katsuno, T., Nakiri, T., and Furukawa, Y., On The Manoeuvering Performance of A Ship With The Parameter of Loading Condition, *The Society of Naval Architecture of Japan*, Vol. 168, pp. 141-148, 1990.

[21] Kijima, K., Nakiri, Y., Furukawa, Y., Hori, T., and Aoki, I., On a Study for Influence of Loading Condition on a Prediction of Ship Manoeuvrability, *The Japan Society of Naval Architects and Ocean Engineers*, Vol. 89, pp. 155-166, 1995. (in Japanese)

[22] Liu, J., Quadvlieg, F., and Hekkenberg, R., Impacts of the Rudder Profile on Maneuvering Performance of Ships. *Ocean Engineering*, 124, pp.226-240, 2016.

[23] Maruo, H., Wave Resistance of a Ship in Regular Head Sea, The Bulletin of the Faculty of Eng., Yokohama National University, Vol.9, pp.73-91, 1960.

[24] Nagarajan, V., Kang, D. H., Hasegawa, K. and Nabeshima, K., Comparison of the Mariner Schilling Rudder and the Mariner Rudder for VLCCs in Strong Winds, *J. Marine Science and Technology*, Volume 13, Issue 1, pp.24-39, 2008.

[25] Nguyen, T. V., and Ikeda, Y., Hydrodynamic Characteristic of Rudder Sections with High Lift Force, *Conference Proceedings of JASNAOE*, 17, 2013A-GS7-1, pp.121-124, 2013.

[26] Nomoto, K., Taguchi, K., Honda, K. and Hirano, S., On the Steering Quality of Ships, *International Shipbuilding Progress*, Vol. 4, pp. 354-370, 1957.

[27] SIMMAN. Part B Benchmark Test Cases, KVLCC2 Description, Workshop on Verification and Validation of Ship Maneuvering Simulation Method, Workshop Proc., Vol.1, Copenhagen, page B7-B10, 2008.

[28] Tachi, K., and Endo, M., Estimated Manoeuvrability of T. S. Wakashio-maru-I –Wind Tunnel Test and Rudder Open Test– (in Japanese). *Journal of Japan Institute of Navigation*, 94, pp.17-26, 1996.

[29] Takahashi, T. and Asai, S., Experimental Study on Rough-Sea Performance of a Lower-Powered Large Full Ship, *Trans. of West-Japan Society of Naval Architects*, No.65 , pp.51-61, 1983. (in Japanese)

[30] Tsujimoto, M., Kuroda, M., and Sogihara, N., Development of a Calculation Method for Fuel Consumption of Ships in Actual Seas with Performance Evaluation, Proc. ASME 2013,

32nd International Conference on Ocean, Offshore and Arctic Engineering, OMAE2013, Nantes, France, paper no.OMAE2013-11297, 2013.

[31] United Nation Conference on Trade and Development, United Nations. *Review of Maritime Transport 2016*, Geneva, November 2016, retrived from http://unctad.org/transportnews, 2016.

[32] Watanabe, I., Toki, N., and Ito, A., Chapter 2 Strip Method, Theory of Seakeeping performance and its Application to Ship Design, The 11th Marine Dynamic Symposium, The Society of Naval Architects of Japan, pp.167-187, 1994. (in Japanese)

[33] Yasukawa, H., Simulations of Ship Maneuvering in Waves (2nd report: zig-zag and stopping maneuvers), *Journal of the Japan Society of Naval Architects and Ocean Engineers*, Vol. 7, (2008), pp. 163-170. (in Japanese)

[34] Yasukawa, H., Hirata, N., Matsumoto, A., Kuroiwa, R., and Mizokami, S., Evaluations of Wave-Induced Steady Forces and Turning Motion of a Full Hull Ship in Waves, *J. Marine Science and Technology* (2017), to be submitted.

[35] Yasukawa, H., Hirata, N., Yonemasu, I., Terada, D., and Matsuda, A., Maneuvering Simulation of a KVLCC2 Tanker in Irregular Waves, *International Conference on Marine Simulation and Ship Maneuverability* (MARSIM'15), Newcastle, UK, CD-R, 2015.

[36] Yasukawa, H., and Nakayama, Y., 6-DOF Motion Simulations of a Turning Ship in Regular Waves, Proc. *International Conference on Marine Simulation and Ship Maneuverability*, Panama City, 2009.

[37] Yasukawa, H. and Yoshimura, Y., Introduction of MMG Standard Method for Ship Maneuvering Predictions, *J. Marine Science and Technology*, Volume 20, Issue 1 , pp.37-52, 2015.

[38] Yasukawa, H., Zaky, M., Yonemasu, I., and Miyake, R., Effect of Engine Output on Maneuverability of a VLCC in Still Water and Adverse Weather Conditions, *J. of Marine Science and Technology*, Vol.22, Issue 3, pp.574-586, 2017.

[39] Yasukawa, H., Hirata, N., Kayama, Y., Sano, M., Yonemasu, I., and Hashizume, Y., Maneuverability of Cb-Series Full Hull Ships (1st report: Tank Tests) (in Japanese), *J. Society of Naval Architects of Japan*, to be published.

[40] Yasukawa, H., Yamazaki, Y., Zaky, M., and Amii, H., Maneuverability of C_b-Series Full Hull Ships (2nd report: maneuvering simulations) (in Japanese), *J. Society of Naval Architects of Japan*, to be published.

[41] Yasukawa, H., Hirata, N., Matsumoto, A., Kuroiwa and Mizokami, S., Evaluations of Wave-Induced Steady Forces and Turning Motion of a Full Hull Ship in Waves, *Journal of Marine Science and Technology*, 2018, in press, DOI: 10.1007/s00773-018-0537-3 (Published online: 2018.2.24).

[42] Yoshimura, Y., Prediction of Ship Manoeuvrability Of SR221 Series Model With Full Load And Ballast Conditions, Proceeding of the *Workshop on Ship Maneuverability*, Kyushu, Japan, 1998.

[43] Yoshimura, Y. and Nagashima, J., Estimation of the Manoeuvring Behaviour of Ship in Uniform Wind, *J. Society of Naval Architects of Japan*, No.158, pp.125-136, 1985. (in Japanese)

[44] Yoshimura, Y., Nakao I., Kanamoto, M., and Nakamura, M., Ship Manoeuvrability at Ballast Condition (Open Water Characteristics of Rudder), *The Journal of Japan Institute of Navigation*, Vol. 126, pp. 99-104, 2012. (in Japanese)

[45] Zaky, M., Sano, M., and Yasukawa, H., Improvement of Maneuverability in a VLCC by a High Lift Rudder, *Journal of Ocean Engineering*, (being reviewed).

[46] Zaky, M., Yasukawa, H., and Miyake, R., Simulation Study on Maneuverability of a VLCC in Still Water and Adverse Weather Conditions, Proc. of *Workshop on Environmental Technologies in Naval Architecture and Ocean Engineering* (2016), Vol.64, pp.93-96, Hiroshima, Japan, Dec. 2016.

[47] Zaky, M., and Yasukawa, H., Manoevring Simulations of a VLCC in Adverse Weather Conditions, Proceeding of *10th International Workshop on Ship and Marine Hydrodynamics* (IWSH 2017), pp.1-10, Keelung, Taiwan, Nov. 2017.

[48] Zaky, M., Sano, M., and Yasukawa, H., Improving the Maneuvering Performance of a VLCC in Adverse Weather Conditions by a High Lift Rudder, Proc. of *Workshop on Environmental Technologies in Naval Architecture and Ocean Engineering* (2017), Vol.65, pp.43-46, Hiroshima, Japan, Nov. 2017.

[49] Zaky, M., and Yasukawa, H., Effect of Load Condition on Turning Performance of a VLCC in Adverse Weather Conditions, *Journal of Advanced Research in Ocean Engineering*, to be published.

[50] Zhang, Z., and Li, X, M., Global Ship Accidents and Ocean Swell-Related Sea States, *Journal of Natural Hazards Earth System Science*, Vol.17, pp. 2041-2051, 2017.